AD

CONTRACT REPORT ARBRL-CR-00518

MODELING OF RIGIDIZED GUN
PROPELLING CHARGES

Prepared by

Paul Gough Associates, Inc.
P. O. Box 1614
Portsmouth, New Hampshire 03801

November 1983

US ARMY ARMAMENT RESEARCH AND DEVELOPMENT CENTER
BALLISTIC RESEARCH LABORATORY
ABERDEEN PROVING GROUND, MARYLAND

Approved for public release; distribution unlimited.

Destroy this report when it is no longer needed.
Do not return it to the originator.

Additional copies of this report may be obtained
from the National Technical Information Service,
U. S. Department of Commerce, Springfield, Virginia
22161.

The findings in this report are not to be construed as
an official Department of the Army position, unless
so designated by other authorized documents.

REPORT DOCUMENTATION PAGE		READ INSTRUCTIONS BEFORE COMPLETING FORM
1. REPORT NUMBER CONTRACT REPORT ARBRL-CR-00518	2. GOVT ACCESSION NO.	3. RECIPIENT'S CATALOG NUMBER
4. TITLE *(and Subtitle)* MODELING OF RIGIDIZED GUN PROPELLING CHARGES		5. TYPE OF REPORT & PERIOD COVERED Final Report April 1982 – April 1983
		6. PERFORMING ORG. REPORT NUMBER PGA-TR-83-1
7. AUTHOR(s) Paul S. Gough		8. CONTRACT OR GRANT NUMBER(s) DAAK11-82-C-0053
9. PERFORMING ORGANIZATION NAME AND ADDRESS Paul Gough Associates, Inc. P.O. Box 1614 Portsmouth, NH 03801		10. PROGRAM ELEMENT, PROJECT, TASK AREA & WORK UNIT NUMBERS 1L161102AH43
11. CONTROLLING OFFICE NAME AND ADDRESS US Army AMCCOM, ARDC Ballistic Research Laboratory, ATTN: DRSMC-BLA-S(A) Aberdeen Proving Ground, MD 21005		12. REPORT DATE November 1983
		13. NUMBER OF PAGES 203
14. MONITORING AGENCY NAME & ADDRESS*(if different from Controlling Office)*		15. SECURITY CLASS. *(of this report)* UNCLASSIFIED
		15a. DECLASSIFICATION/DOWNGRADING SCHEDULE

16. DISTRIBUTION STATEMENT *(of this Report)*

Approved for public release; distribution unlimited.

17. DISTRIBUTION STATEMENT *(of the abstract entered in Block 20, if different from Report)*

18. SUPPLEMENTARY NOTES

19. KEY WORDS *(Continue on reverse side if necessary and identify by block number)*

Interior Ballistics
Two-Phase Flow
Flamespread
Computer Code

TDNOVA
Solid Propellant Gun
Stick Propellant
Modular Charge

20. ABSTRACT *(Continue on reverse side if necessary and identify by block number)*
slp

The TDNOVA code was developed to simulate the interior ballistics of multi-increment propelling charges by means of a numerical solution of the equations of two-dimensional, two-phase flow. The present work describes extensions to the code, primarily to permit the simulation of rigidized stick propellant charges, and secondarily to explore the ballistic consequences of heat loss to the tube and of slow gas-phase kinetics.

DD FORM 1473 EDITION OF 1 NOV 65 IS OBSOLETE
1 JAN 73

Table of Contents (continued)

1.0 INTRODUCTION

The general topic of interest in this work is the manner in which relatively subtle aspects of propelling charge design influence overall interior ballistic behavior. Specifically, we seek to evaluate theoretically the roles played by the distributed ignition system, the initial free volume (ullage) around the charge, and the properties of the container in which individual increments of the charge are loaded. Our theoretical approach may be summarized as one in which the equations of macroscopic two-dimensional, unsteady, two-phase flow are solved on a multiply connected, time-dependent domain defined by the instantaneous configuration of the propelling charge increments. These equations are solved simultaneously with the balance equations for the single-phase flow in the ullage, subject to external boundary conditions defined by the fixed tube and moving projectile, and internal boundary conditions at the interfaces between the ullage and the propelling charge increments. The influence of the containers is embedded into the internal boundary conditions.

The complexity of the system of governing equations is such as to require numerical solution by the technique of finite differences. The resulting Fortran language computer program is referred to as the TDNOVA code and has been the subject of three previous reports[1,2,3]. In Reference 1 we described an overall computational strategy to such a code and we demonstrated the feasibility of obtaining numerical solutions of the equations governing the macroscopic aspects of the two-dimensional, unsteady flow of a reacting, heterogeneous, two-phase mixture. In Reference 2 we extended the code to treat the complete interior ballistic cycle of a single-increment charge and to model the interplay between the ignition system, the ullage and certain of the properties of the bag used to contain in-service artillery charges. In Reference 3 we described the further extension of the code to treat multi-increment charges of granular propellant.

The principal objective of the present work is to accomplish the further extension of TDNOVA to model a new class of propelling charges described by Einstein et al[4]. The distinguishing features of these

[1] Gough, P. S., "Two-Dimensional Convective Flamespreading in Packed Beds of Granular Propellant," Ballistic Research Laboratory Contract Report ARBRL-CR-00404, 1979 (AD A075326).

[2] Gough, P. S., "A Two-Dimensional Model of the Interior Ballistics of Bagged Artillery Charges," Ballistic Research Laboratory Contract Report ARBRL-CR-00452, 1981 (AD A100751).

[3] Gough, P. S., "Two-Dimensional, Two-Phase Modeling of Multi-Increment Bagged Artillery Charges," Ballistic Research Laboratory Contract Report ARBRL-CR-00503, 1982 (AD A125482).

[4] Einstein, S., Pellington, B. and Westley, S., "Charge Design Technology," Applied Sciences Division, ARRADCOM, Dover, NJ. 1980

new charges are the use of stick propellant and the rigidizing of the case used to package each of the increments.

Neither the fundamental approach nor the overall method of solution have been altered appreciably during the performance of the present effort. Accordingly, we do not attempt to describe completely all aspects of the theoretical basis of the model or of the method of solution. We abstract from the previous reports only those results to which we will need to refer explicitly while discussing the present extensions and revisions. On the other hand, the description of the code structure and use, given in the appendix, is complete as regards both previous and current work.

In Section 1.1 we recapitulate briefly the theoretical and experimental motivation for the development of TDNOVA. We then provide a summary of the code content prior to the performance of the present effort. In Section 1.2 we describe more fully the objectives of the present work. In Section 1.3 we describe the approach taken to achieve our objectives and we summarize the present code content. Attention is given to limitations as well as capabilities.

1.1 Background Information

An ideal type of interior ballistic cycle may be described as follows. At some initial instant the entire charge is uniformly ignited. The chamber pressure increases smoothly and monotonically to some maximum value, determined by the competition between the rate of energy release due to combustion of the propellant and the rate of chamber expansion due to motion of the projectile. Then, as the rate of chamber expansion begins to dominate, the pressure decreases smoothly and monotonically. If we take the gun and the projectile as given then the only charge design parameters of interest are the rate of energy release, the thermodynamic properties of the gas-phase, and the fraction of the chamber volume occupied by the unburnt propellant. This ideal sort of behavior is the basis for the widely used lumped parameter model of Baer and Frankle[5] in which the rate of energy release is expressed in terms of a subgroup of charge parameters, namely, grain geometry, linear burn rate and gas-phase thermochemical properties.

In practice, however, significant departures from the ideal are apparent from an inspection of the histories of chamber pressure. In many cases, the pressure does not rise smoothly and monotonically through a maximum value; oscillations, whose amplitudes are strongly charge-dependent, are seen to be superimposed on the ideal pressure

---

[5]Baer, P. G., and Frankle, J. M., "The Simulation of Interior Ballistic Performance of Guns by Digital Computer Program," Ballistic Research Laboratory Report 1183, 1962 (AD 299980).

history. These oscillations may be made even more apparent by plotting the history of the difference between the values of pressure in the breech and the mouth of the chamber of the gun. It is customary to refer to the oscillations as pressure waves.

As early as 1935 Kent[6] studied the manner in which pressure waves in the 155mm gun could be alleviated by modifications to the path of ignition through the charge and the initial distribution of ullage around the charge. The dependence of pressure waves on the path of flamespreading through a Navy charge was studied experimentally by Heddon and Nance[7] who noted that the presence of pressure waves did not necessarily disqualify a charge from service. However, it was observed in the extensive review of Budka and Knapton[8] that a correlation could be detected between the existence of pressure waves and the possible occurrence of catastrophic malfunction due to overpressure of the gun.

Obviously, the prediction of pressure waves is inherently outside the scope of a lumped parameter model. The NOVA code[9] is one of several models which were advanced to extend the scope of numerical simulation to recognize details of the distributed ignition system and its influence on flamespreading. The NOVA code is based on the equations of quasi-one-dimensional two-phase flow. Provided that careful attention is given to details of the axial distribution of the propellant and the properties of the end closures of the container, it yields predictions of axial pressure wave structure which are in good agreement with observations of case gun ammunition for which the assumption of one-dimensional flow is reasonable.[10,11]

[6]Kent, R. H., "Study of Ignition of 155mm Gun"
Ballistic Research Laboratory Report 22, 1935 (AD 494703).

[7]Heddon, S. E., and Nance, G. A., "An Experimental Study
of Pressure Waves in Gun Chambers," Naval Proving Ground
Report 1534   1957

[8]Budka, A. J., and Knapton, J. D., "Pressure Wave Generation
in Gun Systems--A Survey," Ballistic Research Laboratory
Memorandum Report 2567, 1975 (AD B008893L).

[9]Gough, P. S., "The NOVA Code: A User's Manual"
Naval Ordnance Station Contract Report IHCR 80-8   1980

[10]Horst, A. W., Smith, T. C., and Mitchell, S. E., "Key Design
Parameters in Controlling Gun Environment Pressure Wave
Phenomena--Theory versus Experiment," Proc. 13th JANNAF
Combustion Meeting   1976

[11]Horst, A. W., and Gough, P. S., "Influence of Propellant
Packaging on Performance of Navy Case Gun Ammunition"
J. Ballistics v.1, p. 229   1977

However, the prediction of the structure of pressure waves in bagged artillery charges has proven to be generally outside the scope of one-dimensional models. As already anticipated by the work of Kent,[6] the list of significant charge parameters must be extended to include at least two-dimensional details of the initial distribution of propellant. Exploratory calculations based on a quasi-two-dimensional representation to account for ullage around the charge indicated significant theoretical sensitivity to the presence of annular ullage[12] and, moreover, to certain of the properties of the sidewall of the bag, namely its mechanical strength and its permeability to the gas-phase.[13] With regard to the importance of the properties of the material used to contain the charge we note the remark by May and Horst[14] that in one instance, at least, a change in the type of cloth resulted in a breech-blow of a 155mm howitzer charge. Accordingly, it was determined that an appropriate extension to the NOVA code would involve an analysis not only of multidimensional flow but also of the properties of the propellant bag. The development of TDNOVA was therefore begun. The remainder of this section provides a description of TDNOVA as it existed prior to the onset of the present effort.

Figure 1.1 is a schematic illustration of a charge consisting of three increments. It was assumed that the increments are packed end-to-end; coaxial increments were not considered. Each increment was permitted, however, to incorporate a centercore igniter charge, as has been shown in Figure 1.1. The various components of the gun/projectile/charge assembly were represented as follows.

Gun Tube and Spindle

These were treated as rigid, stationary, impermeable surfaces.

Projectile

The projectile was treated as a rigid body whose motion was determined by the total forces acting on the wetted portion of the afterbody and by a predetermined law of resistance due to interference of the rotating band with the gun tube.

[12] Gough, P. S., "Theoretical Study of Two-Phase Flow Associated with Granular Bag Charges," Ballistic Research Laboratory Contract Report ARBRL-CR-00381, 1978 (AD A062144).

[13] Horst, A. W., and Gough, P. S., "Modeling Ignition and Flame-spread Phenomena in Bagged Artillery Charges," Ballistic Research Laboratory Technical Report ARBRL-TR-02263, 1980 (AD A091790).

[14] May, I. W., and Horst, A. W., "Charge Design and Pressure Waves in Guns," Progress in Astronautics and Aeronautics, Vol. 68, Interior Ballistics of Guns, edited by H. Krier and M. Summerfield   1979
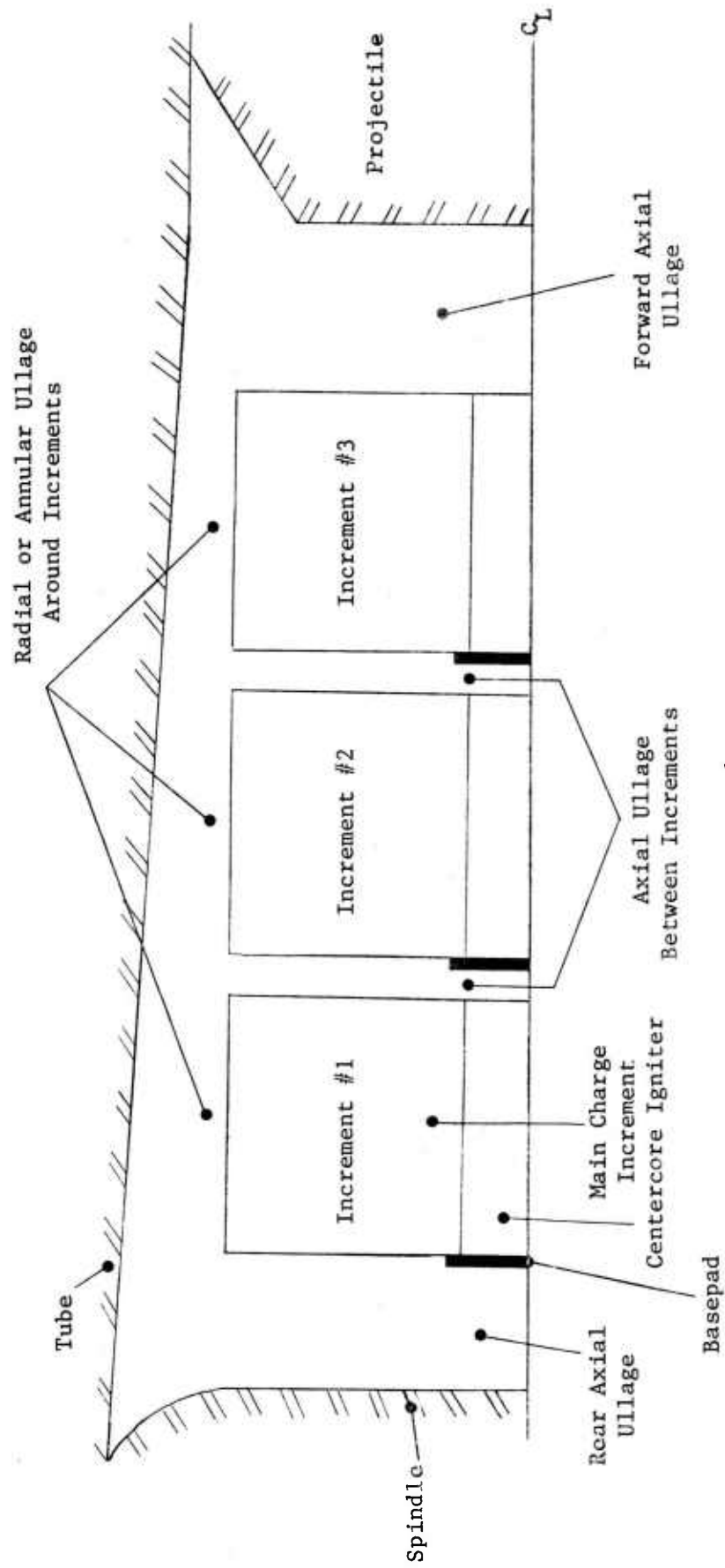
Figure 1.1   Representation of Multi-Increment Charge by TDNOVA

Projectile

Forward Axial
Ullage

Radial or Annular Ullage
Around Increments

Increment #3

Increment #2

Increment #1

Axial Ullage
Between Increments

Main Charge
Increment
Centercore Igniter

Basepad

Tube

Rear Axial
Ullage

Spindle

C_L

9

Main Charge Increments

Each increment was assumed to consist of granular propellant. The behavior of the solid- and gas-phases in each region occupied by an increment was assumed to be governed by the balance equations for macroscopic two-phase flow. These describe the evolution of what may be viewed as average state variables and they require independent constitutive laws to define sub-scale-of-heterogeneity processes such as combustion, assumed to be governed by an exponential dependence of surface regression rate on ambient pressure; interphase heat transfer, assumed to be governed by the correlation of Gelperin and Einstein,[15] and interphase drag, assumed to be governed by the correlation of Ergun[16] for packed beds, extended into the fluidized regime by the tortuosity factor of Andersson.[17] The gas-phase was assumed to obey the covolume equation of state and the ratio of specific heats and the molecular weight were taken to vary with composition. The average stress in the solid-phase was assumed to reflect intergranular stresses as well as the ambient gas-phase pressure. The intergranular stresses depend on the porosity and were assumed to be path-dependent. The surface area and volume of individual grains were assumed to be known as functions of surface regression. Ignition of the solid-phase was assumed to occur when the surface temperature, deduced from an approximate solution of the heat conduction equation driven by the interphase heat transfer as a boundary condition, reached a predetermined value.

Ignition Train

When a centercore igniter was present it was modeled in the same fashion as a main charge increment except that the equations governing the centercore igniter were at most one-dimensional-with-area-change. Basepads and other reactive components were viewed as attributes of the envelope of the increment to which they were attached and were represented as source terms according to predetermined tabular data. A distributed tabular source term was also included as an option. Primer discharge through the spindle was not modeled. If the centercore igniter was contained in a combustible nitrocellulose tube, the tube was treated as an attribute of the main charge boundary in the same fashion as a basepad.

---

[15]Gelperin, N. I., and Einstein, V. G., "Heat Transfer in Fluidized Beds," Fluidization, edited by Davidson, J. F. and Harrison, D., Academic Press, NY   1971

[16]Ergun, S. "Fluid Flow Through Packed Columns" Chem. Eng. Progr., v. 48, p. 89   1952

[17]Andersson, K. E. B. "Pressure Drop in Ideal Fluidization" Chem. Eng. Sci., v. 15, p. 276   1961

Bag Material and Additives

We have already noted that source terms were used to represent exothermic components of the bag, like the basepad and the centercore tube. A similar technique was used to represent such endothermic additives as, for instance, a salt bag attached to the front of an increment. The reactive components were represented as sources of mass, momentum and energy, and were embedded in the model by reference to the gas-phase boundary conditions which couple the two-phase flow in the mixture region, defined by each charge increment, to the single-phase flow in the contiguous ullage, or, possibly, to the two-phase flow in a contiguous centercore igniter charge. The bag had other attributes, however, namely resistance to the flow of the gas-phase, mechanical integrity, resistance to the motion of the solid-phase, and thickness. The gas-phase flow resistance was, like the reactivity, represented as a source (or sink) term in the gas-phase normal momentum flux boundary condition. The bag was taken to impede radial motion of the solid-phase on the inner sidewall (the centercore tube), provided that rupture had not occurred. Similarly, the bag was assumed to resist outward radial motion of the solid-phase on the outer sidewall, provided that the outer sidewall was fully dilated. Rupture was taken to occur locally when a given value of pressure differential was exceeded. The bag was permitted to have an arbitrary initial distribution of thickness.

Ullage

The ullage was assumed to be occupied by a single-phase flow. The gas in the ullage was taken to be compressible, inviscid, and non-heat-conducting. The covolume equation of state was assumed to apply and, as in the mixture regions, the ratio of specific heats and the molecular weight were taken to be composition-dependent.

The governing equations consisted of a number of partial differential equations supported by algebraic constitutive laws and subject to external boundary conditions--at the tube, spindle, and projectile-- and internal boundary conditions--at the interfaces between regions. The code contained two distinct modes of representation, the dynamic mode, which permitted a two-dimensional analysis of regions of ullage, and a static mode in which the regions of ullage were at most quasi-one-dimensional. Complete calculations have only been attempted in the static mode which we now proceed to describe. Reference may be made to the previous reports[2,3] for discussions of the dynamic mode.

Figure 1.2 depicts two-dimensional and quasi-two-dimensional representations of the charge shown in Figure 1.1. In the static mode,

2D2P – Two-Dimensional, Two-Phase
Q1DA – Quasi-One-Dimensional, Axial (Single- or Two-Phase)
Q1DR – Quasi-One-Dimensional, Radial
  LP – Lumped Parameter
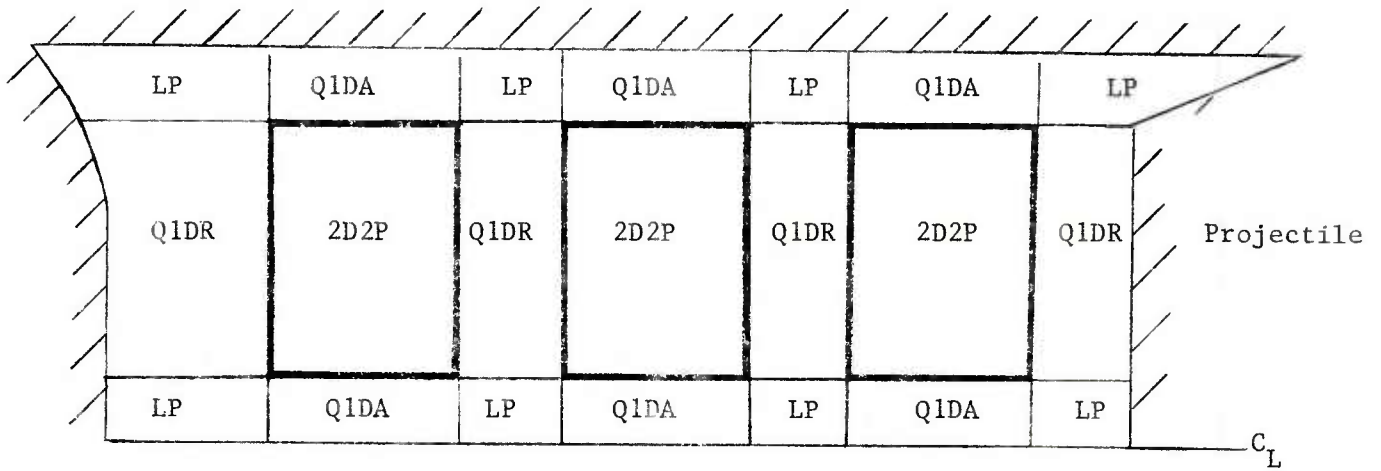
(a)   Two-Dimensional Representation

Q1DA – Quasi-One-Dimensional, Axial (Single- or Two-Phase)
  LP – Lumped Parameter
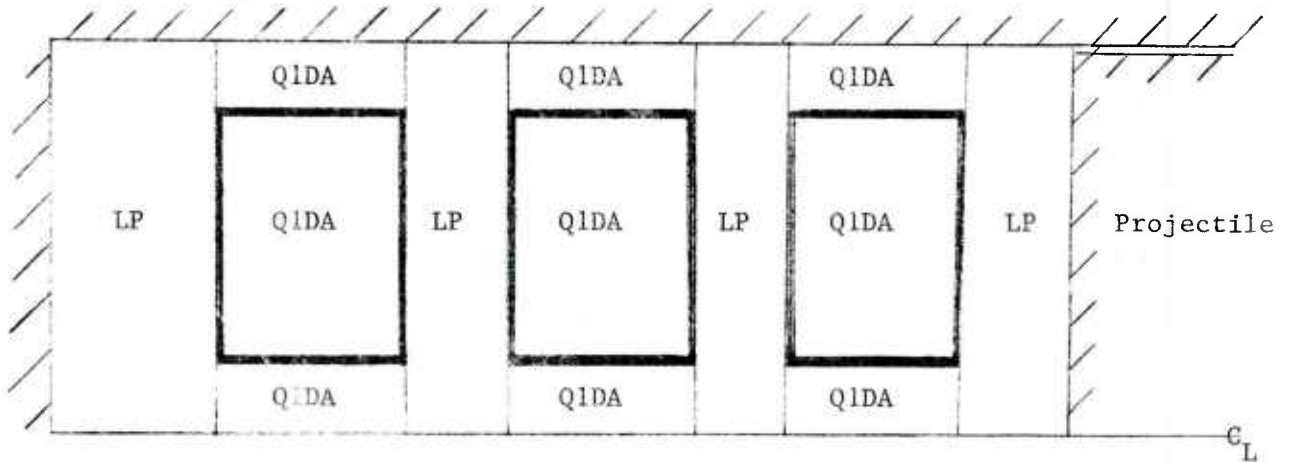
(b)   Quasi-Two-Dimensional Representation

Figure 1.2   Two-Dimensional and Quasi-Two-Dimensional Representations
              Associated with Static Mesh Allocation Mode

the two-dimensional representation applied until flamespreading was complete, all sidewalls of all bags had completely ruptured, and the radial gradient of pressure had subsided to less than some user-selectable tolerance at each cross section of the tube. When the foregoing conditions were met, an irreversible transformation was made to a quasi-two-dimensional representation which permitted an economical determination of the longitudinal structure of the pressure field throughout the remainder of the interior ballistic cycle.

The finite difference mesh in each of the two-dimensional regions was established by means of the equipotential algorithm of Thompson et al[18] Dirichlet data were specified for the mesh on the boundaries. The mesh in the quasi-one-dimensional regions contiguous with the mixture boundaries was tied to the mesh on the mixture boundaries. An explicit two-step marching scheme based on the algorithm of MacCormack[19] was used at all interior mesh points. Convective derivatives, however, were evaluated by means of the second order two-step scheme of Moretti[20] which only uses upstream data. The integration time step was limited by the Courant condition and calculations to date have been performed with Courant numbers in the range 0.5-0.9.

Characteristic forms of the equations were used to update the solution at the boundaries. In the mixture regions there is significant differential coupling between the solid-phase and gas-phase state variables. The gradient of porosity (fraction of a unit volume occupied by the gas-phase) appears in the gas-phase continuity equation, and also in the energy equation if it is expressed in terms of internal energy. The gradient of gas-phase pressure appears in the solid-phase momentum equation. Some simplification of the analysis was obtained by using pseudo-characteristic forms in which the gradient of gas-phase pressure was treated as an algebraic or inhomogeneous term in the solid-phase momentum equation. The gas-phase normal mass flux and pressure were treated implicitly--that is to say that they were expressed as future level properties--in the characteristic forms for the mixture, the jump conditions at the internal boundaries, and in the algebraic forms which capture mass transfer to the contiguous regions of quasi-one-dimensional flow.

---

[18] Thompson, J. F., Thames, F. C., and Mastin, C. W., "Automatic Numerical Generation of Body-Fitted Curvilinear Coordinate Systems for Field Containing Any Number of Arbitrary Two-Dimensional Bodies," J. Comp. Phys. v. 15, p. 299   1974

[19] MacCormack, R. W. "The Effect of Viscosity in Hypervelocity Impact Cratering," AIAA Paper No. 69-354   1969

[20] Moretti, G. "Calculation of the Three-Dimensional, Supersonic, Inviscid, Steady Flow Past an Arrow-Winged Airframe" POLY-AE/AM Report No. 76-8, Polytechnic Institute of New York   1976

Full details of the physical content of the model and the method of solution may be found in References 1, 2 and 3. A baseline evaluation of the code is described by Horst.[21]

1.2 Present Objectives

Because of the increasing importance of stick propellant in current charge designs, the first, and most important objective of the present effort is the formulation and encoding into TDNOVA of a model of stick propellant with the following features.

Representation of Stick Charges

(i) The charge may incorporate one or more increments of stick propellant, each having chemical and physical properties independent of other increments.

(ii) Each increment may consist of zero-, single-, seven-, or nineteen-perforation unslotted sticks or single-perforation slotted sticks.

(iii) Prior to local burnthrough in each increment, it is assumed that the values of all the gas-phase variables in the interstices between individual sticks differ from the values within the perforations at the same macroscopic location. Heat transfer, ignition and surface regression are represented independently for the exterior and interior flows. In the case of slotted stick propellant, consideration must be given to mass transfer through the slot. For perforated stick propellant, the possibility of transformation to a slotted form is required when the internal pressure exceeds the external pressure by a specified amount.

(iv) Anisotropic formulations are required in respect to the interphase drag and heat transfer.

(v) An anisotropic constitutive law is required for the description of stresses in the solid-phase.

The previously existing code version did not recognize any impediment to motion of the solid-phase due to the presence of the endwalls of the bag. This feature was omitted due to the requirement that endwall constraint be coupled to the axial stress-field in the sidewall.

---

[21] Horst, A. W. "Baseline Evaluation of the TDNOVA Code" Ballistic Research Laboratory Memorandum Report ARBRL-MR-03198, 1982 (AD A120718).

At any section of the container, only one reactive source was considered and its combustion characteristics were taken to be predetermined. A second objective of the present work is to relax these modeling limitations as follows.

Representation of Rigidized Cases

(i) It is assumed that prior to rupture of any portion of each container, the endwalls are rigid and the sidewalls obey a linear elastic law with respect to the axial deformation field.

(ii) Each segment of the container has finite thickness and inertia. Provision is made for the specification of two reactive layers on each side of each segment. One such layer is to represent the combustion of the container wall and the other is to represent an attached component, such as a basepad. The rates of discharge may be determined according to predetermined tabular data or by reference to an ignition and combustion model driven by local flow conditions.

A number of extensions to the constitutive physics of the model are included in the present work, over and above those referred to in respect to the treatment of stick charges and rigidized cases. It has been suggested that stick charges may induce higher rates of heat transfer to the tube than do granular charges.[22] To determine whether the same theoretical conclusion holds in the context of a two-dimensional model, we incorporate heat loss models of the same type as those contained in the one-dimensional NOVA code.[9] While erosive combustion has not yet been demonstrated to play a significant role in respect to granular charges, the same conclusion is unlikely to be true of perforated stick charges and a model of erosive combustion is therefore desirable.

In some cases the region of annular ullage can become quite narrow and it is possible that wall friction may be significant. We explore this possibility by encoding a steady-state correlation. Better data are available to describe the flow resistance in a packed bed than the Ergun law used hitherto. We encode a correlation due to Robbins and Gough[23] as formulated by Gough[24] for use in the one-dimensional NOVA code. Finally, we seek to relax the assumption that the combustion of

---

[22]Horst, A. W., "A Comparison of Barrel-Heating Processes for Granular and Stick Propellant Charges," Ballistic Research Laboratory Memorandum Report ARBRL-MR-03193, 1982 (AD A118394).

[23]Robbins, F. W., and Gough, P. S., "Influence of Length and Diameter of Cylinders on Packed Bed Flow Resistance" Proc. 16th JANNAF Combustion Meeting   1979

[24]Gough, P. S., "Extensions to NOVA Flamespread Modeling Capacity," Final Report, Task I, Contract N00174-80-C-0316 Paul Gough Associates Report PGA-TR-81-2   1981

the solid-phase is completed instantaneously and locally, all the chemical energy being released simultaneously with the regression of the surface.

The third objective can be summarized as follows.

Extensions to Constitutive Laws

(i) A two-step model of the combustion of the solid-phase is encoded, part of the chemical energy being released at the surface simultaneously with the regression of the surface, and the balance being released at a finite rate in the gas-phase.

(ii) A representation is made of frictional losses in regions of quasi-one-dimensional single-phase flow. The correlation describing steady state flow resistance in packed beds of granular propellant is revised.

(iii) Heat loss to the tube wall is modeled. The heat loss may be deduced according to a steady-state correlation or according to an unsteady boundary layer model. The wall temperature may be updated according to a cubic profile approximation or by reference to a numerical solution of the heat conduction equation.

(iv) A model of erosive burning is encoded.

The three preceding topics constitute the principal objectives of the present effort. We note, however, that certain other minor objectives have also been met in the present contract. These include the following.

Revisions to Problem Processing

(i) Variably scheduled logout of the solution is supported.

(ii) Histories of global mass and energy balance are tabulated at the conclusion of the run as a check on the numerical accuracy of the solution.

(iii) A detailed debugging print package is encoded to expedite code maintenance at BRL. Provisions are also made to use the large core memory of the CYBER 7600.

(iv) To assist in preliminary evaluations of the revised code, the previously encoded constitutive laws may be used on an optional basis. The solid-phase Lagrangian mesh used in Reference 2 has been restored as an option in addition to the fully equipotential mesh described in Reference 3.

As a final comment we note that an objective of this work has been to link all new features to one another and to all pre-existing features in a physically reasonable manner.

1.3 Summary of Approach

Full details of the analysis required to meet the objectives associated with stick charges, rigidized cases, and revisions to the constitutive laws are respectively contained in Sections 2.0, 3.0 and 4.0. Our purpose in the present section is simply to state the major modeling assumptions and limitations pertinent to each of these three topics. Details of the revisions to problem processing are contained in the appendix and receive no further attention here.

Representation of Stick Charges

The extension of TDNOVA to permit the modeling of stick charges involves both conceptual and practical revisions. The conceptual revision is associated with the interpretation of the macroscopic state variables, which will be the first topic of this section. It will lead to a discussion of the anisotropic formulations required to represent the interphase drag and heat transfer as well as the state of stress of the solid-phase. We will then comment on the representation of the perforations and the treatment of slotted propellant.

The formulism of TDNOVA is based on the macroscopic equations of two-phase flow. The macroscopic equations may be deduced formally by averaging the balance equations for the microflow, which are known, at least in principle. The equations derived in this manner are form indifferent with respect to the precise definition of the average. It is tacitly assumed, however, that average values can be defined which depend smoothly on position and time. If the average is formed by sampling values over some volume then it is assumed that the average varies negligibly over length scales comparable to those which characterize the averaging volume. A similar requirement is associated with time averaging and is a familiar feature of turbulence modeling[25] in single-phase flow. It is customarily assumed, in applications to granular charges, that the macroscopic state variables may be formed by averaging over a region which is large by comparison with the scale of heterogeneity. In the one-dimensional treatment of NOVA, the average may be thought of as formed over a disc bounded by two cross sections of the tube separated by a distance equal to a few multiples of the average grain dimensions. In the two-dimensional treatment of TDNOVA, the averaging region becomes an annulus, formed from the same disc as in the NOVA

---

[25]Hinze, J. O., "Turbulence", McGraw-Hill   1959

representation, by taking an intersection with two cylindrical surfaces whose diameters differ by a few multiples of the grain dimensions. We have previously noted[1] that since, in fact, the tube diameter itself is only a few multiples of the typical grain dimensions, the radial flow structure modeled by TDNOVA is actually at the limit of applicability of the macroscopic equations.

When we seek to apply the macroscopic approach to the simulation of stick charges, the conceptual definition of the averaging region involves a length scale of heterogeneity which reflects only the diameter of the grains and not their lengths. We assume that the microflow is sufficiently regular in the longitudinal direction of the stick bundle that only the transverse variation requires filtering by an averaging operator. The only exception to this statement occurs at the ends of the bundles where exit and entrance effects may be pronounced. In general, however, we expect the macroscopic approach to be more rather than less applicable when we turn from granular to stick charges.

An important conceptual point to understand in respect to stick charges is that the anisotropy of the mixture plays no role in the formal structure of the macroscopic equations. A direction dependent voidage or porosity is not required. The anisotropy is embedded in the constitutive laws. The intuitive perception that the transverse flux in a stick charge will be much less than the longitudinal flux is captured theoretically not by an expression of limited transverse flow area but rather by an expression of strong transverse flow resistance. Anisotropic formulations apply to both the interphase drag and the heat transfer. These are resolved by reference to available empirical correlations for duct flow, to capture the longitudinal components, and to correlations for tube bundles, to capture the transverse components. The solid-phase stress components in the transverse direction are assumed to have an irreversible dependence on porosity which is perfectly analogous to that which governs the isotropic stress in a granular bed. The longitudinal component of stress is, however, assumed to follow from a linear elastic law.

A basic assumption of the NOVA and TDNOVA codes is that ignition and combustion of individual perforated grains of propellant exhibit negligible variation over the entire surface of the grains within a local averaging volume. Under certain conditions this assumption may be incorrect[26] possibly, it may be untrue during extended ignition delays in artillery charges. In general, however, it appears to be a satisfactory working hypothesis for properly ignited granular charges.

[26] Jakus, K., "Feasibility of a Laboratory Ignition Test for Lot Acceptance of Gun Propellant," Report No. ASR-SD-QA-A-P-59-74 ARRADCOM, Dover, N.J.   1974

As the length to diameter ratio of the grains is increased from the values of 1 or 2 typical of granular propellant to values of 50 or 100 typical of stick propellant, the assumption of uniformity of ignition and combustion obviously fails to be true with respect to the length of the grains. Inasmuch as our state variables do not involve longitudinal averaging it is apparent that the variation over the length of the sticks will be captured by the model. But an additional extension is required to capture the local lack of uniformity between the exterior and interior combustion processes in perforated propellants.

With reference to the gas-phase properties we regard the averages as formed independently over the interstitial and perforation regions. The same is true of the surface temperature of the stick propellant, prior to ignition, and of the regression rate subsequently. Previous theoretical studies based on a purely one-dimensional dual-voidage model of perforated stick propellant have indicated that ignition of the perforations may be delayed by several milliseconds relative to the ignition of the exterior. Subsequently, the pressure in the perforations, computed according to a quasi-steady burn rate law, may exceed that in the interstices by several tens of MPa. Such high pressure differentials may exceed the mechanical capacity of the propellant. We therefore include a simple rupture model according to which the propellant is treated as slotted once a threshold pressure differential is exceeded.

The consideration of the mass transfer through the slot raises a number of theoretical questions. Slotted propellant is manufactured with an extremely narrow slot, actually nothing more than a cut, initially. The flow rates through the slot obviously will be influenced by the instantaneous width of the slot. This, in turn, will depend on the surface regression due to progressive combustion of the slot sidewalls and, on the structural characteristics of the individual sticks. We assume that until the interior pressure exceeds the exterior pressure, there is no mass transfer through the slot. This assumption embeds the expectation that under an exterior pressure excess, the slot will close sufficiently tightly as to form an effective seal, unless burning of the slot sidewalls has previously occurred to enlarge it. Once the interior pressure exceeds the exterior pressure, in the absence of mass transfer, we assume that the slot is opened by the mechanical forces and that the subsequent rate of mass transfer is such as to equilibrate locally the interior and exterior pressures. The contribution of the combustion of the sidewalls of the slot is included in the analysis of the mass transfer. The possible erosive influence of the mass transfer through the slot is not considered.

Representation of Rigidized Cases

We first discuss the mechanical properties of the case and then we turn to its reactive properties. It is convenient to divide the container into three parts: the external sidewall, which we will simply refer to as the sidewall; the internal sidewall, presumably a center-core tube and referred to as such henceforward; and the endwalls.

The principal difference between the current mechanical attributes of the container and those of the previous code versions is as follows. Previously, mechanical constraints on the solid-phase were assumed to occur only on the sidewall and the centercore. Since the container has relatively little inertia it is only capable of impeding the motion of the solid-phase by virtue of its structural characteristics. For the endwalls to impede the motion of the solid-phase it is evident that the entire sidewall must be intact and capable of transmitting the total stress induced on the endwall by the confined propellant. Moreover, for flexible endwalls, as are typical of bag charges, the structural response is that of a membrane and significant impediment can occur only after the endwall has deformed sufficiently as to develop curvature. Here, we assume that the endwalls are sufficiently stiffened that they may be treated as rigid. Moreover, we construct the axial stress field in the sidewalls from a solution to the equations of motion of a linear elastic solid. Only the axial equation of motion is solved. Radial motion of the container sidewall, independently of the motion of the propellant is not considered. It is not difficult to include the radial motion of the sidewall, but we have viewed this further extension as a topic to be addressed following an evaluation of the current code version.

The coupling of the centercore tube to the endwalls is neglected. The influence of the centercore tube is unchanged from the previous model. The endwall is taken to impede the motion of the solid-phase at any radial location provided that it is unruptured at all radial positions equal to or greater than the location in question. If rupture occurs at a given radial location on the endwall, it is assumed that the end-wall is no longer capable of impeding the motion of the solid-phase anywhere within the disc defined by the point of rupture.

On each segment of the endwalls and the sidewalls we distinguish between the volumetric, or total, thickness and the structural thickness. The volumetric thickness corresponds to the total intrusion of the container segment and includes the complete presence of the additives or attached components. The structural thickness is intended to reflect only the case material itself and defines both the load-carrying capacity and the inertia of the segment insofar as the analysis of the axial stress field is concerned. The rate of decrease of the volumetric thickness, due to combustion, reflects all four reactive sources at

20

each location. The rate of decrease of the structural thickness reflects only the reactive sources attributed to the case itself.

Failure of a rigidized container is presently determined from an inspection of the equivalent or von Mises stress in the sidewall. Once rupture is determined to occur anywhere on the sidewall, the container in question ceases to be viewed as rigidized since an essential mechanical linkage for the endwalls to provide confinement has been broken. The subsequent analysis of the container in question is conducted as in the previous work;[3] it is viewed as flexible and subsequent failure is due to progressive overpressure of the sidewalls. Independently of whether the sidewall is treated as rigidized or flexible, failure of the endwalls is taken to occur locally when the internal pressure-- including solid-phase contributions--exceeds the external pressure by a pre-specified amount.

Rigidized container increments may be described as initially linked by a bond of prespecified strength. Once the bond tensile strength is exceeded, the increments are free to move apart.

Each segment of the container--whether situated on the sidewall, the centercore, or the endwalls--is permitted to have as many as four reactive sources. Two are attributed to the exterior and two are attributed to the interior. Proceeding from the inside of the container to the exterior, the reactive layers are assumed to be encountered in the following order: internal attached component, container inner surface, container outer surface, external attached component. The interior is understood to be the side occupied by the main charge increment, so that if a centercore tube is present, the exterior of the container refers to the inside of the tube, where the igniter charge is located.

The ordering of the reactive layers is given careful attention in the numerical solution so as to avoid a spurious diffusion of properties across a relatively impermeable segment which has, for example, an endothermic reactive layer on one side and an exothermic layer on the other. The ideas of inside and outside are expressed analytically by predicating the normal gas-phase flow resistance in terms of the total mass flux through the segment.

The rate of discharge of a reactive layer may be prespecified in tabular form, as in the previous code version,[3] or it may be modeled as follows. Heat transfer to the surface is computed from a convective heat transfer correlation. The surface temperature of the layer is computed from an approximate solution to the heat conduction equation and ignition is assumed to occur at a prespecified temperature. Subsequently, the surface of the layer is assumed to regress according to a steady state exponential dependence on local gas-phase pressure. On a given segment, one may specify layers of different types.

21

Extensions to Constitutive Laws

Erosive combustion is modeled according to the formulation of Lenoir and Robillard[27] in the same fashion as in the NOVA code. The frictional losses in quasi-one-dimensional regions of ullage are represented according to correlations for fully developed turbulent duct flow.[28] Finite rate chemistry is supported for at most one propellant species. Preheat and ignition are assumed to occur in accordance with the pre-existing criteria. No attempt is made to model the unsteady thermal profile in the solid-phase subject to the combined influence of heat feedback from the flame, following ignition, and the convective stimulus which induced the ignition. Combustion, following ignition, is assumed to obey a steady-state exponential dependence on pressure, but the products are viewed as intermediate species whose formation releases only part of the available chemical energy of the propellant. The balance of the energy is assumed to be released in the gas-phase according to an Arrhenius dependence on temperature.

The analysis of heat loss to the tube is treated from the same perspective as in the NOVA code. The heat transfer to the tube is coupled to the two-phase flow as a volumetric heat loss based on the rate of convective heating of the wall at each cross section. No attempt is made to analyze thermal diffusion within the two-phase mixture. Principally, it is desired to estimate the ballistic consequence of heat loss which is most noticeably manifested as a loss of muzzle velocity, the influence on maximum pressure being relatively small. Where estimates of thermal erosion are of interest, the unsteady integral boundary layer model of Shelton et al[29] may be used to compute the rate of heating. The wall temperature history may be ignored, updated according to a cubic profile approximation fully coupled to the calculation of heat loss, or evaluated according to the method of invariant embedding[30] at selected stations. The invariant embedding solutions are not fully coupled to the calculation of heat loss. As in the NOVA code,[9] they play a passive role.

[27] Lenoir, J. M., and Robillard G., "A Mathematical Method to Predict the Effects of Erosive Burning in Solid-Propellant Rockets," Sixth Symposium (International) on Combustion Reinhold, New York   1957

[28] Holman, J. P., "Heat Transfer," McGraw-Hill   1968

[29] Shelton, S., Bergles, A., and Saha, P., "Study of Heat Transfer and Erosion in Gun Barrels," Air Force Armament Lab., AFATL-TR-73-69   1973

[30] Meyer, G. M., "Initial Value Methods for Boundary Value Problems," Academic Press, NY   1973

2.0 ANALYSIS OF STICK CHARGES

Our conceptual approach to the modeling of stick propellant has been summarized in Chapter 1.0. Here we provide a discussion of the analysis insofar as it involves differences from the previous treatment of granular charges. In Section 2.1 we summarize the fully-two-dimensional and the quasi-two-dimensional (one-dimensional-with-area-change) forms of the balance equations for two-phase flow as used in the previous version of the code.[3] These serve as a convenient point of departure for the present discussion and, moreover, they help to make the present report more self-contained in respect to the discussion of Chapter 4.0.

In Section 2.2 we introduce the two components of voidage--exterior (interstitial) and interior (perforation)--which must be considered when we model perforated stick propellant. The dual-voidage balance equations for the gas-phase follow from the single-voidage forms of Section 2.1 in a straightforward manner. It will be noted that we incorporate a fully-two-dimensional representation of the flow within the perforations. The inherently one-dimensional nature of the flow in the perforations is embedded into the model by requiring that the transverse flow resistance be infinite. This analytical approach has been taken for the following reasons. First, it should be noted that the transverse flow resistance may be infinite for the interstitial flow if the sticks are packed tightly together. Thus it is necessary to incorporate a provision for infinite transverse flow resistance within the numerical analysis of the fully-two-dimensional model of the interstitial flow. Once this provision is incorporated, it becomes relatively straightforward to use the same method to analyze the one-dimensional flow in the perforations. Second, a significant reduction in the number of partial derivatives to be evaluated numerically for the interior flow only arises if we choose the computational mesh so that one family of coordinate lines is always aligned with the perforations. Such a requirement is not difficult to satisfy, and might in fact be desirable from the point of view of numerical accuracy. For the present, however, we have preferred to allow the computational mesh to evolve in accordance with the equipotential algorithm and to accept the possibility that the flow through the perforations may fail to be aligned with the computational mesh.

In Section 2.3 we discuss the constitutive laws for stick propellant insofar as they differ from those for granular propellant. The discussion of Section 2.3 is accordingly confined to the mechanical behavior or rheology of the stick charge, the interphase drag and the interphase heat transfer. The treatment of rupture of single-

perforation stick propellant and the related topic of the flow through the slot of slotted stick propellant are taken up in Section 2.4.

The two-phase modeling of stick propellant was first addressed in connection with the one-dimensional NOVA code.[31] On the assumption that the propellant was microscopically incompressible, it was shown that the constitutive law for the rheology of granular and stick charges could be folded into a unified representation. A consequence of this finding was the indifference of the characteristic forms of the equations with respect to the type of propellant. Since the characteristic forms were used to determine boundary values in NOVA,[31] the unified representation resulted in some simplification of the method of solution. This first analysis of stick charges was, however, based on the assumption that a single set of gas-phase properties was adequate to describe the state of the mixture at any macroscopic location. The analysis was therefore limited to unperforated stick charges.

Subsequently[24] the NOVA code was extended to incorporate a dual-voidage model of stick charges, essentially a one-dimensional limit of the present analysis. In addition, the assumption of microscopic incompressibility of the propellant was dropped and the stick charge was assumed to obey a linear elastic law insofar as the longitudinal strain field was concerned. The revised constitutive law for the solid-phase stress produced the result that the unified treatment of stick and granular charges was lost, new differential terms appearing in the solid-phase momentum equation, except in the limiting case when the value of Poisson's ratio became equal to 0.5, which corresponds to incompressible behavior. Revisions to the characteristic forms were therefore required.

We had previously established, in connection with the development of TDNOVA,[1,2,3] that mathematically rigorous characteristic forms were not required in order to obtain stable numerical solutions. In the development of TDNOVA we used pseudo-characteristic forms in which the pressure gradient in the solid-phase momentum equation was treated as a nonhomogeneous or algebraic term. With this in mind it was decided to go one step further in Reference 24 and use pseudo-characteristic forms in which the gas-phase and the solid-phase state variables were uncoupled at the differential level. The convective derivative of porosity which appears in the gas-phase continuity equation was treated as an algebraic term as were the several new differential terms appearing in the solid-phase momentum equation.

---

[31] Gough, P. S., "Numerical Analysis of a Two-Phase Flow with Explicit Internal Boundaries," Naval Ordnance Station Contract Report IHCR 77-5   1977

The situation is significantly more complicated in the present two-dimensional analysis of stick propellant. As in Reference 23, we are faced with the requirement that the characteristic forms be revised. Following the example of Reference 23 we assume that the differential uncoupling of the gas-phase and solid-phase state variables can be effected for the fully-two-dimensional two-phase flow without introducing a loss of numerical accuracy. The revised characteristic analysis is summarized in Section 2.5 and includes the effect of a transformation from cylindrical to computational coordinates. The characteristic forms are used computationally to determine boundary values of those state variables which are not defined directly by the physical boundary conditions. For instance, at an impermeable boundary the physical condition directly determines the normal velocity component; the characteristic forms are used to deduce the remaining state variables. The initial and boundary conditions pertinent to stick charges are summarized in Section 2.6.

The basic method of solution is unchanged from that used previously[1,2,3] even though many detailed revisions were required to incorporate the present extensions to the physical basis of the model. Throughout this chapter we will comment on substantive revisions to the method of solution in the context of the relevant modeling topics.

2.1 Single-Voidage Balance Equations for Two-Phase Flow

The balance equations stated in this section are those which we have used previously in connection with the modeling of granular propellant. We take these equations as a starting point and, in Section 2.2, we note the revisions required to effect a dual-voidage model of stick charges. It should be noted that, with the exception of the solid-phase momentum equation, the present results apply to stick charges whenever a single-voidage model is appropriate. Single-voidage modeling of stick charges is obviously appropriate when the sticks are unperforated. As we discuss further in Section 2.4, however, single-voidage modeling--with appropriate revisions to the form functions of the propellant--is adopted whenever the slots have opened completely for a given bundle of slotted propellant and also when a bundle of single-perforation propellant is completely ruptured.

In previous reports[1,2,3] we have tabulated separately the balance equations in cylindrical coordinates for two-dimensional two-phase flow, two-dimensional single-phase flow, quasi-one-dimensional two-phase flow, quasi-one-dimensional single-phase flow and lumped parameter single-phase flow. The single-phase equations are essentially limiting forms of the two-phase equations except that we express the quasi-one-dimensional results for two-phase flow by reference to the axial coordinate z and those for the single-phase flow by refer-

ence to arc length over an arbitrary path. Here we will only tabulate the two-phase results since these will suffice for the subsequent discussion of the revisions and extensions to the models. As in the previous report[3] we include the equations for the time dependence of the molecular weight and the specific heats.

2.1.1 Two-Dimensional Flow

In cylindrical coordinates such that z is the axial coordinate, r is the radial coordinate and t is the time, the balance equations take the following forms.

Balance of Mass of Gas-Phase

$$\frac{D\varepsilon\rho}{Dt} + \varepsilon\rho\left[\frac{\partial u}{\partial z} + \frac{\partial v}{\partial r}\right] = \dot{m} + \psi - \frac{\varepsilon\rho v}{r} \qquad 2.1.1.1$$

The notation conforms with that used previously.[2] We have ρ, the density of the gas, ε the porosity, u and v the z- and r-components of gas-phase velocity, D/Dt the convective derivative along the gas-phase streamline, ψ the source term associated with a stimulus, $\dot{m}$ the rate of production of gas due to combustion of the solid-phase.

We recall:

$$\frac{D}{Dt} \equiv \frac{\partial}{\partial t} + u \frac{\partial}{\partial z} + v \frac{\partial}{\partial r} \qquad 2.1.1.2$$

$$\dot{m} = (1 - \varepsilon) \frac{S_p}{V_p} \dot{d}\rho_p = s_p \dot{d}\rho_p \qquad 2.1.1.3$$

Here S_p, V_p are the surface area and volume of an individual grain and $\dot{d}$ is the rate of surface regression. We have introduced s_p as the surface area per unit volume.

Balance of Momentum of Gas-Phase

$$\varepsilon\rho\frac{D\vec{u}}{Dt} + \varepsilon g_o \nabla p = -\vec{f} + \dot{m}(\vec{u}_p - \vec{u}) - \psi\vec{u} \qquad 2.1.1.4$$

Here $\vec{u}$ is the velocity with components u and v, and $\vec{f}$ represents the velocity dependent interphase drag.

Balance of Energy of Gas-Phase

$$\epsilon\rho\frac{De}{Dt} + \epsilon p[\frac{\partial u}{\partial z} + \frac{\partial v}{\partial r}] + p\frac{D\epsilon}{Dt} = \frac{\vec{f}}{g_o} \cdot (\vec{u} - \vec{u}_p) - s_p q$$

$$+ \dot{m}(e_p - e + \frac{p}{\rho_p} + \frac{|\vec{u} - \vec{u}_p|^2}{2g_o})$$

$$+ \psi(e_{IG} - e + \frac{\vec{u} \cdot \vec{u}}{2g_o}) - \epsilon p\frac{v}{r}$$

2.1.1.5

Here $e = e(p,\rho)$ is the internal energy of the gas-phase and q is the interphase heat transfer per unit surface area of the solid-phase.

Balance of Mass of Solid-Phase

$$\frac{D\epsilon}{Dt_p} - (1 - \epsilon)[\frac{\partial u_p}{\partial z} + \frac{\partial v_p}{\partial r}] = \frac{\dot{m}}{\rho_p} + (1 - \epsilon)\frac{v_p}{r}$$

2.1.1.6

The subscript p denotes properties of the solid-phase and D/Dt_p is defined by analogy with 2.1.1.2.

Balance of Momentum of Solid-Phase

$$(1 - \epsilon)\rho_p\frac{D\vec{u}_p}{Dt_p} + (1 - \epsilon)g_o\nabla p + g_o\nabla\sigma = \vec{f}$$

2.1.1.7

Time-Dependence of Molecular Weight

$$\frac{DM_w}{Dt} = \frac{M_w}{\epsilon\rho}\left\{(1 - \frac{M_w}{M_{IG}})\psi + (1 - \frac{M_w}{M_{PROP}})\dot{m}\right\}$$

2.1.1.8

Here M_{IG} and M_{PROP} are respectively the molecular weights of the combustion products of the external stimulus and the solid propellant.

Time-Dependence of Specific Heats

With c used to signify a specific heat at either constant volume or constant pressure we have

$$\frac{Dc}{Dt} = \frac{1}{\varepsilon\rho} \left\{ (c_{IG} - c)\psi + (c_{PROP} - c)\dot{m} \right\}$$ 2.1.1.9

where c_{IG} and c_{PROP} are the corresponding specific heats of the combustion products of the external stimulus and the propellant, respectively.

2.1.2 Quasi-One-Dimensional Flow

The nontrivial spacewise coordinate is aligned with the axis of the tube so that u, u_p are the nontrivial components of gas- and solid-phase velocity respectively. The cross-sectional area of the annulus through which the flow occurs is taken to be $A(z,t)$ and therefore depends upon both position and time. It is supposed that the circumferential boundaries are permeable to the gas-phase and that mass transfers must be considered. We use R_i and R_o to denote respectively the radii of circumferential surfaces on which influx ($\dot{m}_i$) or efflux ($\dot{m}_o$) occur. Attention should be paid to this convention. The subscripts i and o do <u>not</u> refer to the interior and exterior surfaces, only to the direction of mass transfer. We understand $\dot{m}_i$ and $\dot{m}_o$ to represent rates of transfer per unit surface area. Moreover, we will also denote the properties transported with $\dot{m}_i$ by the subscript i. Thus u_i will be the axial velocity associated with the incoming gas. The exiting properties are, of course, those of the gas in the quasi-one-dimensional region presently under consideration.

Balance of Mass of Gas-Phase

$$\frac{\partial}{\partial t} \varepsilon A\rho + \frac{\partial}{\partial z} \varepsilon A\rho u = A\dot{m} + A\psi + 2\pi[\Sigma R_i \dot{m}_i - \Sigma R_o \dot{m}_o]$$ 2.1.2.1

The summations are over all entering and all exiting fluxes.

Balance of Momentum of Gas-Phase

$$\varepsilon\rho\frac{Du}{Dt} + \varepsilon g_o \frac{\partial p}{\partial z} = - f - \psi u + \dot{m}(u_p - u) + \frac{2\pi}{A} \Sigma R_i \dot{m}_i (u_i - u) \qquad 2.1.2.2$$

Balance of Energy of Gas-Phase

$$\varepsilon\rho\frac{De}{Dt} + \frac{p}{A}\frac{D\varepsilon A}{Dt} + \varepsilon p \frac{\partial u}{\partial z} = \frac{f}{g_o} (u - u_p) - s_p q \qquad 2.1.2.3$$

$$+ \psi[e_{IG} - e + \frac{u^2}{2g_o}]$$

$$+ \dot{m}[e_p - e + \frac{p}{\rho_p} + \frac{(u - u_p)^2}{2g_o}]$$

$$+ \frac{2\pi}{A} \Sigma\dot{m}_i R_i[e_i + \frac{p_i}{\rho_i} + \frac{(u - u_i)^2}{2g_o} - e]$$

$$- \frac{2\pi}{A} \frac{p}{\rho} \Sigma\dot{m}_o R_o$$

Balance of Mass of Solid-Phase

$$\frac{1}{A}\frac{D}{Dt_p} (1 - \varepsilon)A + (1 - \varepsilon) \frac{\partial u_p}{\partial z} = - \frac{\dot{m}}{\rho_p} \qquad 2.1.2.4$$

Balance of Momentum of Solid-Phase

$$\rho_p(1 - \varepsilon) \frac{Du_p}{Dt_p} + (1 - \varepsilon)g_o \frac{\partial p}{\partial z} + g_o \frac{\partial\sigma}{\partial z} = f \qquad 2.1.2.5$$

29

Time-Dependence of Molecular Weight

$$\frac{DM_w}{Dt} = \frac{M_w}{\varepsilon\rho} \left\{ (1 - \frac{M_w}{M_{IG}})\psi + (1 - \frac{M_w}{M_{PROP}})\dot{m} \right\} \qquad 2.1.2.6$$

$$+ \frac{2\pi M_w}{\varepsilon\rho A} \Sigma\dot{m}_i R_i (1 - \frac{M_w}{M_{w_i}})$$

Here M_{w_i} is the molecular weight of the gas transferred into the quasi-one-dimensional region. An efflux, of course, has no effect on M_w.

Time-Dependence of Specific Heats

$$\frac{Dc}{Dt} = \frac{1}{\varepsilon\rho} \left\{ (c_{IG} - c)\psi + (c_{PROP} - c)\dot{m} \right\} + \frac{2\pi}{\varepsilon\rho A} \Sigma\dot{m}_i R_i (c_i - c) \qquad 2.1.2.7$$

where c_i is a specific heat of the same type as c for the entering gas.

2.2 Dual-Voidage Balance Equations for Perforated Stick Charges

In Section 2.2.1 we introduce the decomposition of the voidage or porosity into exterior and interior components and we relate these components to the exterior and interior form functions. In Section 2.2.2 we discuss the revisions to the gas-phase balance equations of Section 2.1 which must be introduced in the dual-voidage model. These revisions are straightforward and require only minimal attention. In Section 2.2.3 we discuss the solid-phase balance equations. The solid-phase continuity equation presents no diffi-culty and we also note the differential equations which relate the exterior and interior components to the total voidage. The discussion of the solid-phase momentum equation, however, cannot be completed without introducing constitutive assumptions concerning the stress tensor. Accordingly, the result given in 2.2.3 is incomplete in certain respects and the final form of the solid-phase momentum equation is established in Section 2.3.1 following the discussion of the solid-phase stress tensor.

2.2.1 Interior and Exterior Voidage

If ε is the total voidage or porosity, as used in Section 2.1, we assume that it can be decomposed into an exterior (interstitial) component ε_e and an interior (perforation) component ε_i. We assume

30

for the time being that the sticks are not slotted or ruptured. The additional complications which attach to the presence of the slots are discussed in Section 2.4. In connection with granular propellant we have previously referred to S_p and V_p, the surface area and volume of an individual grain; see Equation 2.1.1.3.

We use a similar nomenclature in reference to stick propellant. However S_p and V_p are understood to be defined per unit length of the stick in accordance with our supposition that minimal longitudinal averaging is involved. With this in mind we define V_{p_e} as the volume per unit length defined by the exterior envelope of a stick, and V_{p_i} as the volume per unit length defined by the perforations. Evidently,

$$V_p = V_{p_e} - V_{p_i} \qquad\qquad 2.2.1.1$$

Let n_p be the number of sticks per unit volume. Then by definition

$$n_p V_p = 1 - \varepsilon$$
$$n_p V_{p_e} = 1 - \varepsilon_e$$
$$n_p V_{p_i} = \varepsilon_i$$

and thus

$$\frac{1 - \varepsilon}{V_p} = \frac{1 - \varepsilon_e}{V_{p_e}} = \frac{\varepsilon_i}{V_{p_i}} \qquad\qquad 2.2.1.2$$

For subsequent reference we also define the exterior and interior rates of mass generation due to combustion as

$$\dot{m}_{p_e} = \left(\frac{1 - \varepsilon_e}{V_{p_e}}\right) S_{p_e} \dot{d}_e \rho_p = s_{p_e} \dot{d}_e \rho_p \qquad\qquad 2.2.1.3$$

31

and

$$\dot{m}_{p_i} = \frac{\varepsilon_i}{V_{p_i}} S_{p_i} \dot{d}_i \rho_p = s_{p_i} \dot{d}_i \rho_p \qquad 2.2.1.4$$

respectively. We use the double subscript to avoid possible confusion with $\dot{m}_i$, in Section 2.1.2, which is a rate of mass transfer from one region to another. The quantities $\dot{d}_e$ and $\dot{d}_i$ in Equations 2.2.1.3 and 2.2.1.4 indicate the exterior and interior rates of regression which are assumed to differ as a consequence of the differing gas-phase pressures.

2.2.2 Gas-Phase Balance Equations

The fully-two-dimensional gas-phase balance equations follow from 2.1.1.1, 2.1.1.4 and 2.1.1.5 by simply interpreting all quantities as exterior or interior quantities, including a provision for mass transfer through the slot of slotted sticks, and by noting that $\psi = 0$ for the interior flow. We only state explicit results for the exterior flow.

Balance of Mass of Exterior Gas-Phase

$$\frac{D}{Dt}\varepsilon_e \rho_e + \varepsilon_e \rho_e \left[\frac{\partial u_e}{\partial z} + \frac{\partial v_e}{\partial r} \right] = \dot{m}_{p_e} + \psi - \frac{\varepsilon_e \rho_e v_e}{r} + \dot{m}_{s\ell_e} \qquad 2.2.2.1$$

we have used subscript e to denote exterior properties and $\dot{m}_{s\ell_e}$ is the mass added to the exterior as a consequence of transfer through the slot. We define $\dot{m}_{s\ell_i}$ analogously and note the convention that both $\dot{m}_{s\ell_e}$ and $\dot{m}_{s\ell_i}$ are positive when they correspond to additions to the exterior and interior, respectively. Further discussion of $\dot{m}_{s\ell_e}$ and $\dot{m}_{s\ell_i}$ is given in Section 2.4.2.

Balance of Momentum of Exterior Gas-Phase

$$\varepsilon_e \rho_e \frac{D\vec{u}_e}{Dt} + \varepsilon_e g_o \nabla p_e = -\vec{f}_e + \dot{m}_{p_e}(\vec{u}_p - \vec{u}_e) - \psi \vec{u}_e \qquad 2.2.2.2$$

$$+ \dot{m}_{s\ell_e}(\vec{u}_{s\ell_e} - \vec{u}_e)$$

We note that when $\dot{m}_{s\ell_e} < 0$, $\vec{u}_{s\ell_e} = \vec{u}_e$ so that the last term vanishes

32

in this case. In the corresponding equation for the interior flow it is to be understood that $\vec{f}_i$ is determined analytically to enforce the one-dimensional character of the flow through the perforations. Accordingly only the longitudinal component of ∇p_i has any net effect on the internal flow. As we will see subsequently, the internal pressure distribution is assumed to have negligible effect on the motion of the solid-phase. Moreover, we will take care to ensure that only the longitudinal component of $\vec{f}_i$ contributes to the motion of the solid-phase. This latter condition is not precisely correct since, if the sticks are bent, the part of $\vec{f}_i$ which corresponds to the transverse constraint of the gas flow also includes a centrifugal component which will affect the motion of the solid-phase.

Balance of Energy of Exterior Gas-Phase

$$\varepsilon_e \rho_e \frac{De_e}{Dt} + \varepsilon_e p_e [\frac{\partial u_e}{\partial z} + \frac{\partial v_e}{\partial r}] + p_e \frac{D\varepsilon_e}{Dt}$$

$$= \frac{\vec{f}_e}{g_o} \cdot (\vec{u}_e - \vec{u}_p) - s_{p_e} q_e + \dot{m}_{p_e} (e_p - e_e + \frac{p_e}{\rho_p} + \frac{|\vec{u}_e - \vec{u}_p|^2}{2g_o})$$

$$+ \psi(e_{IG} - e_e + \frac{\vec{u}_e \cdot \vec{u}_e}{2g_o}) - \varepsilon_e p_e \frac{v_e}{r}$$

$$+ \dot{m}_{s\ell_e} (e_{s\ell_e} - e_e + \frac{p_{s\ell_e}}{\rho_{s\ell_e}} - \frac{p_e}{\rho_e} + \frac{|\vec{u}_{s\ell_e} - \vec{u}_e|^2}{2g_o}) \qquad 2.2.2.3$$

It is perhaps worth noting that the divergence term $\frac{v_i}{r}$ which will appear in the interior counterparts to 2.2.2.1 and 2.2.2.3 is correctly included. If the stick bundle were directed radially it might seem that the v_i/r term would be spurious in view of the patently one-dimensional nature of the flow. It is not difficult to see, however, that it is cancelled by the terms involving the radial gradient of ε_i which must occur in such a case.

We do not state the equations which govern the time-dependence of the molecular weight and the specific heats. Their extensions from 2.1.1.8 and 2.1.1.9 to include the presence of slotted propellant will be obvious.

The quasi-one-dimensional forms of the gas-phase balance equations follow directly from 2.1.2.1, 2.1.2.2 and 2.1.2.3 with the introduction of the appropriate subscripts. We do not state them explicitly. It

33

should be noted, as discussed further in Section 2.4, that the terms
corresponding to mass transfer through the slot of a slotted stick
charge are not considered in the quasi-one-dimensional forms of the
equations. The quasi-one-dimensional forms are used for the center-
core charge, which is assumed never to consist of perforated sticks,
and for the main charge following the transition to a quasi-two-
dimensional representation. In the latter case, it is assumed that
the transition is delayed until all slotted increments have fully
opened slots whereupon a single-voidage representation is instituted.
Similar considerations apply in respect to the rupture of single-
perforation sticks.

2.2.3 Solid-Phase Balance Equations

The fully-two-dimensional form of the balance of mass of the
solid-phase follows directly from 2.1.1.6 as

$$\frac{D\varepsilon}{Dt_p} - (1 - \varepsilon)[\frac{\partial u_p}{\partial z} + \frac{\partial v_p}{\partial r}] = \frac{\dot{m}_{p_e} + \dot{m}_{p_i}}{\rho_p} + (1 - \varepsilon)\frac{v_p}{r} \qquad 2.2.3.1$$

The quasi-one-dimensional form follows similarly from 2.1.2.4. From
the relations 2.1.1.2 it is not difficult to show that

$$\frac{1}{1 - \varepsilon} \{\frac{D}{Dt_p}(1 - \varepsilon) + \frac{\dot{m}_{p_e} + \dot{m}_{p_i}}{\rho_p}\} = \frac{1}{1 - \varepsilon_e} \{\frac{D}{Dt_p}(1 - \varepsilon_e) + \frac{\dot{m}_{p_e}}{\rho_p}\}$$

$$= \frac{1}{\varepsilon_i} \{\frac{D\varepsilon_i}{Dt_p} - \frac{\dot{m}_{p_i}}{\rho_p}\} \qquad 2.2.3.2$$

These results provide the values of $\frac{D\varepsilon_e}{Dt_p}$ and $\frac{D\varepsilon_i}{Dt_p}$ as required in the dual-
voidage gas-phase equations. The quasi-one-dimensional form of the
solid-phase continuity equation follows from 2.1.2.4 with a simple
revision to the right-hand side to reflect $\dot{m}_{p_e} + \dot{m}_{p_i}$ rather than $\dot{m}$.

The single-voidage solid-phase momentum Equation 2.1.1.7 already
incorporates a constitutive assumption concerning the solid-phase
stress tensor. Equation 2.1.1.7 follows from the more general result[32]
which we express in a coordinate free form as

---

[32]Gough, P. S., "On the Closure and Character of the Balance
Equations for Heterogeneous Two-Phase Flow"
Dynamics and Modelling of Reactive Flow Systems, Academic Press, 1980

$$(1 - \epsilon)\rho_p \frac{D\vec{u}_p}{Dt_p} + (1 - \epsilon)g_o \nabla p - g_o \nabla \cdot (1 - \epsilon)(p\overleftrightarrow{I} - \overleftrightarrow{\sigma}_p) = \vec{f} \qquad 2.2.3.3$$

where $\overleftrightarrow{I}$ is the unit tensor of order 2 and $\overleftrightarrow{\sigma}_p$ is the intrinsic average stress in the solid-phase with the convention that a compressive component of $\overleftrightarrow{\sigma}_p$ is positive. Equation 2.1.1.7 follows when we adopt the constitutive assumption

$$\overleftrightarrow{\sigma}_p = (p + R)\overleftrightarrow{I} \qquad 2.2.3.4$$

where R is an intrinsic average property which is assumed to embed the stresses communicated from grain to grain. Evidently, the scalar quantity σ in 2.1.1.7 is related to R according to

$$\sigma = (1 - \epsilon)R \qquad 2.2.3.5$$

We have previously assumed that σ has an irreversible dependence on porosity.[1,2,3]

To proceed from 2.2.3.3 to a result suitable for modeling perforated stick charges, three topics must be addressed. First, we note that 2.2.3.3 is based on the assumption that the gas-phase pressure is a single-valued macroscopic variable. In the present context the pressure is dual-valued. Second, the interphase drag $\vec{f}$ must be decomposed into exterior and interior components with due regard to that part of $\vec{f}_i$ which compensates analytically for the presence of the full pressure gradient in the gas-phase momentum equation. Third, the isotropic behavior implied by 2.2.3.4 must be replaced by a nonisotropic law. The first two topics are dealt with here and the third is the subject of the next section.

With regard to the value of the gas-phase pressure which appears in Equation 2.2.3.3 we assume that it can be represented with sufficient accuracy as the exterior or interstitial value. As far as the transverse motion of the solid-phase is concerned, it is clear that only the external pressure field can exert any influence. The relative influence of the external and internal pressures on the longitudinal motion of the solid-phase was discussed previously in connection with the one-dimensional NOVA code.[24] It was shown from a consideration of the average longitudinal stress in a thick-walled cylinder that the external pressure would always be expected to exert a dominant influence.

As far as the interphase drag is concerned it is easy to see that we must have

$$\vec{f} = \vec{f}_e + (\vec{f}_i \cdot \vec{x}_1)\vec{x}_1 \qquad\qquad 2.2.3.6$$

where $\vec{f}_e$ and $\vec{f}_i$ are the external and internal drag forces on the gas-phase and $\vec{x}_1$ is a unit vector directed locally along the axis of the stick.

2.3 Constitutive Laws for Perforated Stick Charges

In the previous section we introduced $\vec{x}_1$ as a unit vector directed along the axis of the stick. For the present discussion we will also refer to $\vec{x}_2$ and $\vec{x}_3$ which, with $\vec{x}_1$, form an orthonormal triad. We will consistently refer to the direction defined by $\vec{x}_1$ as the longitudinal direction and to the directions defined by $\vec{x}_2$ or $\vec{x}_3$ as transverse. Subscripts L and T will also be introduced to indicate certain longitudinal and tranverse properties, respectively. We refer to the triad $\vec{x}_1$, $\vec{x}_2$, $\vec{x}_3$ as the intrinsic coordinate frame of the stick bundle.

The idea that there exists locally a unique longitudinal direction, $\vec{x}_1$, embeds an important assumption. The stick charge is initially assembled into bundles in each of which all the sticks are aligned. Initially, therefore, there is no difficulty in defining a unique longitudinal direction at each macroscopic location. As combustion is induced and motion of the sticks begins, it is necessary to assume that the sticks do not become entangled with one another. This assumption is probably on safe ground when long sticks are used with high loading densities, at least until a significant fraction of the propellant has been consumed. An experimental investigation of the distribution and orientation of the sticks throughout a typical interior ballistic cycle would be of great interest. Not only does the distribution of the propellant influence the pressure gradient; it also influences the rate of heat transfer to the tube.[22]

The constitutive laws addressed in this section include the rheology of the stick bundle, Section 2.3.1; the interphase drag, Section 2.3.2; and the interphase heat transfer, Section 2.3.3. We do not discuss the ignition and combustion of the stick charge. These phenomena are treated as in the previous models of granular charges and were summarized in Section 1.1. Of course, ignition and combustion are modeled separately for the exterior and interior surfaces. The effects of erosion and finite rate gas-phase chemical kinetics as described in Chapter 4.0 are fully linked to the dual-voidage model.

The form functions for the stick charge are straightforward and require no further attention here.

2.3.1 Solid-Phase Stress Tensor

We return now to the discussion of the tensor $\overset{\leftrightarrow}{\sigma}_p$ as used in the solid-phase momentum Equation 2.2.3.3. We recall that for granular propellant the dependence of the scalar intergranular pressure σ, Equation 2.2.3.5, on porosity is as follows

$$\frac{D\sigma}{Dt_p} = -\rho_p \frac{a^2}{g_o} \frac{D\varepsilon}{Dt_p} \qquad\qquad 2.3.1.1$$

where the rate of propagation of intergranular disturbances, a, satisfies

$$a(\varepsilon) = \begin{cases} a_1 \varepsilon_o/\varepsilon & \text{if } \dot{\varepsilon} \leqq 0, \ \sigma_p = \sigma_{nom}, \ \varepsilon \leqq \varepsilon_o \\[2em] a_2 & \text{if } 0 \leqq \sigma_p < \sigma_{nom}, \ \varepsilon \leqq \varepsilon_o \\ & \text{or if } \dot{\varepsilon} > 0, \ \sigma_p = \sigma_{nom}, \ \varepsilon \leqq \varepsilon_o \\[2em] 0 & \text{if } \sigma_p = 0 \text{ and } \dot{\varepsilon} > 0 \text{ or if } \varepsilon > \varepsilon_o \end{cases} \qquad 2.3.1.2$$

where we understand $\dot{\varepsilon}$ to mean $D\varepsilon/Dt_p$ and the nominal loading curve, defined by monotonic compaction of the bed from the settling porosity ε_o to a smaller value ε is given by

$$\sigma_{nom}(\varepsilon) = \rho_p \frac{a_1^2}{g_o} \varepsilon_o^2 \left(\frac{1}{\varepsilon} - \frac{1}{\varepsilon_o}\right) \qquad\qquad 2.3.1.3$$

The values a_1 and a_2 respectively correspond to loading of the bed and unloading/reloading.

We next discuss the constitutive law for stick charges in the intrinsic coordinate frame. Then we consider the transformation to cylindrical coordinates. We conclude by stating the momentum equations for the solid-phase.

Constitutive Law in Intrinsic Coordinate Frame

We assume that the mechanical behavior of the stick bundle is anisotropic. Transverse loads are assumed to obey a functional dependence on porosity similar to that for granular charges. Longitudinal loads are assumed to obey a linear elastic law with respect to the longitudinal strain field. We make the following assumptions.

(1) We assume that in the $\vec{x}_1$, $\vec{x}_2$, $\vec{x}_3$ coordinate frame, the intrinsic coordinate frame, the stress tensor $\vec{\sigma}_p$ is diagonal. This is tantamount to the assumption that the sticks offer no significant resistance to bending. The component τ_{23} vanishes as a consequence of the assumption of axisymmetry.

(2) If the diagonal components are σ_{p_1}, σ_{p_2}, and σ_{p_3} we assume that $\sigma_{p_2} = \sigma_{p_3}$. This is tantamount to the assumption that the bundle offers negligible resistance to deformation in the 2-3 plane and is equivalent to the current assumption of isotropy of $\vec{\sigma}_p$ in respect to granular propellant.

(3) The transverse components obey a law similar to that for granular propellant as given in Equation 2.2.3.4. Specifically

$$\sigma_{p_2} = \sigma_{p_3} = p_e + R_T \qquad\qquad 2.3.1.4$$

where we note the use of the external pressure p_e in accordance with the discussion of Section 2.2.3. Then introducing σ_T by analogy with σ_p in 2.2.3.5 we have

$$\sigma_T = (1 - \varepsilon)R_T \qquad\qquad 2.3.1.5$$

and we assume

$$\frac{D\sigma_T}{Dt_p} = -\rho_p \frac{a_T^2}{g_o} \frac{D\varepsilon}{Dt_p} \qquad\qquad 2.3.1.6$$

where a_T is governed by an equation of the form 2.3.1.2 based on values a_{T_1} and a_{T_2}.

(4) The longitudinal stress is assumed to obey a linear elastic law with modulus E and Poisson ratio ν such that

38

$$\sigma_{p_1} = - Ee_1 + 2\nu(p_e + R_T) \qquad\qquad 2.3.1.7$$

where e_1 is the longitudinal component of strain, positive in tension. Then, introducing R_L such that

$$R_L = - Ee_1 \qquad\qquad 2.3.1.8$$

and

$$\sigma_L = (1 - \varepsilon)R_L \qquad\qquad 2.3.1.9$$

it follows for small strains[31] that

$$\frac{DR_L}{Dt_p} = - E \frac{\partial u_{p_1}}{\partial x_1} \qquad\qquad 2.3.1.10$$

where u_{p_1} is the longitudinal velocity component of the solid-phase. Then, introducing $a_L = (g_o E/\rho_p)^{\frac{1}{2}}$, we have
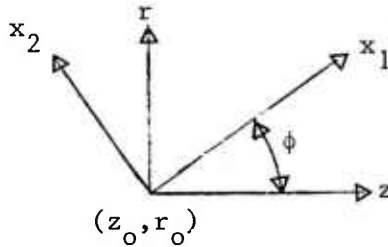
$$\frac{D\sigma_L}{Dt_p} = - \frac{\sigma_L}{1 - \varepsilon} \frac{D\varepsilon}{Dt_p} - (1 - \varepsilon)\rho_p \frac{a_L^2}{g_o} \frac{\partial u_{p_1}}{\partial x_1} \qquad\qquad 2.3.1.11$$

The representation of the longitudinal stress in Equation 2.3.1.7 differs from that used in the original NOVA code analysis[31] by virtue of the use of a value of Poisson's ratio and the recognition of the contribution of the transverse intergranular stress. The latter term also represents a constitutive extension with respect to the more recent dual-voidage analysis of NOVA.[24]

The foregoing constitutive assumptions are thought to represent the simplest anisotropic law which will lead to a well-posed boundary value problem in two dimensions. If the transverse stress σ_T were neglected, for example, there would be no mechanism to prevent the porosity from becoming arbitrarily small due to radial compaction of the stick bundle as a consequence of igniter blast. On the other hand, to assume $\sigma_T = \sigma_L$ would result in a radial propagation of stresses even when the sticks were no longer in contact with one another.

Transformation to Cylindrical Coordinates

Since we are only concerned with the axisymmetric case we consider only the transformation from (x_1, x_2) to (z,r). Let the intrinsic coordinates be defined by a local counterclockwise rotation ϕ as shown in the sketch. Evidently

$$z - z_o = x_1 \cos\phi - x_2 \sin\phi \qquad 2.3.1.12$$

$$r - r_o = x_1 \sin\phi + x_2 \cos\phi \qquad 2.3.1.13$$

It is not difficult to see that the time variation of ϕ satisfies

$$\frac{D\phi}{Dt_p} = \frac{\partial u_{p_2}}{\partial x_1} \qquad 2.3.1.14$$

The cylindrical velocity components (u_p, v_p) are related to the intrinsic components (u_{p_1}, u_{p_2}) according to

$$u_{p_1} = u_p \cos\phi + v_p \sin\phi \qquad 2.3.1.15$$

$$u_{p_2} = - u_p \sin\phi + v_p \cos\phi \qquad 2.3.1.16$$

Equation 2.3.1.14 may therefore be expressed in cylindrical coordinates as follows

$$\frac{D\phi}{Dt_p} = \cos\phi \frac{\partial}{\partial z}\{-u_p \sin\phi + v_p \cos\phi\} + \sin\phi \frac{\partial}{\partial r}\{-u_p \sin\phi + v_p \cos\phi\} \qquad 2.3.1.17$$

The quantity ϕ becomes an additional state variable to be integrated simultaneously with the balance equations. The two-step MacCormack scheme is used to perform the integration although upwind differencing is used for the convective terms and values of ϕ at the boundaries are simply continued from the interior in the present code version. For the time being we have neglected the terms which involve $\sin\phi$ in 2.3.1.17.

In cylindrical coordinates the components of the stress tensor $\overleftrightarrow{\sigma}_p$ become:

$$\sigma_{p_{zz}} = \cos^2\phi\sigma_{p_1} + \sin^2\phi\sigma_{p_2} \qquad\qquad 2.3.1.18$$

$$\sigma_{p_{rr}} = \sin^2\phi\sigma_{p_1} + \cos^2\phi\sigma_{p_2} \qquad\qquad 2.3.1.19$$

$$\sigma_{p_{zr}} = \sigma_{p_{rz}} = \cos\phi\sin\phi(\sigma_{p_1} - \sigma_{p_2}) \qquad\qquad 2.3.1.20$$

It will be evident that the effect of the orientation of the sticks on the components of $\overleftrightarrow{\sigma}_p$ in cylindrical coordinates will not be pronounced. To an order of approximation consistent with the state of knowledge of the constitutive coefficients it seems reasonable to neglect the effect of ϕ on the stress tensor components. For the sake of future work we deduce the equations of motion without neglecting the effect of ϕ. However, we treat the ϕ-dependence as being perturbative in nature. To simplify the determination of the pseudo-characteristic forms, in Section 2.5, we write the momentum equations so as to retain explicitly only the dominant differential terms and we formally treat the ϕ-dependent correction terms, as well as the gas-phase pressure terms, as though they were inhomogeneous or algebraic in nature.

The terms which express the ϕ-dependence of the stress tensor have not been coded into TDNOVA. Their effect is not expected to be large and they can easily be added, if subsequent calculations so require, following the demonstration of satisfactory numerical results with the existing code. We do note, however, that the effect of the orientation of the sticks on the axial component of the interphase drag is not expected to be negligible and, as discussed in Section 2.3.2, the ϕ-dependence of $\vec{f}$ is encoded into TDNOVA.

To emphasize the perturbative character of ϕ on $\overleftrightarrow{\sigma}_p$ we recast 2.3.1.18-2.3.1.20 as follows.

$$\sigma_{p_{zz}} = \sigma_{p_1} + (\cos^2\phi - 1)\sigma_{p_1} + \sin^2\phi\sigma_{p_2} = \sigma_{p_1} + \sigma_{p_1}^* \qquad\qquad 2.3.1.21$$

$$\sigma_{p_{rr}} = \sigma_{p_2} + \sin^2\phi\sigma_{p_1} + (\cos^2\phi - 1)\sigma_{p_2} = \sigma_{p_2} + \sigma_{p_2}^* \qquad\qquad 2.3.1.22$$

$$\sigma_{P_{zr}} = 0 + \cos\phi\sin\phi(\sigma_{P_1} - \sigma_{P_2}) = 0 + \sigma_{P_3}^* \qquad 2.3.1.23$$

Thus $\sigma_{P_1}^*$, $\sigma_{P_2}^*$, $\sigma_{P_3}^*$ embed the ϕ-dependence. To express the divergence of the stress tensor in cylindrical coordinates we will also need to evaluate $\sigma_{P_{rr}} - \sigma_{P_{\theta\theta}}$. Since $\sigma_{P_{\theta\theta}} = \sigma_{P_3} = \sigma_{P_2}$ we evidently have

$$\sigma_{P_{rr}} - \sigma_{P_{\theta\theta}} = \sigma_{P_2}^* \qquad 2.3.1.24$$

Equations of Motion in Cylindrical Coordinates

In cylindrical coordinates, but retaining the convective time derivative, Equation 2.2.3.3 may be broken into the following components. We have the axial momentum equation:

$$(1 - \varepsilon)\rho_p \frac{Du_p}{Dt_p} + (1 - \varepsilon)g_o \frac{\partial p_e}{\partial z} - g_o \frac{\partial}{\partial z}[(1 - \varepsilon)(p_e - \sigma_{P_{zz}})]$$

$$+ \frac{g_o}{r} \frac{\partial}{\partial r}[(1 - \varepsilon)r\sigma_{P_{zr}}] = f_z \qquad 2.3.1.25$$

and the radial momentum equation:

$$(1 - \varepsilon)\rho_p \frac{Dv_p}{Dt_p} + (1 - \varepsilon)g_o \frac{\partial p_e}{\partial r} - g_o \frac{\partial}{\partial r}[(1 - \varepsilon)(p_e - \sigma_{P_{rr}})] \qquad 2.3.1.26$$

$$+ g_o \frac{\partial}{\partial z} (1 - \varepsilon)\sigma_{P_{zr}} + g_o \frac{(1 - \varepsilon)}{r}(\sigma_{P_{rr}} - \sigma_{P_{\theta\theta}}) = f_r$$

Then, using Equations 2.3.1.4, 2.3.1.5, 2.3.1.7-2.3.1.9 and 2.3.1.21-2.3.1.24, we express the momentum equations as follows.

Axial Momentum Equation

$$(1 - \varepsilon)\rho_p \frac{Du_p}{Dt_p} + g_o \frac{\partial}{\partial z}[\sigma_L + 2\nu\sigma_T] = \xi_6 \qquad 2.3.1.27$$

where the pseudo-non-homogeneous term ξ_6 is given by

$$\xi_6 = f_z - g_o(1 - \varepsilon) \frac{\partial p_e}{\partial z} + g_o(1 - 2\nu) \frac{\partial}{\partial z} [(1 - \varepsilon)p_e]$$

$$- g_o \frac{\partial}{\partial z} [(1 - \varepsilon)\sigma_{p_1}{}^*] - \frac{g_o}{r} \frac{\partial}{\partial r} [(1 - \varepsilon)r\sigma_{p_3}{}^*] \qquad 2.3.1.28$$

The subscript for ξ is chosen to conform with the conventions of earlier work.[1,2,3]

Radial Momentum Equation

$$(1 - \varepsilon)\rho_p \frac{Dv_p}{Dt_p} + g_o \frac{\partial \sigma_T}{\partial r} = \xi_7 \qquad 2.3.1.29$$

where

$$\xi_7 = f_r - g_o(1 - \varepsilon) \frac{\partial p_e}{\partial r} - \frac{g_o}{r} \frac{\partial}{\partial r} [(1 - \varepsilon)r\sigma_{p_2}{}^*] \qquad 2.3.1.30$$

$$- g_o \frac{\partial}{\partial z} [(1 - \varepsilon)\sigma_{p_3}{}^*]$$

To conclude, we require the quasi-one-dimensional form of the solid-phase momentum equation. From Reference 24, extended to reflect the influence of σ_T, we see that the required result is just Equation 2.3.1.27 but with ξ_6 given by

$$\xi_6 = f_z - \frac{g_o}{A} (\sigma_L + 2\nu\sigma_T) \frac{\partial A}{\partial z} - g_o(1 - \varepsilon) \frac{\partial p_e}{\partial z} \qquad 2.3.1.31$$

$$+ \frac{g_o}{A} (1 - 2\nu) \frac{\partial}{\partial z} [A(1 - \varepsilon)p_e] + \frac{g_o\sigma_T}{(1 - \varepsilon)A} \frac{\partial}{\partial z} [(1 - \varepsilon)A]$$

where A is the cross-sectional area of the region occupied by the mixture.

43

2.3.2 Interphase Drag

We begin by noting the form of the correlation used in previous one-dimensional models of stick charges.[9,24,31]   As far as the interior flow is concerned--and even for the exterior flow, once a quasi-two-dimensional formulation is adopted--these previous results are still applicable. With regard to the exterior flow in a fully-two-dimensional analysis, it is necessary to recognize the anisotropy of the flow resistance through the bundle. We establish an anisotropic law of flow resistance by combining available data for transverse flow through tube bundles with the data used previously to describe the longitudinal flow.

The natural coordinate frame for the formulation of the law of flow resistance is the intrinsic frame used in the previous section. As in the previous section we shall first establish results in the intrinsic frame and then transform these results into cylindrical coordinates.

Previous Results

The previous results pertained solely to the longitudinal flow component and we express them by reference to u_1 and u_{p_1} which are understood to be the gas-phase and solid-phase velocity components in the x_1-direction. The interphase drag was expressed by reference to a correlation for the turbulent shear stress at the wall of a duct[28]

$$\tau = 0.023 \frac{\mu}{D_p} (u_1 - u_{p_1}) \, Re_p^{0.8} \qquad\qquad 2.3.2.1$$

in which a coefficient $Pr^{0.07}$ has been treated as unity and[24]

$$D_p = \begin{cases} 6V_{p_e}/S_{p_e} & \text{for the exterior flow.} \\ \\ 4V_{p_i}/S_{p_i} & \text{for the interior flow.} \end{cases} \qquad\qquad 2.3.2.2$$

$$Re_p = \rho |u_1 - u_{p_1}| \frac{D_p}{\mu}$$

We therefore have the longitudinal component of the exterior inter-phase drag as $f_{s_{e_1}}$ where[24]

$$f_{s_{e_1}} = 0.138\mu \frac{u_1 - u_{p_1}}{D_{p_e}^2} (1 - \varepsilon_e)Re_p^{0.8} \qquad \qquad 2.3.2.3$$

in which exterior gas-phase properties are used to determine μ and Re_p. The interior component is[24]

$$f_{s_{i_1}} = 0.092\mu \frac{u_1 - u_{p_1}}{D_{p_i}^2} \varepsilon_i Re_p^{0.8} \qquad \qquad 2.3.2.4$$

We have assumed, in previous work.[9,24,31] that due to the mitigation of the shear stress by the blowing effect associated with the combustion of the propellant surface, both $f_{s_{e_1}}$ and $f_{s_{i_1}}$ will vanish at a point where ignition has occurred.

As noted in the preamble to this section, Equations 2.3.2.3 and 2.3.2.4 describe completely the interphase drag in the present code version following the transition to a quasi-two-dimensional representation. Moreover, as far as the interior flow is concerned, 2.3.2.4 describes the total influence of the drag on the motion of the solid-phase, even when the fully-two-dimensional representation is in effect. The transverse flow resistance for the interior flow is taken to be infinite in order to embed the one-dimensional motion into the two-dimensional equations. The transverse flow resistance for the interior is therefore determined analytically as part of the method of solution which we comment on at the conclusion of this section. The following discussion of transverse flow resistance is accordingly to be understood as referring solely to the exterior flow.

Transverse Flow Resistance

The transverse flow resistance through bundles of tubes depends on the arrangement of the tubes. In conventional heat exchangers, for which flow resistance data have been acquired, the arrangement is controlled by the designer and is fixed once and for all. In our application, the configuration is neither known nor controlled. We therefore make the simplest possible assumption, namely that the packing is locally isotropic in the transverse plane. We introduce S_n, the center-to-center spacing as shown in the sketch. Using D

to signify the external diameter of a stick, it follows that S_n is related to the exterior voidage ε_e according to
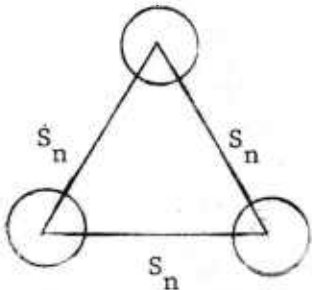
$$1 - \varepsilon_e = \frac{\pi}{2\sqrt{3}} \frac{D^2}{S_n^2} \qquad\qquad 2.3.2.5$$

We therefore have the result

$$\frac{S_n}{D} = \sqrt{\frac{\pi}{2\sqrt{3}} \frac{1}{1 - \varepsilon_e}} \qquad\qquad 2.3.2.6$$

which we will require in order to translate the existing data for tube bundles into the nomenclature of our model.

Holman[28] reports the pressure drop through a staggered array in the form

$$\Delta p = \frac{f' G_{max}^2 N}{2.09 \times 10^8 \rho} \qquad\qquad 2.3.2.7$$

where G_{max} = mass velocity at minimum flow area in $lbm/hr\text{-}ft^2$

ρ = density in lbm/ft^3

N = number of rows

and the dimensionless friction factor f' is given by

$$f' = \left\{ 0.25 + \frac{0.118}{\left[\frac{S_n - D}{D} \right]^{1.08}} \right\} Re_{max}^{-0.16} \qquad\qquad 2.3.2.8$$

where $Re_{max} = G_{max} D / \mu$

We interpret Equation 2.3.2.7 as

$$\frac{\Delta p}{\Delta x} = \frac{f' G_{max}^2}{2.09 \times 10^8 \rho S_n} \qquad\qquad 2.3.2.9$$

since the pressure drop Δp occurs over a length NS_n. Moreover,

changing the units to those of the present report and identifying $\Delta p / \Delta x$ with $-\partial p / \partial x$ we have

$$-g_o \frac{\partial p}{\partial x} = \frac{1}{2} \frac{f' G_{max}^2}{\rho S_n} \qquad\qquad 2.3.2.10$$

We express the maximum flow rate in our nomenclature as

$$G_{max} = \varepsilon_e \rho (u_2 - u_{p_2}) \frac{S_n/D}{S_n/D - 1} \qquad\qquad 2.3.2.11$$

whereupon, with $Re_D = \rho|u_2 - u_{p_2}|D/\mu$, we have

$$Re_{max} = \varepsilon Re_D \frac{D}{D_p} \frac{S_n/D}{S_n/D - 1} \qquad\qquad 2.3.2.12$$

Finally, for steady incompressible flow the gas-phase momentum equation reduces to

$$f_{s_{e_2}} = -\varepsilon_e g_o \frac{\partial p}{\partial x} \qquad\qquad 2.3.2.13$$

Thus substituting 2.3.2.10 and 2.3.2.11 into 2.3.2.13 we deduce the following correlation for the transverse flow resistance.

$$f_{s_{e_2}} = \frac{f'}{2} \frac{\rho \varepsilon_e^3}{D} \frac{S_n/D}{(S_n/D - 1)^2} |u_2 - u_{p_2}|(u_2 - u_{p_2}) \qquad\qquad 2.3.2.14$$

Since S_n/D is given by 2.3.2.6, f' by 2.3.2.8 and Re_{max} by 2.3.2.12, Equation 2.3.2.14 is expressed entirely in terms of the two-phase flow nomenclature.

Combined or Oblique Flow

When the exterior flow is purely longitudinal, Equation 2.3.2.3 describes the flow resistance. When the flow is purely transverse, Equation 2.3.2.14 applies. In the general case we assume that the two components of the flow resistance satisfy

$$f_{s_{e_1}} = 0.138\mu \; \frac{u_1 - u_{P_1}}{D_{P_e}^2}(1 - \epsilon_e)Re_p^{0.8} \qquad\qquad 2.3.2.15$$

where

$$Re_p = \frac{\rho|\vec{u} - \vec{u}_p|}{\mu} D_p \qquad\qquad 2.3.2.16$$

so that in contrast to 2.3.2.3, Re_p is based on the total magnitude of the relative velocity, and

$$f_{s_{e_2}} = \frac{f'}{2} \; \frac{\rho\epsilon_e^3}{D} \; \frac{S_n/D}{(S_n/D - 1)^2} \; |\vec{u} - \vec{u}_p|(u_2 - u_{P_2}) \qquad\qquad 2.3.2.17$$

which involves the total magnitude of the relative velocity as a prefactor and for which f' is based on Re_p as given in 2.3.2.16.

We note that $\vec{f}$ is not parallel to $\vec{u} - \vec{u}_p$ due to the anisotropy of the flow resistance. This reflects the tendency of the bundle to turn the incident flow towards the longitudinal direction.

The formulation given here is hypothetical and is constructed, in part, with a view to computational tractability. It is of interest therefore to have some experimental confirmation. Kutateladze[33] has presented a correction factor which relates the transverse pressure drop to that which is obtained at an angle of obliquity θ where $\theta = 90°$ corresponds to purely transverse flow. If S_n is the spacing between tube centers, it follows that there are
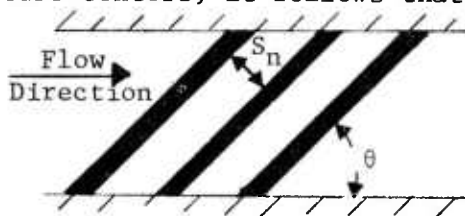
$$N = \frac{\sin\theta}{S_n} \text{ tubes per unit length}$$

in the axial direction. We assume that the transverse component of resistance is dominant so that the axial flow resistance is $f_z = f_{s_{e_2}} \sin\theta$ and $f_{s_{e_2}}$ is based on $u_2 - u_{P_2} = |\vec{u} - \vec{u}_p|\sin\theta$. From Equation 2.3.2.17 it follows that the axial flow resistance satisfies

$$f_z(\theta) = f_z(90°)\sin^2\theta \qquad\qquad 2.3.2.18$$

---

[33]Kutateladze, S. S., and Borishanskii, V. M., "A Concise Encyclopedia of Heat Transfer," Pergamon Press   1966

However, the correction factor given by Kutateladze is applied to the formula for the pressure drop per row of pipes. Evidently f_z, which expresses pressure drop per unit length, must be divided by N to yield the pressure drop per row of pipes so that we find

$$\Delta p(\theta) = \Delta p(90°)\sin\theta \qquad\qquad\qquad 2.3.2.$$

Thus we have concluded that the correction factor should vary with $\sin\theta$. We compare this expectation with Kutateladze's observation in the following table. A comparison with $\sin^2\theta$ is also included.

θ (Degrees)	Experimental Correction Factor[33]	$\sin\theta$	$\sin^2\theta$
90	1	1	1
80	1	0.99	0.97
70	0.95	0.94	0.88
60	0.83	0.87	0.75
50	0.69	0.77	0.59
40	0.53	0.64	0.41
30	0.38	0.50	0.25
20	0.24	0.34	0.12
10	0.15	0.174	0.03

The agreement is fair and, overall, is better than the $\sin^2\theta$ dependence which would follow if we based 2.3.2.17 entirely on $u_2 - u_{p_2}$. It seems likely that errors in our proposed law for oblique flow resistance will be affected more strongly by the uncertainties in the estimate of the transverse component alone. For example, entrance effects in a bank of tubes are pronounced.[33] The friction factor for the first few rows may be of the order of 60% of the value obtained after ten or more rows have been traversed. Additional uncertainties derive from our state of knowledge of the transverse arrangement of the sticks, an influential factor. Finally, in the initial condition the sticks may be in contact with one another, a situation not encountered in the data base for heat exchangers.

Transformation to Cylindrical Coordinates

If ϕ describes the orientation of the stick bundle in the sense of Section 2.3.1, and with the convention

$$\hat{f}_{s_{e_1}} = 0.138\mu \frac{(1 - \epsilon_e)}{D_{p_e}^2} Re_p^{0.8} \qquad 2.3.2.20$$

$$\hat{f}_{s_{e_2}} = \frac{f'}{2} \frac{\rho\epsilon_e^3}{D} \frac{S_n/D}{(S_n/D - 1)^2} |\vec{u} - \vec{u}_p| \qquad 2.3.2.21$$

we have the cylindrical components of the exterior flow resistance as

$$f_{e_z} = \hat{f}_{s_{e_1}} [(u - u_p)\cos\phi + (v - v_p)\sin\phi]\cos\phi \qquad 2.3.2.22$$

$$- \hat{f}_{s_{e_2}} [-(u - u_p)\sin\phi + (v - v_p)\cos\phi]\sin\phi$$

$$f_{e_r} = \hat{f}_{s_{e_1}} [(u - u_p)\cos\phi + (v - v_p)\sin\phi]\sin\phi \qquad 2.3.2.23$$

$$+ \hat{f}_{s_{e_2}} [-(u - u_p)\sin\phi + (v - v_p)\cos\phi]\cos\phi$$

Whereas the components of the stress tensor $\overleftrightarrow{\sigma}_p$ are thought to be in-sensitive to small departures of ϕ from zero, as discussed in **Section** 2.3.1, the same is not true of the interphase drag. Since $\hat{f}_{s_{e_2}}$ is

expected to exceed $\hat{f}_{s_{e_1}}$ by two or more orders of magnitude, a small

value of ϕ can alter significantly the axial component of the drag and, accordingly, the time-dependent distribution of the stick charge.

Computational Considerations

We have previously treated the interphase drag for granular charges according to a semi-implicit scheme[2,3] in which the gas-phase velocity was evaluated at the future time level. In the present case it is mandatory that the transverse component be treated implicitly. Moreover, because $\hat{f}_{s_{e_2}}$ may actually become infinite, both the gas-

phase and the solid-phase velocity components require implicit treatment in the computation of the interphase drag.

Using u^{n+1} to denote the $(n + 1)$-level solution of u and $\tilde{u}$ to denote the corresponding value with $\hat{f}_{s_{e_2}} = 0$ we write

$$u^{n+1} = \tilde{u} + \frac{\hat{f}_{s_{e_2}}}{\varepsilon_e \rho} \overline{\Delta t} \{-(u^{n+1} - u_p^{n+1})\sin^2\phi + (v^{n+1} - v_p^{n+1})\cos\phi\sin\phi\}$$

and similarly for v^{n+1}, u_p^{n+1} and v_p^{n+1}. We have $\overline{\Delta t} = \Delta t$ on a predictor step and $\overline{\Delta t} = \Delta t/2$ on a corrector step. Following the integration of momentum equations with $\hat{f}_{s_{e_2}} = 0$, the values of $\tilde{u}$, $\tilde{v}$, $\tilde{u}_p$ and $\tilde{v}_p$ are known, whereupon values of u^{n+1}, v^{n+1}, u_p^{n+1} and v_p^{n+1} follow from the solution of four simultaneous linear equations.

In the subsequent integration of the interior flow, only the longitudinal motion of the solid-phase is affected. The transverse component of the interior gas-phase velocity is simply set to zero by a suitable modification to the cylindrical components.

2.3.3   Interphase Heat Transfer

As with the interphase drag, we assume that the previous one-dimensional formulation of the interphase heat transfer[24] describes adequately the situation for purely longitudinal flow. Existing data for tube bundles are assumed to describe the situation in the case of purely transverse flow. The two components are combined according to a hypothetical formulation.

In longitudinal flow the heat transfer is described by

$$Nu_{P_1} = h_1 \frac{D_p}{k_f} = 0.023 Re_p^{0.8} Pr^{0.4} \qquad\qquad 2.3.3.1$$

where D_p is defined as in the previous section, Equation 2.3.2.2 and k_f is the thermal conductivity of the gas at the film temperature. We understand 2.3.3.1 to apply to both the exterior and interior flows with the appropriate values of D_p.

Transverse flow is relevant only to the exterior flow. According to Holman,[28] the heat transfer to tube bundles in transverse flow may be expressed as a function of Re_{max}, Equation 2.3.2.12, expressed in the form

51

$$Nu_{p_2} = CRe_{max}^n \qquad\qquad 2.3.3.2$$

and C and n are expressed in tabular form as a function of the arrangement of the tubes within the bank. Values of C and n near the fully packed condition are not available but it appears that suitable values might be $C \approx n \approx 0.5$.

Under conditions of combined or oblique flow we assume that the Nusselt number is given by

$$Nu_p = \frac{1}{|\vec{u} - \vec{u}_p|} \{(u_1 - u_{p_1})Nu_{p_1} + (u_2 - u_{p_2})Nu_{p_2}\} \qquad 2.3.3.3$$

It is emphasized that 2.3.3.3 is speculative in nature and that further study of this topic is desirable.

2.4 Rupture and the Presence of Slots

When single-perforation stick propellant is initially slotted or when it is unslotted but ruptures over its length at some time, it becomes necessary to consider mass transfer between the interior and exterior flows. We note the treatment of rupture in TDNOVA in Section 2.4.1 together with some additional comments on mechanical failure of stick propellant. Mass transfer through the slot is discussed in Section 2.4.2.

An important point to keep in mind in the present discussion is that explicit modeling of mass transfer through the slot--whether present initially or due to rupture--is performed only in the fully-two-dimensional part of the calculation. If increments of slotted stick propellant are present, the transition to a quasi-two-dimensional representation is delayed until all slots are opened and venting freely in all increments. If increments of unslotted single-perforation stick propellant are present, the transition is delayed until such a point in time as all the sticks in a given increment are entirely ruptured or all are entirely unruptured.

When all the slots of a given increment are fully open, or when an increment is fully ruptured, the dual-voidage representation of that particular increment is terminated. A single-voidage model is initiated in which the gas-phase state variables are initialized to mass weighted averages of the interior and exterior values at each location. The subsequent analysis of the solid-phase form functions recognizes explicitly the effect of the presence of the

slot on the surface area and volume per unit length of the sticks. A transition to a single-voidage model is also effected when slivering or burnthrough occurs at any point in a given increment. Following the transition to a single-voidage model all surfaces of the stick regress at the same rate under the influence of a common value of pressure. The differences in total regression at the instant of transition are saved, however, and are used to correct the subsequent calculations of the form functions.

2.4.1 Mechanical Failure of Stick Propellant

The importance of the possibility of rupture of single-perforation stick propellant has been emphasized in recent experimental studies.[34,35] The present treatment of rupture in TDNOVA is extremely crude and is intended only to permit diagnostic simulations. We assume that there exists a maximum value of the excess of the interior over the exterior pressure which can be supported by the sticks. When this value, which is set by the code user, is exceeded at any point in the computational mesh it is assumed that a longitudinal crack is instantaneously opened over the full length of the increment. For simplicity, the coding allows the crack to open along a computational line of constant η which is approximately a line of constant radius.[3] For a given increment to become fully ruptured it is therefore necessary that the rupture criterion be satisfied at each radial location. The precise axial location is irrelevant. In the quasi-two-dimensional representation, however, rupture of an increment occurs when the rupture criterion is satisfied at any axial location since radial structure is not modeled.

A more complete model could be incorporated using the theory of thick cylinders[36] to compute the stress within the propellant, provided suitable constitutive data become available. Consideration could also be given to the finite rate of propagation of the crack. This sort of elaboration is only recommended, however, if it becomes necessary to accommodate stick rupture as part of the intended combustion process.

---

[34]Robbins, F. W., "Continued Study of Stick Propellant Combustion Processes," Proc. 19th JANNAF Combustion Meeting   1982

[35]Juhasz, A., Robbins, F. W., Bowman, R. E., and Doali, J. O. "Combustion Characteristics of NOSOL 363 Single-Perforated and Slotted Stick Propellant," Proc. 19th JANNAF Combustion Meeting   1982

[36]Harvey, J. F., "Theory and Design of Modern Pressure Vessels" van Nostrand Reinhold   1974

Before leaving this topic we offer some additional observations on the mechanical failure of stick propellant. Even if the sticks are not perforated, rupture can occur due to nonuniformity of the pressure distribution. As an example consider the situation in the sketch. We assume that symmetry prevails so that the pressure in
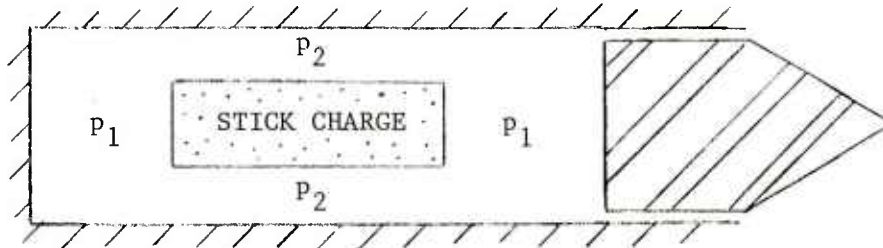
both of the end regions of ullage is p_1. Due to the burning of the propellant, the pressure at the midpoint is p_2 and presumably $p_2 > p_1$. We suppose that events unfold sufficiently slowly that the transient nature of the loads can be ignored and the principles of statics can be applied to the determination of the stresses in the stick. Neglecting shear due to drag, it is evident that the axial stress in the sticks, positive in compression to conform with Section 2.3.1, has everywhere the value

$$\sigma_z = p_1 \qquad\qquad\qquad 2.4.1.1$$

Because the stick is solid we have $\sigma_r = \sigma_\theta$, both being equal to the pressure at each cross section. In the midpoint, in particular

$$\sigma_r = \sigma_\theta = p_2 \qquad\qquad\qquad 2.4.1.2$$

These simple considerations lead to a state of stress consistent with the assumption of static equilibrium. But arbitrary states of stress are not accessible in real materials. In particular, the maximum difference between principal stresses is limited by the strength of the material, or its resistance to shear. If one supposes that the von Mises criterion of maximum distortional energy[36] is a reasonable failure criterion, then 2.4.1.1 and 2.4.1.2 define a state of equilibrium provided that the equivalent stress σ_{eq} does not exceed the tensile yield strength of the propellant σ_y

where

$$\sigma_{eq}{}^2 = \frac{1}{2} \{(\sigma_z - \sigma_r)^2 + (\sigma_r - \sigma_\theta)^2 + (\sigma_\theta - \sigma_z)^2\} \qquad 2.4.1.3$$

Evidently, therefore, failure of the stick bundle will occur at the midpoint if

$$p_2 - p_1 > \sigma_y \qquad 2.4.1.4$$

and it is noteworthy that the failure is extensional, the bundle breaking into two halves.

TDNOVA incorporates the foregoing stress principles with due allowance for transient wave propagation. However, the possibility of axial rupture is not presently considered.

Finally we note the possibility of rupture or damage to the propellant due to impact against the projectile base. While this does not seem to be a likely eventuality for case charge stick increments, it becomes a distinct possibility when the increments are loaded into individual, impermeable and mobile containers.

2.4.2 Mass Transfer Through the Slot

Let σ_{rup} be the maximum pressure differential which can be supported by unslotted single-perforation propellant. Then, as discussed in the preceding section, rupture occurs over the length of the stick when the following relation is satisfied at any point

$$p_i - p_e \geq \sigma_{rup} \qquad 2.4.2.1$$

In the present version of TDNOVA, Equation 2.4.2.1 is also used to determine the time at which venting through the slot of slotted stick propellant commences locally. Venting through the slot does not occur at any location where 2.4.2.1 has not been satified at some time. Once 2.4.2.1 is satisfied at a given location, venting is assumed always to occur and to maintain local equality of the external and internal pressures.

The magnitude of the mass flux through the slot is found by integrating the gas-phase Equations 2.2.2.1-2.2.2.3 with $\dot{m}_{s\ell_e} = \dot{m}_{s\ell_i} = 0$.

The resulting values of pressure may be denoted by $\tilde{p}_e$ and $\tilde{p}_i$. From the right-hand side of the balance equations it is possible to identify the partial derivative $\partial p_e / \partial \dot{m}_{s\ell_e}$ such that for a nonzero value of $\dot{m}_{s\ell_e}$

$$p_e^{n+1} = \tilde{p}_e + \left(\frac{\partial p_e}{\partial \dot{m}_{s\ell_e}}\right)\dot{m}_{s\ell_e} \qquad\qquad 2.4.2.2$$

and similarly for p_i^{n+1}. The values of $\dot{m}_{s\ell_e}$ and $\dot{m}_{s\ell_i}$ follow from 2.4.2.2 and its counterpart for p_i^{n+1} together with the quasi-steady mass balance

$$\dot{m}_{s\ell} - \dot{m}_{s\ell_e} - \dot{m}_{s\ell_i} = 0 \qquad\qquad 2.4.2.3$$

where $\dot{m}_{s\ell}$ is the rate of mass production due to combustion of the faces of the slot.

It should be noted that 2.4.2.3 is only valid provided that the total volume of the slot remains small during the dual-voidage representation of slotted or ruptured propellant. Once the single-voidage model is initiated the changing volume of the slot is automatically taken into account by the form functions.

When the values of $\dot{m}_{s\ell_e}$ and $\dot{m}_{s\ell_i}$ have been found it is necessary to correct all the gas-phase state variables in the exterior and interior flows. The state of the transported gas is determined using the same method as that described in Section 3.4 in relation to the transport of gas through the reactive container. The influence of $\dot{m}_{s\ell}$ on the internal energy, specific heats, molecular weight, reactant mass fraction and velocity components is captured by the quasi-steady transfer conditions.

At present we perform the equilibration of interior and exterior pressures on the boundaries prior to the imposition of the physical conditions which link the gas-phase boundary values to the neighboring computational regions or the external boundaries. Therefore a small departure from precise equilibration will be expected following the imposition of the external boundary conditions.

2.5 Pseudo-Characteristic Forms of the Dual-Voidage Balance Equations

At all continuum boundaries we use characteristic forms of the balance equations to determine those boundary values which are not captured by the physical conditions. As we have discussed in the introduction to this chapter, mathematically complete characteristics are not essential for the determination of stable numerical results. We merely need to extract the differential relationship between the pressure, or normal stress, and the normal velocity component. The results presented here differ from those in the previous versions of TDNOVA[1,2,3] not only because of the additional complications stemming from the consideration of the rheology of the stick charge, but also because of the degree of differential uncoupling of the gas-phase and solid-phase state variables.

Only the results of the characteristic analysis are tabulated here. The method of derivation follows the discussion of Reference 1 and while laborious, it is straightforward. Actually, due to the treatment of the derivatives of porosity as nonhomogeneous terms in the gas-phase balance equations, the present results for the gas-phase are formally similar to those of Reference 1 for single-phase flow.

2.5.1 Gas-Phase Pseudo-Characteristic Forms

As in previous work it is assumed that the continuity Equation 2.2.2.1 is substituted into the energy Equation 2.2.2.3 and that the internal energy is eliminated in favor of pressure and density. Derivatives of porosity remain only in 2.2.2.1 and are treated as algebraic terms. With the understanding that the following results refer either to the exterior or the interior gas-phase properties, and accordingly suppressing the subscripts e or i we write

$$\xi_1 = \frac{1}{\varepsilon} \{ \dot{m}_p + \psi - \frac{\varepsilon \rho v}{r} + \dot{m}_{s\ell} - \rho [\frac{\partial \varepsilon}{\partial t} + u \frac{\partial \varepsilon}{\partial z} + v \frac{\partial \varepsilon}{\partial r}] \} \qquad 2.5.1.1$$

$$\xi_2 = \frac{1}{\varepsilon} \{ -f_z + \dot{m}_p (u_p - u) - \psi u + \dot{m}_{s\ell} (u_{s\ell} - u) \} \qquad 2.5.1.2$$

$$\xi_3 = \frac{1}{\varepsilon} \{ -f_r + \dot{m}_p (v_p - v) - \psi v + \dot{m}_{s\ell} (v_{s\ell} - v) \} \qquad 2.5.1.3$$

$$\xi_4 = \frac{1}{\varepsilon\rho\left(\frac{\partial e}{\partial p}\right)_\rho} \left\{ \frac{f_z}{g_o}(u - u_p) + \frac{f_r}{g_o}(v - v_p) - s_p q \right.$$

$$+ \dot{m}_p \left(e_p - e + p\left(\frac{1}{\rho_p} - \frac{1}{\rho}\right) + \frac{|\vec{u} \cdot \vec{u}|^2}{2g_o} \right)$$

$$+ \psi\left(e_{IG} - e - \frac{p}{\rho} + \frac{\vec{u} \cdot \vec{u}}{2g_o} \right)$$

$$\left. + \dot{m}_{s\ell}\left(e_{s\ell} - e + \frac{p_{s\ell}}{\rho_{s\ell}} - \frac{p}{\rho} + \frac{|\vec{u}_{s\ell} - \vec{u}|^2}{2g_o} \right) \right\}$$

2.5.1.4

Care should be taken not to confuse $\dot{m}_{s\ell}$ with the mass production due to the slot sidewalls as used in Section 2.4.2. The terms subscripted $s\ell$ are implicitly understood to carry the additional subscript e or i.

The characteristic forms are deduced after first considering the transformation from cylindrical coordinates (t,z,r) to computational coordinates (τ,ζ,η) as described previously.[1] We recall the following definition

$$w = (u - u_m)\zeta_z + (v - v_m)\zeta_r \qquad\qquad 2.5.1.5$$

$$x = (u - u_m)\eta_z + (v - v_m)\eta_r \qquad\qquad 2.5.1.6$$

where $u_m = z_\tau$ and $v_m = r_\tau$ are the velocity components of the computational mesh in cylindrical coordinates. As previously, we record results only for a boundary on which η = constant and we define the following:

$$\xi_1{}^* = \xi_1 - [x\rho_\eta + \rho\eta_z u_\eta + \rho\eta_r v_\eta] \qquad\qquad 2.5.1.7$$

$$\xi_2{}^* = \xi_2 - [\rho x u_\eta + g_o\eta_z p_\eta] \qquad\qquad 2.5.1.8$$

$$\xi_3{}^* = \xi_3 - [\rho x v_\eta + g_o\eta_r p_\eta] \qquad\qquad 2.5.1.9$$

$$\xi_4{}^* = \xi_4 - x\left[p_\eta - \frac{c^2}{g_o}\rho_\eta\right] \qquad\qquad 2.5.1.10$$

58

Then the acoustic condition of compatibility is

$$-\frac{g_o}{c^2}\, y p_\alpha = -\frac{\xi_A}{1+\dfrac{w}{y}} + \rho\left(\zeta_z u_\alpha + \zeta_r v_\alpha\right) \qquad 2.5.1.11$$

where c is the isentropic speed of sound of the gas-phase and y is the characteristic root

$$y = \frac{d\zeta}{d\tau} - w = \pm\, c\left(\zeta_z^{\,2} + \zeta_r^{\,2}\right)^{\frac{1}{2}} \qquad 2.5.1.12$$

We also have

$$\xi_A = \xi_1^* + \frac{g_o}{c^2}\, \xi_4^* + \frac{\zeta_z \xi_2^* + \zeta_r \xi_3^*}{y} \qquad 2.5.1.13$$

Finally, the characteristic derivative p_α is related to the τ- and ζ-derivatives according to[1,2]

$$p_\alpha = p_\zeta + p_\tau \Big/ \left(\frac{d\zeta}{d\tau}\right) \qquad 2.5.1.14$$

In addition to the acoustic condition 2.5.1.11 which relates the pressure, p, to the normal velocity component $\zeta_z u + \zeta_r v$ there are material characteristic forms which relate p and ρ and which describe changes in γ or M_w. These are unchanged from the previous results and require no further attention here.

2.5.2 Solid-Phase Pseudo-Characteristic Forms

Let ξ_5 denote the right-hand side of Equation 2.2.3.1 and let ξ_6 and ξ_7 be as given in Equations 2.3.1.28 and 2.3.1.30, respectively. Let ξ_8 and ξ_9 represent the nonhomogeneous parts of 2.3.1.6 and 2.3.1.11, respectively. Evidently $\xi_8 = 0$. However, $\xi_9 = 0$ only in the limit as the angle of orientation of the sticks $\phi \to 0$. At present, in accordance with the discussion of Section 2.3.1, we have neglected the influence of ϕ on the solid-phase stress tensor components in cylindrical coordinates. Therefore ξ_9 is understood to be zero in the subsequent discussion. We nevertheless retain it so as to identify its analytical role for future studies in which the corrections due to finite values of ϕ become of interest. As in the previous section we consider explicitly a boundary on which η = constant. Then we

define w_p and x_p by analogy to w and x, Equations 2.5.1.5 and 2.5.1.6, and we have

$$\xi_5{}^* = \xi_5 - [x_p\epsilon_\eta - (1 - \epsilon)\eta_z u_{p_\eta} - (1 - \epsilon)\eta_r v_{p_\eta}] \qquad 2.5.2.1$$

$$\xi_6{}^* = \xi_6 - [(1 - \epsilon)\rho_p x_p v_{p_\eta} + 2\nu g_o \eta_z \sigma_{T_\eta} + g_o \eta_z \sigma_{L_\eta}] \qquad 2.5.2.2$$

$$\xi_7{}^* = \xi_7 - [(1 - \epsilon)\rho_p x_p v_{p_\eta} + g_o \eta_r \sigma_{T_\eta}] \qquad 2.5.2.3$$

$$\xi_8{}^* = \xi_8 - [\frac{\rho_p a_T{}^2}{g_o} x_p \epsilon_\eta + x_p \sigma_{T_\eta}] \qquad 2.5.2.4$$

$$\xi_9{}^* = \xi_9 - [\frac{\sigma_L}{1 - \epsilon} x_p \epsilon_\eta + (1 - \epsilon)\frac{\rho_p a_L{}^2}{g_o}\eta_z u_{p_\eta} + x_p \sigma_{L_\eta}] \qquad 2.5.2.5$$

The acoustic characteristic condition is found to be

$$\zeta_z{}^2 \sigma_{L_\alpha} + \frac{1}{y_p{}^2}[y_p{}^2(2\nu\zeta_z{}^2 + \zeta_r{}^2) - a_L{}^2\zeta_r{}^2\zeta_z{}^2]\sigma_{T_\alpha} - \frac{\zeta_z\zeta_B}{g_o(1 + \frac{w_p}{y_p})}$$

$$+ (1 - \epsilon)\frac{\rho_p y_p}{g_o}[\zeta_z u_{p_\alpha} + \zeta_r v_{p_\alpha}(\frac{y_p{}^2 - a_L{}^2\zeta_z{}^2}{y_p{}^2})] = 0 \qquad 2.5.2.6$$

where the characteristic root $y_p = \frac{d\zeta}{d\tau} - w_p$ satisfies

$$y_p{}^4 - y_p{}^2[a_T{}^2(\zeta_r{}^2 + 2\nu\zeta_z{}^2) + a_L{}^2\zeta_z{}^2 + \frac{g_o\sigma_L\zeta_z{}^2}{(1 - \epsilon)\rho_p}] + a_T{}^2 a_L{}^2\zeta_z{}^2\zeta_r{}^2 = 0$$

$$2.5.2.7$$

and we have

$$\xi_B = \zeta_z\xi_6{}^* + \frac{g_o}{y_p}\zeta_z{}^2\xi_9{}^* + \frac{2\nu}{y_p}g_o\zeta_z{}^2\xi_8{}^* \qquad 2.5.2.8$$

$$- \frac{\rho_p}{y_p}(y_p{}^2 - a_L{}^2\zeta_z{}^2)[\xi_5{}^* - \frac{\zeta_r\xi_7{}^*}{\rho_p y_p} - \frac{g_o\zeta_r{}^2}{\rho_p y_p{}^2}\xi_8{}^*]$$

We observe that 2.5.2.6 introduces certain complications which can only be resolved through elements of judgment when we seek to apply it to the determination of the solid-phase boundary values. First, we observe that both σ_L and σ_T are present. Moreover, the only material characteristic condition which emerges is the constitutive relation for σ_T and ϵ already anticipated by Equation 2.3.1.6. The constitutive law 2.3.1.11 yields a characteristic form only in the one-dimensional case when $\partial u_p/\partial z$ can be related to $D\epsilon/Dt_p$ through the continuity equation. Therefore the physical boundary conditions and the characteristic conditions will be insufficient in number to determine all the solid-phase properties. This problem is resolved in Section 2.6 when we discuss the physical boundary conditions.

The second complication relates to the velocity components. Equation 2.5.1.11, for example, establishes a direct relation between the pressure and a normal gas-phase velocity component. But Equation 2.5.2.6 involves the expression

$$\hat{u}_p = \zeta_z u_p + \zeta_r v_p K \qquad\qquad 2.5.2.9$$

where

$$K = \frac{y_p^2 - a_L^2 \zeta_z^2}{y_p^2} \qquad\qquad 2.5.2.10$$

We assume that we can express $\hat{u}_p$ as a linear combination of a normal component $u_{p_N} = \zeta_z u_p + \zeta_r v_p$ and a tangential component $u_{p_T} = -\zeta_r u_p + \zeta_r v_p$. It then follows that the characteristic relations to be used in the determination of compatible boundary values are

$$\frac{\partial \sigma_L}{\partial u_{p_N}} = -(1-\epsilon)\frac{\rho_p y_p}{g_o} \frac{\zeta_z^2 + K\zeta_r^2}{\zeta_z^2(\zeta_z^2 + \zeta_r^2)} \qquad\qquad 2.5.2.11$$

$$\frac{\partial \sigma_T}{\partial u_{p_N}} = -(1-\epsilon)\frac{\rho_p y_p}{g_o} \frac{y_p^2}{\{y_p^2(2\nu\zeta_z^2 + \zeta_r^2) - a_L^2 \zeta_r^2 \zeta_z^2\}} \frac{\zeta_z^2 + K\zeta_r^2}{\zeta_z^2 + \zeta_r^2}$$

$$2.5.2.12$$

We discuss the use of these results at the conclusion of the next section.

Equation 2.5.2.6 pertains to the fully-two-dimensional case. The quasi-one-dimensional form follows by setting $\zeta_r = v_p = 0$, deleting the η-derivatives from the $\xi_i{}^*$ and adding the appropriate area dependent terms to the ξ_i.

2.6 Initial and Boundary Conditions

The initial conditions are straightforward and are disposed of in Section 2.6.1. The boundary conditions introduce certain new considerations into TDNOVA and we discuss these in Section 2.6.2 which treats first the physical conditions and subsequently the implications for the method of solution.

2.6.1 Initial Conditions

As in previous work we take both phases to be initially at rest and to have equal temperatures. The porosity is piecewise uniform with discontinuities occurring at the mixture boundaries. The pressure is uniform throughout the chamber. By analogy with the granular charge the transverse stress component σ_T is initially zero. However, the initial value for σ_L is not zero. As previously noted in the one-dimensional dual voidage model[24], it may be seen from Equation 2.3.1.7 that since $\sigma_{p_1} = -p_o$, initially, the initial value of σ_L is σ_{L_o} given by

$$\sigma_{L_o} = (1 - 2\nu)(1 - \varepsilon)p_o \qquad 2.6.1.1$$

2.6.2 Boundary Conditions

At an impermeable external boundary the physical condition to be satisfied is the vanishing of the normal velocity component of each of the phases, independently of whether we are dealing with a granular or a stick charge. New considerations arise only when we consider an internal boundary defined by a discontinuity in porosity. In previous work pertaining to granular charges[31] we have made use of the jump conditions which connect macroscopic states on either side of a discontinuity. These are formally similar to the Rankine-Hugoniot conditions which connect the single-phase states on either side of the gas-dynamic discontinuity and are nothing more than finite balances of mass, momentum and energy. Even for granular charges a theoretical obstacle is observed in connection with the finite momentum balance. The balance can only be written for the

mixture and constitutive assumptions have to be made, or resolved experimentally, concerning the exchange of momentum between the phases. We have consistently made the assumption that the intergranular stresses satisfy $\sigma_1 = \sigma_2$ where subscripts 1 and 2 refer to the two sides of the discontinuity and σ is as defined by Equation 2.2.3.5.

When we turn to the consideration of the finite momentum balance for the stick charge, two additional factors must be taken into account. First, the finite balance will now include the combined effects of the exterior and interior gas-phase flows. Second, if the normal to the surface of discontinuity lies in the transverse direction we must use σ_T in place of σ in the balance equation and if the normal lies in the longitudinal direction, we must replace σ by $\sigma_L + 2\nu\sigma_T - (1 - 2\nu)(1 - \varepsilon)p_e$. This latter consideration is an extension of the result used in connection with the NOVA code[24] inasmuch as it introduces the influence of σ_T on the boundary value of σ_L.

Splitting the momentum balance is accomplished by means of the same assumptions used in Reference 24. We assume that if subscript i denotes any of the gas-phase streamlines intercepting the macroscopic discontinuity, then

$$p_i + \varepsilon_i \rho_i \frac{u_{n_i}^2}{g_o} = p_*$$

2.6.2.1

where u_{n_i} is the normal velocity component and p_* may be thought of as a reference pressure which is determined during the computation of the boundary values. Concerning the solid-phase we assume that the relevant condition is, in general

$$\sigma_1{}^* = \sigma_2{}^*$$

2.6.2.2

where

$$\sigma_i{}^* = \begin{cases} \sigma & \text{if side i is granular} \\ \sigma_T & \text{if side i is stick and normal to boundary is in transverse direction} \\ \sigma_L + 2\nu\sigma_T - (1 - 2\nu)(1 -\varepsilon)p_e & \text{if side i is stick and normal to boundary is in longitudinal direction} \end{cases}$$

2.6.2.3

63

The hypothetical nature of 2.6.2.1 was pointed out in Reference 24 and is reiterated here. Both theoretical and experimental studies are desirable in connection with the gas-phase mechanical boundary condition. We also note that 2.6.2.1 is only used provided that the resulting boundary state corresponds to a subsonic flux. If 2.6.2.1 results in a supersonic flux for streamline i then it is replaced by a condition of sonic flow. Finally, we note the observation of Reference 24 that when we are dealing with a longitudinal boundary, 2.6.2.1 and 2.6.2.2 only satisfy the normal momentum balance to an order of accuracy in the difference between the exterior and interior gas-phase pressures similar to that which justifies the use of p_e alone in the solid-phase momentum equation.

To conclude, we comment on the method of solution. This is essentially unchanged except in regard to certain details of the solid-phase, specifically the interpretation of Equation 2.5.2.6. Previously,[3] we have first updated the solid-phase state variables u_p, v_p, ε and σ. The solid-phase tangential velocity component was defined at the boundary by continuation from the interior. The normal velocity component u_{p_N} was assumed to be unchanged from current storage and a compatible value of σ was determined from the characteristic form. The value of ε followed from the solid-phase material characteristic if the rate of propagation of intergranular disturbances did not vanish and from the continuity equation otherwise. Then the value of either σ or u_{p_N} was varied so as to satisfy the physical boundary condition and the other solid-phase state variables were correspondingly changed in order to ensure the satisfaction of all relevant characteristic forms.

In the present case, if the normal to the boundary is transverse we update σ_L directly from the constitutive law 2.3.1.11. Equation 2.5.2.6 then yields a characteristic relation between u_{p_N} and σ_T which is used in the same fashion as in the earlier granular case except that 2.5.2.12 is used to identify the characteristic relation between σ_T and u_{p_N}. If the boundary is longitudinal we update the porosity by reference to the continuity equation and the value of σ_T by reference to the constitutive law 2.3.1.6. Then σ_L follows from the characteristic form 2.5.2.6. Equation 2.5.2.11 expresses the characteristic relation between σ_L and u_{p_N}. Further discussion of the solid-phase boundary conditions is given in Section 3.3.

64

As in previous work[3] the update of the gas-phase state variables is accomplished by first solving the mechanical equations--the finite mass and momentum balances and the acoustic characteristic forms. The remaining state variables follow from the gas-phase material characteristic forms or from the transport conditions at the discontinuity according as the flow is directed out of or into the region in question. Further details are given in Section 3.4.

We do note the use of a tangential momentum loss for gas entering the mixture.[2,3] At a longitudinal boundary this loss may be total for the exterior flow and is always total for the interior flow. At a transverse boundary, the gas-phase acoustic characteristic form is only applied to the exterior flow. For the interior flow the normal velocity component is simply set equal to zero without perturbation of the remaining state variables.

With regard to the quasi-two-dimensional mode of calculation we merely note that σ_T is used to express the transverse mechanical equilibration of the solid-phase while σ_L pertains to the ends of the increments.

3.0 ANALYSIS OF CHARGE INCREMENT CONTAINERS

With reference to the previous version of TDNOVA[3] there are two new features which require attention in the present work. In Section 3.1 we discuss the equations of motion of the sidewalls and endwalls of the cases used to contain individual charge increments. In Section 3.2 we discuss the revised representation of the reactivity of the container. Corresponding to each of these two topics we have the solid-phase and gas-phase boundary conditions for the mixture within the container. The boundary conditions are discussed in Sections 3.3 and 3.4. The discussion of Sections 3.3 and 3.4 pays attention not only to the formulation of the boundary conditions but also to certain aspects of the method of solution.

3.1 Equations of Motion of the Case

In Figure 3.1 we illustrate schematically a container for one increment of the charge. Following the nomenclature described in the introduction, we refer to the boundaries of the case as the sidewall-- strictly speaking, the outer sidewall--the centercore tube, or inner sidewall, and the endwalls. For the sake of subsequent discussions, particularly in reference to the solid-phase boundary conditions, we arbitrarily show the left-hand endwall as partially ruptured and the right-hand endwall as intact. We also adopt the convention, as illustrated, of regarding the sidewall as extending only over the length of charge increment; the endwalls extend to the outside of the container.

If the container were a flexible bag, no consideration would be given to its motion independently from that of the boundary of the propelling charge increment. When the container is rigidized we adopt the following modeling conventions.

Sidewall

The sidewall is considered to have tangential slip with respect to the propelling charge. The longitudinal equation of motion is based on the assumption that the sidewall is a linear elastic continuum. The inertia and load-carrying capacity of each segment are predicated on a structural thickness which may be less than the total thickness which also reflects the presence of the additives. This assumption implies that the additives are mechanically unlinked from the longitudinal motion. Radial motion of the sidewall independent of the motion of the propellant is not considered.
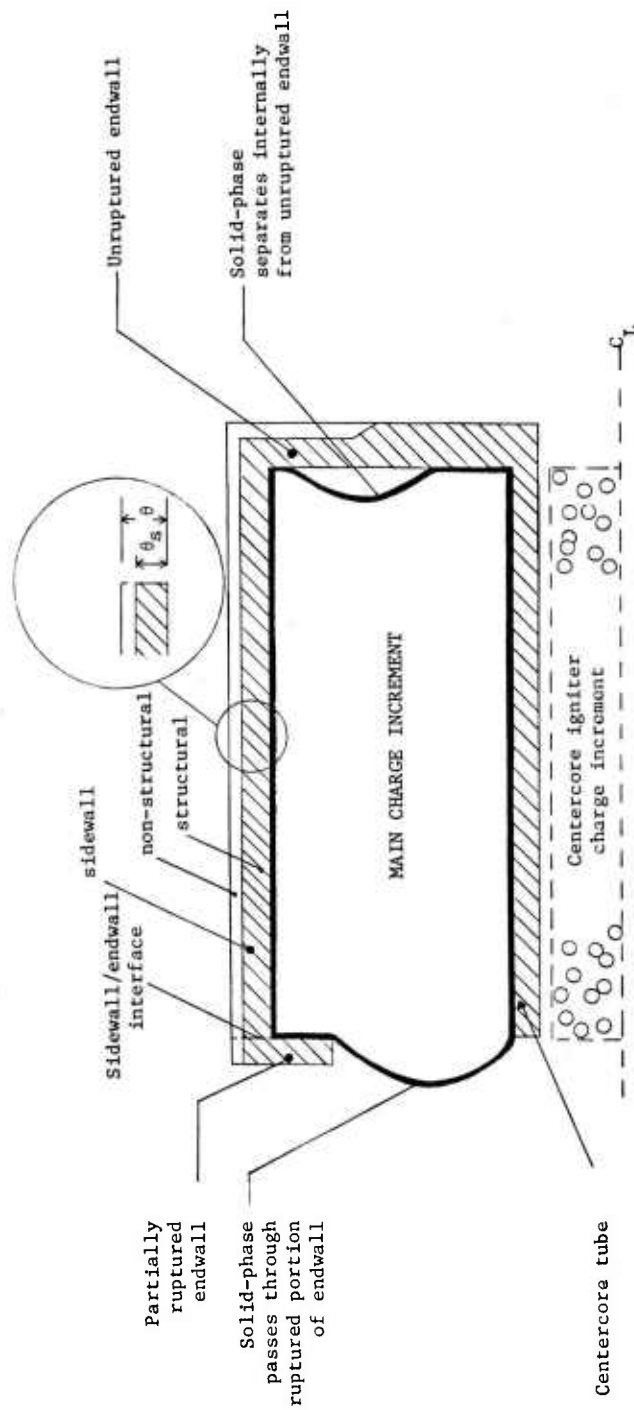
Figure 3.1   Structural Model of Rigidized Case

Unruptured endwall

Solid-phase separates internally from unruptured endwall

Sidewall/endwall interface

non-structural

structural

sidewall

Partially ruptured endwall

Solid-phase passes through ruptured portion of endwall

Centercore tube

MAIN CHARGE INCREMENT

Centercore igniter charge increment

θ_s, θ

C_L

Endwall

The unruptured part of the endwall is assumed to be rigid. The solid-phase is permitted to slip tangentially and also to undergo normal separation from the endwall. The solid-phase is unconfined over the ruptured portion of the endwall. The inertia of the endwalls is based on the instantaneous structural thickness.

Centercore Tube

No revision is involved. Neither normal nor tangential motion of the centercore independently of that of the propelling charge is modeled.

The mechanical problem to be solved when the case is rigidized consists of the longitudinal motion of the sidewall subject to boundary conditions defined by the inertia of the endwalls and the total stresses on the endwalls. The centercore tube is ignored.

Since the momentum flux due to reactivity of the sidewall is presumed to be discharged in a direction normal to the sidewall it offers no contribution to the longitudinal motion. Of course, the structural thickness varies with time. Let θ_s be the structural thickness and let ρ_w be the density of the structural part of the sidewall. Let δ_w and u_w be the longitudinal displacement and velocity of the sidewall and let σ_w be the axial stress, positive in tension. More generally, we can distinguish σ_w as σ_{w_z} and refer also to σ_{w_r}, σ_{w_θ}, the other principal stresses. We have[37]

$$\sigma_w = \sigma_{w_z} = E_w \frac{\partial \delta_w}{\partial z} + \nu_w (\sigma_{w_r} + \sigma_{w_\theta}) \qquad 3.1.1$$

where ν_w is the Poisson's ratio for the sidewall material and E_w is Young's modulus. We assume

$$E_w = \begin{cases} E_t & \text{if } \sigma_w \geqq 0 \\ \\ E_c & \text{if } \sigma_w < 0 \end{cases} \qquad 3.1.2$$

so that we allow the possibility of different moduli in tension and compression.

---

[37] Fung, Y. C., "Foundations of Solid Mechanics"
Prentice-Hall   1965

We expect that σ_{w_r} will be negligible in the applications of interest and we assume θ_s sufficiently small by comparison with the radius of the sidewall r_w that we have

$$\sigma_{w_\theta} = \frac{r_w}{\theta_s} (p_i + \sigma_i - p_o) \qquad\qquad 3.1.3$$

where p_i, σ_i are the gas-phase pressure and intergranular stress inside the sidewall and p_o is the exterior gas-phase pressure.

The displacement field δ_w is assumed to satisfy $\partial\delta_w/\partial z << 1$ in order to permit a linear elastic model to be used, but δ_w itself is not necessarily small in a fixed frame of reference. We write the constitutive equation as

$$\frac{\partial\sigma_w^*}{\partial t} + u_w \frac{\partial\sigma_w^*}{\partial z} = \frac{\rho_w a_w^2}{g_o} \left(\frac{\partial u_w}{\partial t} + u_w \frac{\partial u_w}{\partial z}\right) \qquad\qquad 3.1.4$$

where $a_w^2 = g_o E_w/\rho_w$ and we have introduced

$$\sigma_w^* = \sigma_w - \frac{\nu_w r_w}{\theta_s} (p_i + \sigma_i - p_o) \qquad\qquad 3.1.5$$

The longitudinal equation of motion of the sidewall is

$$\theta_s\rho_w\left(\frac{\partial u_w}{\partial t} + u_w \frac{\partial u_w}{\partial z}\right) = g_o \frac{\partial}{\partial z}(\theta_s\sigma_w) - \mu_w\sigma_i g_o \operatorname{sgn}(u_w - u_p) \qquad\qquad 3.1.6$$

where μ_w is the coefficient of friction between the sidewall and the propellant and u_p is the solid-phase axial velocity component. It should be noted that while we consider the influence of friction on the sidewall we neglect it insofar as the response of the solid-phase is concerned. From a purely physical point of view this omission asserts that the inertia of the sidewall is negligible by comparison with that of the solid-phase to which it is coupled in shear. From the point of view of the equations on which TDNOVA is predicated we may also note that the omission is consistent with the neglect of shear stresses in the solid-phase. Finally, we note that as in the previous versions of the code[2,3] the solid-phase tangential velocity is determined on the boundary by continuation from the interior, which places the influence of the shear exerted by the sidewall still further from our analytical grasp.

The partial differential Equations 3.1.4 and 3.1.6 are solved subject to the initial condition $u_w = \sigma_w{}^* = 0$ and the following boundary condition.

$$\frac{M_{end}}{g_o} \left(\frac{\partial u_w}{\partial t} + u_w \frac{\partial u_w}{\partial z}\right) = 2\pi n_{end} \left\{- r_w \theta_s \sigma_w + \int_{r_i}^{r_w} (p_i + \sigma_i - p_o) r \, dr \right.$$

$$\left. + \frac{F_{contact}}{2\pi} \right\} \qquad\qquad 3.1.7$$

where $n_{end} = \pm 1$ according as we are dealing with a right- or a left-hand boundary, r_i is the inner radius of the unruptured portion of the end-wall, M_{end} is the mass of the endwall, and $F_{contact}$ is the force exerted on the endwall due to contact with a second container, or with an external boundary, and is positive in tension.

The possible influence of the thrust terms due to reactivity of the endwalls is neglected. For ordinary reactive materials this omission is reasonable. Possibly, the thrust terms would be of importance if ultra-high burn rate materials were of interest.

The force of contact between two containers is determined from the condition $u_{w1} = u_{w2}$ where u_{w1} is the velocity of the right-hand boundary of the first container and u_{w2} is the velocity of the left-hand boundary of the second container. Contact is assumed to be main-tained provided that $F_{contact}$ does not exceed F_{bond}, the tensile bond strength between the containers. F_{bond} is set as an input quantity by the user. It is defaulted to zero whenever $F_{contact}$ exceeds F_{bond} or if the containers are initially separated.

A similar consideration applies at the external boundaries where separation is permitted to occur if $F_{contact} > 0$.

Special conventions apply to the determination of p_o in Equation 3.1.7 when the boundary is in contact with that of another container or with an external boundary. Under such a condition p_o is evaluated as the pressure in the external corner region of ullage associated with the boundary in question. This convention implies that the contact condition does not provide a gas-seal over the external surface of the endwall and circumvents the use of gas-phase properties in the collapsed region of axial ullage contiguous with the endwall.

70

Equations 3.1.4 and 3.1.6 are solved, at interior mesh points, using the same algorithm as that used for the regions of quasi-one-dimensional flow, namely, the MacCormack scheme with first order upwind differencing of convective derivatives. The mesh used to define the sidewall properties is collocated with that for the mixture on the external boundary. The endpoints of the sidewall are updated by reference to the characteristic forms of 3.1.4 and 3.1.6, namely:

$$\frac{\partial \sigma_w^*}{\partial t} + (u_w \pm a_w) \frac{\partial \sigma_w^*}{\partial z} \mp \frac{a_w \rho_w}{g_o} \{\frac{\partial u_w}{\partial t} + (u_w \pm a_w) \frac{\partial u_w}{\partial z}\} = \mp \frac{a_w}{g_o} \xi_w \quad 3.1.8$$

where

$$\xi_w = g_o \frac{\sigma_w}{\theta_s} \frac{\partial \theta_s}{\partial z} + g_o \nu_w \frac{\partial \sigma_w}{\partial z} \theta - g_o \mu_w \text{sgn} (u_w - u_p) \sigma_i \quad 3.1.9$$

Special attention is given to the friction term, at all points on the sidewall, when a locking condition occurs. If the sign of $u_w - u_p$ is reversed as a consequence of the friction term, the friction term is reduced to yield $u_w = u_p$.

Equation 3.1.7 is expressed implicitly in respect to σ_w and σ_i to avoid the introduction of oscillations when M_{end} is small. Further details of this topic are given in section 3.3 when we discuss the solid-phase boundary conditions.

The rigidized case analysis is conducted for each increment until either one of the endwalls is completely ruptured or until rupture of the sidewall occurs at any location. Subsequently, the unruptured portions of the container are modeled as in the previous code version.[3] The sidewall is taken to rupture when $\sigma_{eq} \geqq \sigma_y$ when σ_y is the tensile yield stress of the sidewall material and σ_{eq} is the von Mises equivalent stress[36] given by

$$\sigma_{eq}^2 = \frac{1}{2}\{\sigma_{w_z}^2 + \sigma_{w_\theta}^2 + (\sigma_{w_z} - \sigma_{w_\theta})^2\} \quad 3.1.10$$

Failure of the endwall is assumed to occur according to the criterion used previously in respect to flexible walls and which is noted in Section 3.3. In Equation 3.1.7, r_i is understood to be the largest value of r on the endwall for which failure has not yet occurred.

3.2 Ignition and Combustion of Reactive Layers

Each section of the container--endwalls, sidewall or centercore tube--may be characterized as having as many as four reactive substrates. Proceeding from the mixture side to the exterior of the segment, the layers are understood to represent an inner attached component, the inner surface of the segment, the outer surface of the segment and an outer attached component. Each section, moreover, may be described as consisting of a number of segments, and the reactive and mechanical properties may vary from segment to segment. Each substrate is described as reacting at a rate $\dot{m}_{s_j}$ (gm/cm^2-sec) where $j = 1, 2, 3$ or 4.

Each substrate has the following additional characteristics: solid-phase density, ρ_{s_j}, chemical energy, e_{s_j}, gas-phase molecular weight, $M_{w_{s_j}}$ and ratio of specific heats, γ_{s_j}. The thickness of the container varies according to

$$\dot{\theta} = - \sum_{j=1}^{4} \frac{\dot{m}_{s_j}}{\rho_{s_j}} \qquad\qquad 3.2.1$$

But the structural thickness θ_s is governed by

$$\dot{\theta}_s = - \sum_{j=2}^{3} \frac{\dot{m}_{s_j}}{\rho_{s_j}} \qquad\qquad 3.2.2$$

Although the time derivatives in 3.2.1 and 3.2.2 should correspond to a material path line for the container material, it is presently assumed that the convective derivative is negligible in the computational frame.

As in the previous version of the code,[3] $\dot{m}_{s_j}$ may be specified according to predetermined tabular data. Alternatively, $\dot{m}_{s_j}$ may be characterized according to an ignition and combustion model as follows.

We assume that ignition of the segment is due to convective heating in a fashion similar to that used to model the ignition of the propellant. A surface temperature for the substrate is computed by means of a cubic profile approximation and once it reaches a predetermined value the substrate undergoes a surface regression whose rate depends on the local pressure according to the usual exponential form.

The heat transfer coefficient is expressed as

$$h = 0.023 Pr^{0.4} Re^{0.8} \frac{k_f}{D_\star} \qquad\qquad 3.2.3$$

where k_f is the thermal conductivity of the gas at the film temperature, Pr is the Prandtl number and $Re = \rho u_T D_\star / \mu_f$ is the Reynolds number based on the local gas density ρ and tangential velocity u_T, the viscosity μ_f at the film temperature, and the reference length $D_\star$. Equation 3.2.3 corresponds to fully developed turbulent duct flow[28] For substrates on the exterior of the container adjacent to narrow regions of ullage it is tentatively supposed that

$$D_\star = \frac{4A}{P} \qquad\qquad 3.2.4$$

where A is the cross-sectional area of the ullage and P is the wetted perimeter. This assumption is consistent with the basis for the estimation of flow resistance in the ullage as described in Section 4.3. Equation 3.2.4 becomes implausible when the ullage has significant extension normal to the container. For this reason we do not interface this particular modeling option with the dynamic mesh algorithm. On the interior of the container the appropriate choice of $D_\star$ is not obvious. Tentatively, we identify $D_\star$ with the effective particle diameter for the solid propellant. Possibly, the interphase heat transfer correlation would be more appropriate than 3.2.3 on the interior. Such a conjecture is best resolved experimentally.

Because of the uncertainties in the present estimates of the film coefficient, we expect this modeling feature to be of value only when the rate of convection is high and the thermal conductivity of the substrate is low so that ignition occurs shortly after the onset of local convection and the precise value of the delay is insensitive to errors of the order of 100% in h.

The surface temperature of the substrate is deduced from the heat conduction equation by means of a cubic profile approximation. The relevant analysis may be readily ascertained from an inspection of Section 4.6.1 in which we discuss the analogous problem of heat conduction in the wall of the gun tube.

Once ignition occurs we have

$$\dot{m}_{s_j} = \rho_{s_j} \{B_{1_j} + B_{2_j} p^{n_j}\} \qquad\qquad 3.2.5$$

where B_{1_j}, B_{2_j} and n_j are the burn rate parameters of the substrate and p is the ambient gas-phase pressure on the appropriate side of the container.

3.3 Solid-Phase Boundary Conditions

In this section, and in the next, our discussion of the boundary conditions for the two-phase regions covers both the revised and the unrevised portions of the model. We discuss first the boundary conditions as they apply to granular charges at external boundaries and at internal boundaries defined by both flexible and rigidized containers. Then we note the modifications to be taken into account if the propellant consists of sticks.

As far as the method of solution is concerned we only discuss here the implicit analysis of the motion of the endwalls of rigidized containers. The revisions to the numerical analysis which pertain specifically to stick charges have been mentioned in Section 2.6 of this report. We will conclude this section with a discussion of the rupture criterion for flexible sections of the container; this discussion is also pertinent to the endwalls of rigidized containers as was noted in Section 3.1.

Let the boundary of the mixture have velocity $\vec{u}_b$ and outward pointing normal $\vec{n}$. Let $\vec{u}_p$ be the solid-phase velocity on the boundary and let σ_1 be the intergranular stress. Let σ_2 be the intergranular stress on the outside of the boundary. We note that σ as used here pertains to granular beds for the time being. If the mixture is bounded by a region of ullage, $\sigma_2 = 0$. Let Δp_{res} be the pressure drop through the container associated with the normal flux of the gas-phase. We will identify Δp_{res} in the next section. We consider three possible boundary conditions on the solid-phase, namely:

74

$$(\vec{u}_p - \vec{u}_b) \cdot \vec{n} = 0 \qquad\qquad 3.3.1$$

$$\sigma_1 - \sigma_2 = 0 \qquad\qquad 3.3.2$$

$$\sigma_1 - \sigma_2 = -\Delta p_{res} \qquad\qquad 3.3.3$$

and we now consider the circumstances in which they apply.

If the mixture is in contact with an external boundary, Equation 3.3.1 applies and $\vec{u}_b$ is known from the behavior of the boundary in question. However if 3.3.1 results in a negative (tensile) inter-granular stress at the base of the moving projectile, it is assumed that separation is in progress and 3.3.1 is replaced by 3.3.2 with $\sigma_2 = 0$. Although separation of the granular mixture from the stationary boundaries is theoretically possible under some circumstances, we presently enforce 3.3.1 even if the resulting value of σ is negative. The value of σ is replaced by zero when a negative value is produced at stationary external boundaries. For problems of interest to date this apparent overdetermination of the boundary data only has the consequence of filtering out spurious separation due to truncation errors in the numerical solution of the equations.

Now let us consider the internal boundaries. We will refer to these as centercore, sidewall and endwall whether or not the relevant section of the container is actually present.

Centercore

Until it is ruptured the centercore tube is assumed to resist radial displacement. Hence 3.3.1 applies prior to rupture and $\vec{u}_b$ is arbitrary except that it has a zero radial component. Equation 3.3.1 applies to the unruptured tube even when the tube is permeable and/or reactive. The possible separation of the mixture from the tube due to the blowing effect of the gas-phase passing through the boundary is not presently considered. Once the centercore tube is completely ruptured, Equation 3.3.2 applies and σ_2 is the intergranular stress in the igniter charge.

Sidewall

Only when the sidewall is both unruptured and dilated to its original radius do we enforce 3.3.1. If it is unruptured but not fully dilated we use 3.3.2 if the gas is flowing out of the sidewall and 3.3.3

if the gas is flowing in. Once the sidewall is locally ruptured we always use 3.3.2. In both 3.3.2 and 3.3.3 the value of σ_2 is always zero. The use of 3.3.3 asserts that the pressure differential due to impermeability of the sidewall is not supported by the sidewall itself when the external pressure is greater than the internal pressure. For a flexible sidewall this assumption is expected to be on safe ground as a bag offers no resistance to external loads. In the event that the container is rigidized, the use of 3.3.3 is appropriate provided that the structural modulus of the sidewall is much less than that of the propellant bed and that the propellant is loaded tightly into the container without the introduction of radial ullage within the container itself. If E_t and E_b are respectively the compressive modulus of the tube material and the granular aggregate, we require that $E_t \theta_s / E_b r_w < < 1$ for external loads to be supported principally by the propelling charge.

Endwalls

We assume for the moment that the endwall is not locally in contact with the endwall of another container. If the container is rigidized and the endwall is unruptured locally then we use either 3.3.1 or 3.3.2 according to the same principles which apply at a moving external boundary. In 3.3.1 $\vec{u}_b$ is the velocity of the endwall, found from Equation 3.1.7. Separation of the solid-phase from the endwall is explicitly considered in this particular case. If the endwall is flexible and unruptured we use 3.3.2 when the gas is flowing out through the boundary and 3.3.3 when it is flowing in. If the endwall is ruptured we use 3.3.2.

If the endwall is in contact with another endwall and is rigidized, the value of $\vec{u}_b$ is determined implicitly to satisfy both the conditions of continuity of velocity and the force balance across the increment-to-increment interface. If both the endwalls are flexible, $\vec{u}_b$ is determined locally from the application of 3.3.2 or 3.3.3 to each side of the interface and the condition of continuity of velocity. Local separation of flexible endwalls occurs when the computed values of intergranular stress become negative. Separation of rigidized endwalls occurs when the required tensile bond strength exceeds a predetermined value as described in Section 3.1.

Stick Propellant

If we are dealing with stick propellant we interpret σ_1 as σ_T on the centercore and sidewall boundaries. In accordance with the discussion of Section 2.6, however, on the endwalls we must use

$$\sigma_1 = \sigma_{L_1} + 2\nu\sigma_{T_1} - (1 - \varepsilon_1)(1 - 2\nu)p_1 \qquad 3.3.4$$

in both 3.3.2 and 3.3.4.

Computational Considerations

New computational considerations arise only in respect to the analysis of the motion of the endwalls of the rigidized containers. Equation 3.1.7 couples the axial stress in the sidewall to the intergranular stress distribution over the entire endwall. The equation also involves coupling to the gas-phase pressure but our concern is with the stiffness of the boundary condition and the mechanical compliance of the gas-phase is much greater than that of the solid-phase so that we confine our attention to the latter. The computational problem associated with 3.1.7 stems in part from the mechanical stiffness of the sidewall and propellant and in part from the relatively low inertia of the endwall. If 3.1.7 is solved explicitly, using current storage level data to compute the stress terms, oscillations of the endwalls may be expected. Implicit statements of the mechanical boundary conditions are used throughout TDNOVA, but in the present case the coupling is nonlocal. All solid-phase stress values at all mesh points where contact occurs on each endwall have to be made explicitly compatible with the motion of the endwall and hence with each other.

The implicitness is incorporated as follows. Neglecting $F_{contact}$ for the moment, we discretize Equation 3.1.7 as

$$u_w^{n+1} = \tilde{u}_w + \frac{g_o \overline{\Delta t}}{M_{end}} \left\{ - 2\pi r_w \theta_s \sigma_w^{n+1} + \sum_j [p_{i,j} - p_{o,j} + \sigma_j^{n+1}] A_j \right\} n_{end} \qquad 3.3.5$$

where u_w^{n+1} is the updated value and $\tilde{u}_w$ is a current value on a predictor step and the average of the current and the predicted future value on a corrector step. Quantities not labelled with $\sim$ or $n+1$ may be understood to be evaluated as current storage data. A_j is an increment of area and the sum over j includes only those mesh points at which there is contact between the solid propellant and the endwall. We have $\overline{\Delta t} = \Delta t$ or $\Delta t/2$ according as we are dealing with a predictor or a corrector step.

From the hyperbolic structure of the equations we have the following characteristic forms for the sidewall

$$\sigma_w^{n+1} = \tilde{\sigma}_w + \left(\frac{\partial \sigma_w}{\partial u_w}\right)(u_w^{n+1} - \tilde{u}_w) \qquad 3.3.6$$

and the following pseudo-characteristic form for the intergranular stress

$$\sigma_j^{n+1} = \tilde{\sigma}_j + \left(\frac{\partial \sigma}{\partial u_{p_n}}\right)_j (u_{p_{n_j}}^{n+1} - \tilde{u}_{p_{n_j}}) \qquad 3.3.7$$

where $(\tilde{\sigma}_w, \tilde{u}_w)$ and $(\tilde{\sigma}_j, \tilde{u}_{p_{n_j}})$ are compatible values of stress and velocity

77

in a characteristic sense. We understand $u_{p_{n_j}}$ to be the normal component of the solid-phase velocity. Finally, we have the implicit relation

$$u_{p_{n_j}}^{n+1} = u_w^{n+1} \qquad\qquad 3.3.8$$

for all values of j for which there is contact between the propellant and the endwalls. The substitution of 3.3.6, 3.3.7 and 3.3.8 in 3.3.5 immediately yields the value of u_w^{n+1}. Then 3.3.6 and 3.3.7 are used to determine the values of σ_w^{n+1} and $\sigma_{p_j}^{n+1}$.

If the endwall is in contact with another endwall, the force of contact must be found. It follows easily from the requirement $u_{w_1}^{n+1} = u_{w_2}^{n+1}$ at the interface. Contact is maintained provided that $F_{contact}$ does not exceed the bond strength.

We conclude this section with a discussion of the criterion for rupture of the container. In Section 3.1 we discussed the criterion for failure of the sidewall of a rigidized container. The following discussion pertains to the centercore and the endwalls under all circumstances and to the sidewall once the container is no longer viewed as rigidized.

We assume that the container supports a load whose magnitude is F_{bag} given by

$$F_{bag} = \sigma_1 - \sigma_2 + \Delta p_{res} \qquad\qquad 3.3.9$$

provided that the following conditions are met.

Centercore

Equation 3.3.9 applies until rupture occurs, independently of whether the gas-phase is flowing into or out of the main charge increment. Failure is based on the absolute value of F_{bag} so that the crushing and bursting loads are assumed equal.

Sidewall

Equation 3.3.9 applies whenever the gas-phase is flowing out of the main charge increment and also whenever the sidewall is fully dilated.

Endwalls

Equation 3.3.9 applies whenever the gas-phase is flowing out of the main charge increment.

If the container is completely impermeable to the gas-phase, the requirement that the gas flow into the mixture is replaced by the requirement that the external pressure exceed the internal pressure. Rupture commences when F_{bag} exceeds a predetermined input value and is considered to extend over a predetermined interval of time before being completed. Impediment to the motion of the solid-phase is taken to vanish only when rupture is complete. During the rupture interval the container becomes increasingly permeable to the gas-phase as discussed in the next section.

3.4 Gas-Phase Boundary Conditions

The boundary conditions for the gas-phase at the interface between a charge increment and a region of ullage are based on the jump conditions for a macroscopic discontinuity in two-phase flow,[31] as used in the one-dimensional NOVA code. The jump conditions are extended to reflect the two-dimensional nature of the present model and also to reflect the influence of the container. We consider explicitly only the case when the ullage, or possibly a centercore igniter charge, is present. The conditions which apply as the mixture approaches an external boundary follow automatically in the code from the limiting behavior of a region of ullage of vanishing transverse dimension. Similarly, the case defined by an increment-to-increment interface is handled automatically by making each of the respective sets of boundary values compatible with an intervening region of ullage of vanishing transverse dimension.

We use subscript 1 to refer to the mixture and subscript 2 to refer to the exterior state. Quantities having subscript 1 will always be explicitly modeled state variables of the mixture. Quantities with subscript 2, however, will not necessarily be explicitly modeled exterior state variables. If the conditions at the boundary involve transfer to an external quasi-one-dimensional region, the quantities labelled with subscript 2 must be interpreted as characterizing the state of the gas which is subsequently mixed with the exterior gas as reflected by the terms involving $\dot{m}_j$ in quations 2.1.2.1, 2.1.2.2, 2.1.2.3, 2.1.2.6 and 2.1.2.7.

We define $\dot{m}_1 = \varepsilon_1 \rho_1 (\vec{u}_1 - \vec{u}_b) \cdot \vec{n}$ and similarly for $\dot{m}_2$ where, as in the preceding section, $\vec{u}_b$ is the boundary velocity and $\vec{n}$ is the outward pointing normal. At the boundary we assume that we have sources $\dot{m}_{sj}$,

$j = 1$ . . .J which are ordered so that $j = 1$, ..., J_1 are on the inside and $j = J_1 + 1$, ..., J are on the outside. The mass balance at the boundary is

$$\dot{m}_1 + \sum_{j=1}^{J} \dot{m}_{s_j} = \dot{m}_2 \qquad\qquad 3.4.1$$

The normal momentum balance[31] is generalized to reflect the pressure loss due to the impermeability of the container. We have

$$p_1 + \frac{\dot{m}_1^2}{\varepsilon_1 \rho_1 g_o} - \frac{K}{\varepsilon_1^2 \rho_1 g_o} \{ \dot{m}_1 + \sum_{j=1}^{J_1} \dot{m}_{s_j} \} | \dot{m}_1 + \sum_{j=1}^{J_1} \dot{m}_{s_j} | = p_2 + \frac{\dot{m}_2^2}{\varepsilon_2 \rho_2 g_o} \qquad 3.4.2$$

where K is the dimensionless friction factor used to characterize the flow loss through the container. We note that $\dot{m}_1 + \sum_{j=1}^{J_1} \dot{m}_{s_j}$ is the

gas-phase flux through the container. When rupture occurs we allow K to decrease to zero according to a linear dependence on time over the prespecified rupture interval. Referring to Equation 3.3.3 we may now identify Δp_{res} as the third term on the left-hand side of 3.4.2. We note that a positive value of Δp_{res} corresponds to an efflux.

The remaining physical conditions are the energy balance and the laws governing the transport of the tangential velocity component, the specific heats, the molecular weight, and, if finite rate chemistry is of interest—see Section 4.4—the reactant mass fraction. Let x represent any of the following: the total enthalpy, $h = e + \frac{p}{\rho} + \frac{|\vec{u} - \vec{u}_b|^2}{2 g_o}$; the tangential velocity component, u_T; either of the specific heats, c_v or c_p; the reciprocal of the molecular weight, $1/M_w$; or the reactant mass fraction, Y. Let x_{s_j} be the corresponding source attribute. Then

$$x_1 \dot{m}_1 + \sum_{j=1}^{J} x_{s_j} \dot{m}_{s_j} = x_2 \dot{m}_2 \qquad\qquad 3.4.3$$

If the boundary point lies on an endwall of an increment of per-forated stick propellant, Equations 3.4.1-3.4.3 apply separately to the flows in the interstices and the perforations, the appropriate voidage being used to determine ε_1 in each case. The source terms $\dot{m}_{s_j}$ which are specified as attributes of the bounding surface, are

assumed to be allocated to the interstitial and perforation flows in proportion to their respective voidages.

We conclude by commenting on the method of solution. As in the previous version of the code,[3] we view the gas-phase acoustic charac-teristic condition as furnishing an implicit relation between p_1 and $\dot{m}_1$. A similar relation follows for p_2 and $\dot{m}_2$ either from the characteristic condition, if the ullage is two-dimensional, or from the balance Equations 2.1.2.1-2.1.2.3, if the ullage is quasi-one-dimensional. These relations are solved simultaneously with 3.4.1 and 3.4.2 on the assumption that the density is unchanged. Updated values of the density and the remaining state variables follow from the material characteristic conditions and the relations of the form 3.4.3.

Special care is applied when making use of 3.4.3 to isolate the contributions of the source terms to the efflux from each side of the boundary. Attention is paid to the ordering of the source terms and the mixing of properties implicit in 3.4.3 is performed only for those components of the total flux which are found to emerge on the same side of the boundary. The importance of avoiding a spurious numerical mixing of properties becomes obvious if one considers, as an example, the case in which the boundary is impermeable and has an endothermic substrate on one side and an exothermic substrate on the other.

4.0 REVISIONS TO CONSTITUTIVE LAWS

For the most part, the topics dealt with in this chapter represent an attempt to bring the constitutive scope of TDNOVA into line with that of NOVA. We refer specifically to the use of the Robbins-Gough correlation for packed beds of granular propellant, Section 4.1; the influence of erosive burning, Section 4.2; the effect of heat loss to the tube, Section 4.5; and the variation of wall temperature with time, Section 4.6. The revised drag correlation is taken from reference 24, the treatment of erosive burning and heat loss are essentially as in Reference 9. Only the analytical results and the interpretation of these processes in the TDNOVA code are of interest here. References 9 and 25 may be consulted for derivations and additional source material.

The two additional topics--flow resistance in regions of quasi-one-dimensional ullage, Section 4.3, and finite rate combustion in the gas-phase, Section 4.4--are new to TDNOVA and, moreover, have no counterparts in the NOVA code.

As presently coded, the drag correlation of Section 4.1 and the flow resistance of Section 4.3 are default choices. Their selection may be overridden on an optional basis, in which case the previously encoded Ergun correlation is used for the packed granular bed and the flow resistance in the ullage is neglected. This feature has been incorporated to facilitate evaluations of the code during shakedown exercises.

4.1 Revised Interphase Drag Correlation for Granular Beds

We refer to earlier work[24] for a discussion of the derivation of the following correlation. We express the interphase drag in a granular bed in the following form

$$\vec{f}_s = \frac{1 - \varepsilon_e}{D_{p_e}} \left(\frac{\varepsilon}{\varepsilon_e}\right)^3 \rho |\vec{u} - \vec{u}_p| (\vec{u} - \vec{u}_p) \hat{f}_s \qquad 4.1.1$$

This differs from that of Reference 24 only in respect to the vector formulation necessary for the extension to a two-dimensional flow. This extension is identical to that used to extend the Ergun data from one to two dimensions in earlier formulations of TDNOVA.[1,2,3]

Equation 4.1.1 refers to the exterior voidage, ε_e, and the effective diameter, D_{p_e}, based on the exterior volume and surface area. The exterior properties are defined analogously to those of Section 2.2.1 for stick propellants. However, the influence of the ends of the grains and their finite lengths are taken into account when we deal with granular propellants. The remaining quantities in Equation 4.1.1 are defined as follows.

$$\hat{f}_s = \begin{cases} C\hat{f}_{s,RG} & \text{if } \varepsilon_e \leq \varepsilon_{e_o} \\ \max[C\hat{f}_{s,RG}(\dfrac{1-\varepsilon_e}{1-\varepsilon_{e_o}}\dfrac{\varepsilon_{e_o}}{\varepsilon_e})^{0.45}, \hat{f}_{min}] & \text{if } \varepsilon_{e_o} < \varepsilon \leq 1 \end{cases} \qquad 4.1.2$$

$$C = \begin{cases} 0.85 \text{ if the grain is perforated and unignited} \\ \\ 1.0 \quad \text{otherwise} \end{cases} \qquad 4.1.3$$

$$\hat{f}_{min} = \begin{cases} 0.3 \quad \text{for spheres} \\ \\ 0.75 \text{ for cylinders} \end{cases} \qquad 4.1.4$$

$$\hat{f}_{s,RG} = 2.50 \, Re_p^{-0.081} \lambda^{2.17} \qquad 4.1.5$$

$$Re_p = \rho_f \frac{|\vec{u} - \vec{u}_p|}{\mu_f} D_{p_e} \qquad 4.1.6$$

$$\lambda = \begin{cases} 1 & \text{for spheres} \\ \\ (1/2 + L/D)/(3L/2D)^{2/3} & \text{for cylinders} \end{cases} \qquad 4.1.7$$

We have used ε_{e_o} as the value of ε_e in the settled condition of the bed, L as the length of a cylindrical grain and D as its diameter, ρ_f and μ_f as the density and viscosity of the gas at the film temperature, and the remaining quantities correspond with the conventional nomenclature of this report.

4.2 Erosive Burning

According to Lenoir and Robillard,[27] the influence of erosion is presumed to be due to the superposition of the heat transfer due to bulk convection upon the heat feedback due to the flame. The former is ascertained according to the empirical correlation for interphase heat transfer without combustion suitably modified by an exponential blowing factor. When this feature is elected as an option, the steady state burn rate $\dot{d}_s$ is replaced by the erosive value $\dot{d}_{eros}$ according to

83

$$\dot{d}_{eros} = \dot{d}_s + K^* h_{con} \exp\{- \frac{\beta^* \rho_p \dot{d}_{eros}}{\rho |\vec{u} - \vec{u}_p|}\} \qquad 4.2.1$$

Here h_{con} is the convective heat transfer coefficient and K^*, β^* are composition-dependent coefficients which couple the cross flow to the surface regression rate. The definition of $\dot{d}_{eros}$ by Equation 4.2.1 is implicit and the value is determined by Newton's method.

4.3 Flow Resistance in Quasi-One-Dimensional Regions of Ullage

We assume that the wall shear can be described by the following relation for fully turbulent, fully developed, duct flow[28]

$$\tau = \frac{\mu u}{D_{ref}} Pr^{-1/3}(0.023 Re^{0.8} Pr^{0.4}) \qquad 4.3.1$$

where the reference length D_{ref} is related to the perimeter of the duct, P, and the cross-sectional area, A, according to

$$D_{ref} = \frac{4A}{P}$$

and

$$Re = \rho u D_{ref}/\mu$$

If we neglect the weak dependence on Prandtl number in view of the coarseness of the approximation associated with the use of 4.3.1 in the first place, we may express the wall resistance as a force per unit volume in the form

$$f_\omega = \frac{\tau P}{A} = \frac{0.096 \mu Re^{0.8}}{D_{ref}^2} \frac{u^2}{|u|} \qquad 4.3.2$$

In regions of ullage, f_ω is subtracted from the right-hand side of the momentum equation and $f_\omega \cdot u$ is added to the right-hand side of the energy equation. The cited equations are essentially the limiting forms of 2.1.2.2 and 2.1.2.3 as $\epsilon \to 1$.

4.4 Finite Rate Combustion in the Gas-Phase

In all previous work we have assumed that the combustion mechanisms are sufficiently rapid as to permit chemical equilibrium to be reached over an interval of time which is ballistically negligible and prior to transport of the gas out of the macroscopically infinitesimal control volume in which it was produced by decomposition of the solid propellant. Prior attempts to couple a more complex combustion model to the two-phase flow have been limited to studies of quasi-steady burning in which only the finite response time of the solid-phase was of interest.[38,39] The motivation for these earlier transient combustion analyses centered around the question of possible burn rate enhancement during that part of the interior ballistic cycle in which pressures were moderate--of the order of 10 MPa--but changing rapidly--at rates of 10^5 MPa/sec or more--so that the lagging thermal response of the solid-phase would dominate the combustion process.

Our motivation for the present code extension is centered around a different regime, one in which the pressures are very low and the rate of change of pressure is very small. Artillery weapons are frequently observed to have ignition delays of tens or even hundreds of milliseconds between the time the primer is discharged and the time at which significant combustion of the propellant is apparent. During that extensive delay it is possible that part of the charge is undergoing decomposition to intermediate products, that fizz burning is occurring as described by Vest et al,[40] and moreover that these intermediate products are flowing around the charge to form a potentially explosive accumulation of unreleased chemical energy.

To explore the possible consequences of fizz burning in artillery charges we assume that the combustion of the propellant occurs in two steps, namely gasification with heat release χe_p occurring so rapidly as to constitute a macroscopically local phenomenon, followed by a finite rate step governed by Arrhenius kinetics of arbitrary order, in which the balance of the chemical energy $(1 - \chi)e_p$ is released.

---

[38]Nelson, C., Robbins, F. W.,and Gough, P. S., "Predicted Effects of Transient Burning on Gun Flamespreading," Proc. 14th JANNAF Combustion Meeting.   1977

[39]Gough, P. S., "Revisions to the NOVA Code, Part III: Gas-Phase Constitutive Laws," Final Report for Task II, Contract N00174-78-C-0039 Paul Gough Associates Report PGA-TR-79-2   1979

[40]Vest, D. C., Clarke, E. V. Jr., Shoemaker, W. W., and Baker, W. F., "On the Performance of Primers for Artillery Weapons" Ballistic Research Laboratory Report 852, 1953 (AD 13294).

If we refer to the gas produced by the first step as the reactants and we denote the mass fraction of the gas-phase corresponding to the reactants by Y, we have the following balance equation for the reactant mass fraction.

$$\frac{D}{Dt}\varepsilon\rho Y + \varepsilon\rho Y\left[\frac{\partial u}{\partial t} + \frac{\partial v}{\partial r}\right] = \dot{m} - \varepsilon(\rho Y)^N A \exp\left(\frac{-E}{RT}\right) \qquad 4.4.1$$

where N is the reaction order and A and E are respectively the Arrhenius pre-exponential and exponential factors. The other nomenclature follows that of Section 2.1.1, but $\dot{m}$ differs from zero only within an increment consisting of that solid-phase species to which the finite rate combustion process applies. At present we assume that at most one such species is present in the charge. Other species may be present but their combustion is assumed to occur simultaneously with surface regression.

To conform with the present structure of the code we revise the energy equation on the assumption that e contains only the thermal component of the internal energy. It then follows that 2.1.1.5 must be revised to include the heating associated with reactant consumption.

One finds

$$\varepsilon\rho\frac{De}{Dt} + \varepsilon p\left[\frac{\partial u}{\partial z} + \frac{\partial v}{\partial r}\right] + p\frac{D\varepsilon}{Dt} = \frac{\vec{f}}{g_o} \cdot (\vec{u} - \vec{u}_p) - s_p q \qquad 4.4.2$$

$$+ \psi\left(e_{IG} - e + \frac{\vec{u} \cdot \vec{u}}{2g_o}\right) - \varepsilon p\frac{v}{r}$$

$$+ \dot{m}\left(\chi e_p + \frac{P}{\rho_p} + \frac{|\vec{u} - \vec{u}_p|^2}{2g_o} - e\right)$$

$$+ (1 - \chi)e_p\varepsilon(\rho Y)^N A \exp\left(\frac{-E}{RT}\right)$$

and a corresponding revision is required in Equation 2.1.2.3.

4.5   Heat Loss to the Tube

In Section 4.5.1 we describe two steady-state correlations which may be used to estimate the heat loss to the tube by reference to a convective heat transfer coefficient or film coefficient $h_{w_{con}}$. In Section 4.5.2 we describe the estimation of $h_{w_{con}}$ from an unsteady integral boundary layer model.

It should be understood that the two-phase flow defines the heat transfer but that the diffusion of the thermal boundary layer into the flow is not considered. The only influence exerted on the development of the two-phase flow is that defined by a volumetric rate of heat loss in the form

$$q_w = \frac{2}{R_{tube}} h_{w_{con}} (T - T_w) \qquad\qquad 4.5.1$$

Here q_w is the rate of heat loss which is subtracted from the right-hand sides of Equation 2.1.1.5 and 2.1.1.3, R_{tube} is the radius of the tube at the axial location of interest, T_w is the surface temperature of the tube wall and T is the temperature of the gas-phase. Some ambiguity obviously arises when we incorporate a volumetric term like q_w into a two-dimensional model. We have arbitrarily taken T to be a value of temperature in the external regions of annular ullage.

4.5.1   Heat Loss Estimated by Steady-State Correlations

We provide two alternative forms. The first is a correlation for a developing boundary layer on a flat plate. The second is a correlation for fully developed pipe flow. While the former is thought to be more appropriate, the latter is included to permit comparisons of TDNOVA heat loss predictions with those of NOVA in which the pipe flow correlation has been used previously.

Flat Plate Correlation

With z as the distance from the breech we define the film coefficient at z as[28]

$$h_{w_{con}} = 0.0288 \frac{k_f}{z} Pr^{1/3} Re_z^{0.8} \qquad\qquad 4.5.1.1$$

Here Pr is the Prandtl number, k_f is the thermal conductivity of the gas at the film temperature, $Re_z = \rho_f u z / \mu_f$ and u, ρ_f, μ_f are respectively the gas velocity and the gas density and viscosity at the film temperature.

87

Equation 4.5.1.1 has a singularity at $z = 0$. However, in our application it is always the case that $u = 0$ for $z = 0$ so that the singularity can be ignored.

Pipe Flow Correlation

As in the NOVA code[9] we have [28]

$$h_{w_{con}} = 0.023 \frac{k_f}{D_{HYD}} Re_D^{4/5} Pr^{2/5} \qquad 4.5.1.2$$

where $Re_D = \rho_f u D_{HYD}/\mu_f$ and the hydraulic diameter, D_{HYD}, which incorporates the presence of the solid propellant is defined as

$$D_{HYD} = \frac{2\epsilon R_T}{1 + \frac{2R_T(1 - \epsilon)}{D_p}} \qquad 4.5.1.3$$

We evaluate the porosity ϵ and the effective particle diameter D_p on the external boundary of the propelling charge.

4.5.2 Heat Loss Estimated by Transient Boundary Layer Model

Of the two empirical correlations considered in the preceding section, that pertaining to the flat plate is to be preferred on the grounds that it expresses the developing thickness of the wall boundary layer with increasing distance from the breech. The estimation of the boundary layer thickness at each cross section is, however, based on purely local properties of the flow. The integral boundary layer model of Shelton et al[29] provides a basis for expressing the influence, on local boundary layer thickness, of the gradients and rates of change of the core flow state variables. It provides a useful extension of the theoretical basis for estimating heat loss provided that the flow conditions do not vary too rapidly in space or time. The characteristic times of the core flow must be sufficiently long to allow the turbulent structure of the flow to reach steady flow characteristics and must also be long by comparison with the characteristic time for information to diffuse through the boundary layer.

According to Shelton et al, the convective heat transfer coefficient is related to the local momentum displacement thickness θ as follows.

$$h_{w_{con}} = \frac{\rho_f u c_p}{Pr^{2/3}} A \left(\frac{\rho_f u \theta}{\mu_f} \right)^{-B} \qquad 4.5.2.1$$

With $\Theta = \theta^{(1+B)}$ we have the governing equation for the boundary layer thickness as

$$\frac{\partial \Theta}{\partial t} = - \frac{\Theta}{H} \frac{\partial \Theta}{\partial z} + (1 + B) \frac{A}{H} \frac{\mu_f^{B}}{\rho_f^{B}} u^{(1-B)} \qquad 4.5.2.2$$

$$- (1 + B) \Theta \left\{ \frac{1}{\rho_f} \left(\frac{\partial \rho_f}{\partial t} + \frac{u}{H} \frac{\partial \rho_f}{\partial z} \right) + \frac{1}{u} \left(\frac{\partial u}{\partial t} + \frac{H + 2}{H} u \frac{\partial u}{\partial z} \right) \right\}$$

$$+ (1 + B) C \frac{\Theta}{u} \left\{ \frac{1}{\rho_f} \frac{\partial p}{\partial z} + \frac{\partial u}{\partial t} + u \frac{\partial u}{\partial z} \right\}$$

in which A, B, C and H are coefficients to be defined by the user and the remaining nomenclature is as in the preceding section. Experience with the NOVA code has shown that unless the ballistic environment is free from pressure waves, Equation 4.5.2.2 may become unstable. The presence of the factor Θ/u in the last group of terms suggests why this may be so. Following Shelton et al Θ is set equal to zero at the breech and at the base of the projectile.

4.6 Determination of the Temperature of the Tube Wall

The heat loss to the tube wall depends on the wall temperature itself, both directly as shown in Equation 4.5.1 and indirectly, through the evaluation of gas-phase properties at the film temperature. The default options of TDNOVA result in the neglect of both the heat loss and the variation of wall temperature. Even if the heat loss is computed, according to any of the preceding methods, it is still possible to neglect the variation in the temperature of the wall. If the variation of temperature is to be considered, either of the following methods may be used.

4.6.1 Cubic Profile Approximation

Under the assumption that the temperature profile in the tube wall can be represented by a cubic polynomial, it follows that the surface temperature is given by

$$T_w = T_{w_o} - \frac{2}{3} \frac{h_{w_{con}} H_w}{k_w^2} + \left\{ \left(T_{w_o} - \frac{2}{3} \frac{h_{w_{con}} H_w}{k_w^2} \right)^2 + \frac{4}{3} \frac{h_{w_{con}} TH_w}{k_w^2} - T_{w_o} \right\}^{\frac{1}{2}} \quad 4.6.1.1$$

where H_w is a solution of the equation

$$\frac{\partial H_w}{\partial t} = \alpha_w h_{w_{con}} (T - T_w) \quad\quad\quad 4.6.1.2$$

and we have T_{w_o} as the initial value of T_w and k_w as the thermal conductivity of the wall.

4.6.2 Invariant Embedding Solution

When the transient boundary layer model is used to compute the heat loss one may also obtain solutions for the thermal response of the tube at selected stations by means of a finite difference solution of the heat conduction equation. However, the solutions so obtained are passive in the sense that they are not coupled to the heat loss calculation in Equation 4.5.1. Full coupling would require that the solution be obtained at roughly as many axial stations as the number of axial mesh points used to resolve the two-phase flow. The computational expense of such an approach was not thought to be justified in the one-dimensional NOVA code[9] and is accordingly not pursued here either.

Reference 9 may be consulted for a complete discussion of the method of invariant embedding. Here we merely note that it is a computational approach based on an initial timewise discretization of the heat conduction equation, followed by a Ricatti transformation of the resulting ordinary differential equation for the spacewise dependence of temperature. The discussion of Reference 9 includes a provision for a regressing surface since the method is also used to analyze transient combustion mechanisms. The version of the invariant embedding algorithm encoded into TDNOVA does not support the modeling of transient combustion.

ACKNOWLEDGEMENTS

REFERENCES

1. Gough, P. S.
    "Two-Dimensional Convective Flamespreading in Packed
    Beds of Granular Propellant"
    Ballistic Research Laboratory Contract Report ARBRL-CR-00404   1979
                                            (AD A075326)

2. Gough, P. S.
    "A Two-Dimensional Model of the Interior Ballistics
    of Bagged Artillery Charges"
    Ballistic Research Laboratory Contract Report ARBRL-CR-00452   1981
                                            (AD A100751)

3. Gough, P. S.
    "Two-Dimensional, Two-Phase Modeling of Multi-Increment
    Bagged Artillery Charges"
    Ballistic Research Laboratory Contract Report ARBRL-CR-00503   1982
                                            (AD A125482)

4. Einstein, S., Pellington, B., and Westley, S.
    "Charge Design Technology"
    Applied Sciences Division, ARRADCOM, Dover, NJ   1980

5. Baer, P. G., and Frankle, J. M.
    "The Simulation of Interior Ballistic Performance of
    Guns by Digital Computer Program"
    Ballistic Research Laboratory Report 1183 (AD 299980).   1962

6. Kent, R. H.
    "Study of Ignition of 155mm Gun"
    Ballistic Research Laboratory Report 22 (AD 494703).   1935

7. Heddon, S. E., and Nance, G. A.
    "An Experimental Study of Pressure Waves in Gun Chambers"
    Naval Proving Ground Report 1534   1957

8. Budka, A. J., and Knapton, J. D.
    "Pressure Wave Generation in Gun Systems--A Survey"
    Ballistic Research Laboratory Memorandum Report 2567   1975
                                            (AD B008893L)

9. Gough, P. S.
    "The NOVA Code: A User's Manual"
    Naval Ordnance Station Contract Report IHCR 80-8   1980

10. Horst, A. W., Smith, T. C., and Mitchell, S. E.
    "Key Design Parameters in Controlling Gun Environment
    Pressure Wave Phenomena--Theory versus Experiment"
    Proc. 13th JANNAF Combustion Meeting   1976

11. Horst, A. W., and Gough, P. S.
    "Influence of Propellant Packaging on Performance of
    Navy Case Gun Ammunition"
    J. Ballistics v. 1, p. 229   1977

12. Gough, P. S.
    "Theoretical Study of Two-Phase Flow Associated with
    Granular Bag Charges"
    Ballistic Research Laboratory Contract Report ARBRL-CR-00381 1978
                                        (AD A062144)

13. Horst, A. W., and Gough, P. S.
    "Modeling Ignition and Flamespread Phenomena in Bagged
    Artillery Charges"
    Ballistic Research Laboratory Technical Report
    ARBRL-TR-02263 (AD A091790)   1980

14. May, I. W., and Horst, A. W.
    "Charge Design and Pressure Waves in Guns"
    Progress in Astronautics and Aeronautics, Vol. 68,
    Interior Ballistics of Guns, edited by H. Krier and
    M. Summerfield   1979

15. Gelperin, N. I., and Einstein, V. G.
    "Heat Transfer in Fluidized Beds"
    Fluidization, edited by Davidson, J. F., and
    Harrison, D., Academic Press, NY   1971

16. Ergun, S.
    "Fluid Flow Through Packed Columns"
    Chem. Eng. Progr. v. 48, p. 89   1952

17. Andersson, K. E. B.
    "Pressure Drop in Ideal Fluidization"
    Chem. Eng. Sci. v. 15, p. 276   1961

18. Thompson, J. F., Thames, F. C., and Mastin, C. W.
    "Automatic Numerical Generation of Body-Fitted
    Curvilinear Coordinate Systems for Field Containing
    Any Number of Arbitrary Two-Dimensional Bodies"
    J. Comp. Phys. v. 15, p. 299   1974

19. MacCormack, R. W.
    "The Effect of Viscosity in Hypervelocity Impact
    Cratering"
    AIAA Paper No. 69-354   1969

20. Moretti, G.
    "Calculation of the Three-Dimensional, Supersonic,
    Inviscid, Steady Flow Past an Arrow-Winged Airframe"
    POLY-AE/AM Report No. 76-8, Polytechnic Institute of
    New York   1976

21. Horst, A. W.
    "Baseline Evaluation of the TDNOVA Code"
    Ballistic Research Laboratory Memorandum Report
    ARBRL-MR-03198 (AD A120718).   1982

22. Horst, A. W.
    "A Comparison of Barrel-Heating Processes for Granular
    and Stick Propellant Charges"
    Ballistic Research Laboratory Memorandum Report
    ARBRL-MR-03193 (AD A118394).   1982

23. Robbins, F. W. and Gough, P. S.
    "Influence of Length and Diameter of Cylinders on
    Packed Bed Flow Resistance"
    Proc. 16th JANNAF Combustion Meeting   1979

24. Gough, P. S.
    "Extensions to NOVA Flamespread Modeling Capacity"
    Final Report, Task I, Contract N00174-80-C-0316
    Paul Gough Associates Report PGA-TR-81-2   1981

25. Hinze, J. O.
    "Turbulence"
    McGraw-Hill   1959

26. Jakus, K.
    "Feasibility of a Laboratory Ignition Test for Lot
    Acceptance of Gun Propellant"
    Report No. ASR-SD-QA-A-P-59-74, ARRADCOM, Dover, N.J.   1974

27. Lenoir, J. M. and Robillard, G.
    "A Mathematical Method to Predict the Effects of
    Erosive Burning in Solid-Propellant Rockets"
    Sixth Symposium (International) on Combustion
    Reinhold, New York   1957

28. Holman, J. P.
    "Heat Transfer"
    McGraw-Hill   1968

29. Shelton, S., Bergles, A., and Saha, P.
    "Study of Heat Transfer and Erosion in Gun Barrels"
    Air Force Armament Lab. AFATL-TR-73-69   1973

30. Meyer, G. M.
    "Initial Value Methods for Boundary Value Problems"
    Academic Press, NY   1973

31. Gough, P. S.
    "Numerical Analysis of a Two-Phase Flow with Explicit
    Internal Boundaries"
    Naval Ordnance Station Contract Report IHCR 77-5   1977

32. Gough, P. S.
    "On the Closure and Character of the Balance Equations
    for Heterogeneous Two-Phase Flow"
    Dynamics and Modelling of Reactive Flow Systems
    Academic Press   1980

33. Kutateladze, S. S., and Borishanskii, V. M.
    "A Concise Encyclopedia of Heat Transfer"
    Pergamon Press   1966

34. Robbins, F. W.
    "Continued Study of Stick Propellant Combustion Processes"
    Proc. 19th JANNAF Combustion Meeting   1982

35. Juhasz, A., Robbins, F. W., Bowman, R. E., and Doali, J. O.
    "Combustion Characteristics of NOSOL 363 Single-Perforated
    and Slotted Stick Propellant"
    Proc. 19th JANNAF Combustion Meeting   1982

36. Harvey, J. F.
    "Theory and Design of Modern Pressure Vessels"
    van Nostrand Reinhold   1974

37. Fung, Y. C.
    "Foundations of Solid Mechanics"
    Prentice-Hall   1965

38. Nelson, C., Robbins, F. W., and Gough, P. S.
    "Predicted Effects of Transient Burning on Gun
    Flamespreading"
    Proc. 14th JANNAF Combustion Meeting   1977

39. Gough, P. S.
    "Revisions to the NOVA code, Part III: Gas-Phase
    Constitutive Laws"
    Final Report for Task II, Contract N00174-78-C-0039
    Paul Gough Associates Report PGA-TR-79-2   1979

40. Vest, D. C., Clarke, E. V. Jr., Shoemaker, W. W., and
    Baker, W. F.
    "On the Performance of Primers for Artillery Weapons"
    Ballistic Research Laboratory Report 852 (AD 13294)   1953

APPENDIX A

TDNOVA - STRUCTURE AND USE

Appendix: TDNOVA – Structure and Use

The purpose of this Appendix is to provide sufficient information to enable the reader to make use of TDNOVA. To that end we provide, in three successive subsections, an overview of the code macrostructure, a brief discussion of the storage arrays and the principal storage pointers, and a complete description of the code input and output files.

CODE MACROSTRUCTURE

TDNOVA is written in the Fortran IV language. Because it was developed on a 32 bit word machine (ITEL AS-6), all computations are performed in double precision. Thus, users of the code who employ a machine in which the standard word length is 60 or more bits, such as the CYBER 7600 may wish to convert the code to single precision as a measure of economy.

To further expedite execution on a CYBER 7600, TDNOVA contains level 2 storage specification for the major arrays. These are masked as comment cards to provide compatibility with other machines. The level 2 storage specification on the CYBER system may be activated by a global text editing command in which the string C*LCM is replaced by five blanks.

The code macrostructure is illustrated schematically in Figure A.1. The main program TDMAIN is essentially a dummy routine. It executes a call to INPUT, to read and print the problem data, to SETUP, to initialize the problem variables, and then transfers complete control of the calculation to subroutine TDXC, which is, in fact, the principal executive routine. The code version at BRL, following the return from TDXC, also executes a call to a BRL routine called RECAP, whose purpose is to plot data accumulated in the summary tables during the evolution of the solution.

Users who wish to reduce the overall code storage may perform successive overlays onto INPUT and SETUP since these subroutines are each called just once.

The next level of code structure is defined by the principal linkages to the executive TDXC. TDXC is supported by the output routine LOGOUT which is called intermittently to prepare tables of state variables at various times. LOGOUT also stores the solution on disc, if desired, and executes optional calls to PLOTRZ which is responsible for the preparation of graphic representations of the solution. PLOTRZ may be seen to be supported by subroutines PLTLOD, PLTFLO, CONTR, and SEE. Additional output processing is performed by subroutine SUMTAB, which prepares tables of summary data, as

99
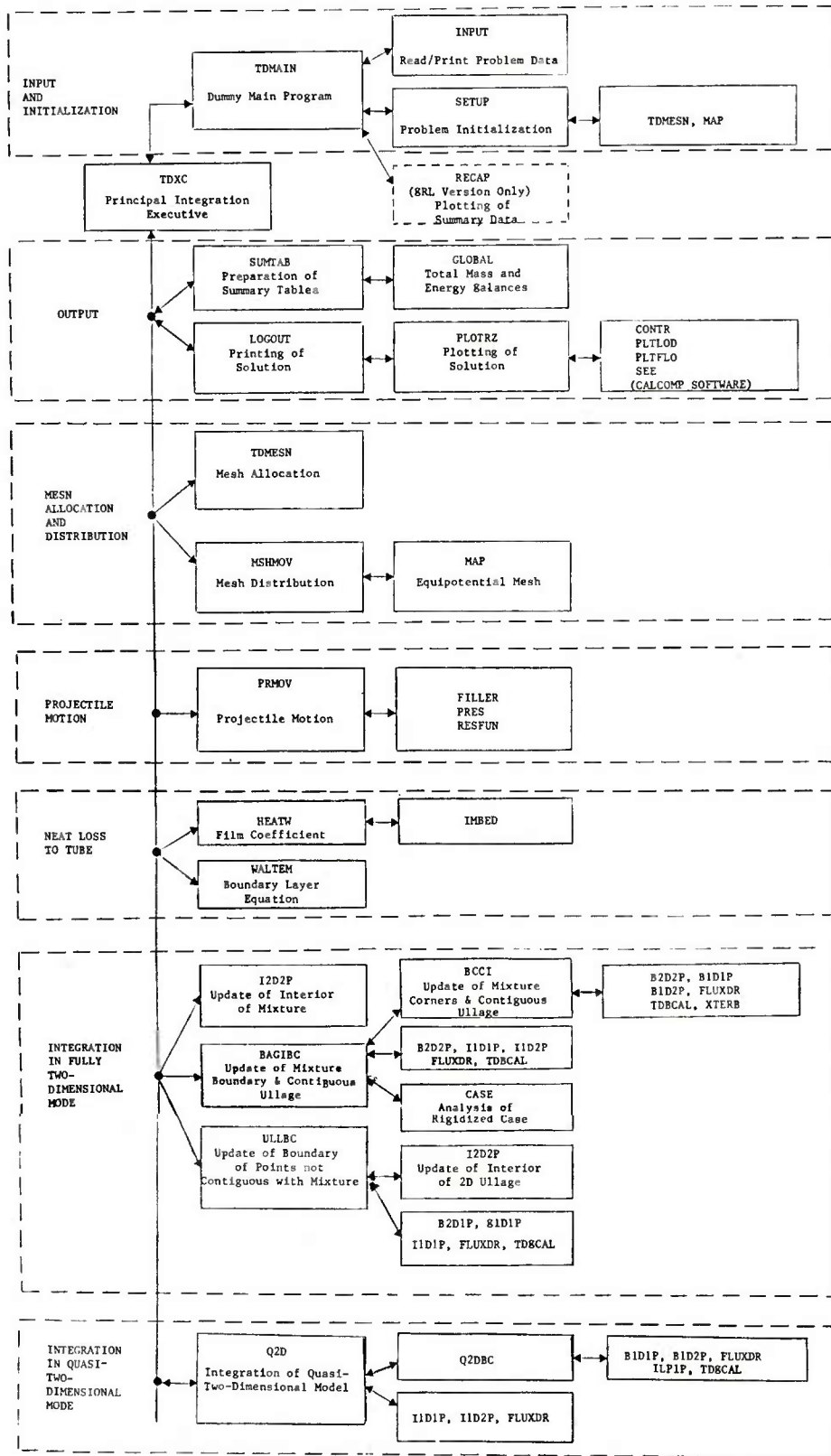
Figure A.1 Schematic Illustration of TDNOVA Macrostructure
(Only principal linkages and routines are shown. See Table A.1)

desired. These, however, are only printed at the conclusion of the run. It is these data which are further processed by the BRL routine RECAP.

SUMTAB is supported by GLOBAL which prepares histories of total system mass and energy. These are printed at the conclusion of the run and serve as an indication of the magnitude of the numerical accuracy of the calculation. Care should be exercised in the interpretation of the tabulated histories of global mass and energy defect. Particular aspects of the calculation may be characterized by numerical accuracy significantly greater or significantly less than the global balances. However, a particularly large defect of mass or energy--in excess of one or two percent--should be viewed as an indication that either additional mesh points are required or that some algorithm refinement is required.

TDXC is further supported by TDMESH and MSHMOV. TDMESH allocates storage to the various computational regions. MSHMOV generally establishes a boundary-fitted equipotential mesh in each two-dimensional region, although a solid-phase lagrangian map may be specified for two-dimensional regions occupied by the mixture.

The integration at all points interior to the mixture is performed by I2D2P. Subroutine ULLBC executes calls to I2D1P to update the solution in the interior of all fully two-dimensional regions of ullage and also performs the update of all ullage boundary points which are not contiguous with the mixture. In the latter capacity it is supported by the routines B1D1P, I1D1P and B2D1P.

Subroutine BACIBC is called by TDXC to effect the update of all points on the boundary of the mixture as well as those points in the ullage which are contiguous with the mixture. For this purpose, mesh points in a region of quasi-one-dimensional ullage adjacent to the mixture are regarded as contiguous with the mixture. BACIBC is supported by the routines I1D1P and I1D2P which update points in the interior of adjacent quasi-one-dimensional regions.

Points on the corners of the mixture are updated by BCCI which calls the computational routines B1D1P, B1D2P and B2D2P. When two-dimensional regions of ullage are present, BCCI also calls XTERB.

The previously existing routines BAGBC and XTERA have been deleted from the present version of the code, their responsibilities having been reassigned to BAGIBC and BCCI.

101

Subroutines I2D2P, ULLBC and BAGIBC are called only until the flow has evolved to such a point as to be amenable to a quasi-two-dimensional analysis. Subsequently TDXC is supported entirely by the routine Q2D which acts as the integration executive for the quasi-two-dimensional representation. Q2D enforces the conditions of physical compatibility between regions and is supported by the subroutines I1D1P, I1D2P at the interior mesh points. At the boundaries Q2D is supported by Q2DBC which in turn makes use of B1D1P, B1D2P and ILP1P.

We also note that TDXC is cycled twice per complete integration step since each step is composed of a predictor and a corrector level as discussed further in the next section when we consider the structure of the storage arrays.

TDNOVA does contain other routines than those which we have mentioned explicitly in this section. A complete summary of the various routines and their linkages to one another is contained in Table A.1. Following the entry for TDMAIN, all the routines are described in alphabetical order. Not shown in Table A.1 are the linkages to standard Fortran functions and to the standard CALCOMP software package. The use of the latter may be system-dependent, particularly with regard to the plot initialization and termination routines.

DATA STORAGE

Table A.2 provides a summary of all the program variables stored in common blocks. Variables which are purely local to a given sub-routine or function are not described in Table A.2.

It should be noted that due to the evolutionary nature of the code, some of the variables listed in Table A.2 may be obsolete or inactive.

The purpose of the present discussion is to provide a description of the principal pointers and to explain the manner in which the state variables are stored.

Each integration step consists of two levels, a predictor and a corrector. The counter NDT, initialized to zero, is bumped by unity on each predictor and each corrector level. The switch INT = MOD(NDT+1,2) is equal to 1 on a predictor level and 0 on a corrector level. At each level the variables NI, NF, NP are used to construct pointers to current, future, and past storage and they cyclically run through the values 1,2,3.

If the total number of propellant increments is denoted by NBAGS, then a total of NRG = 9 + 3*(NBAGS − 1) computational regions are defined. A case involving 3 increments for which NRG = 15 is illustrated in Figure A.2.
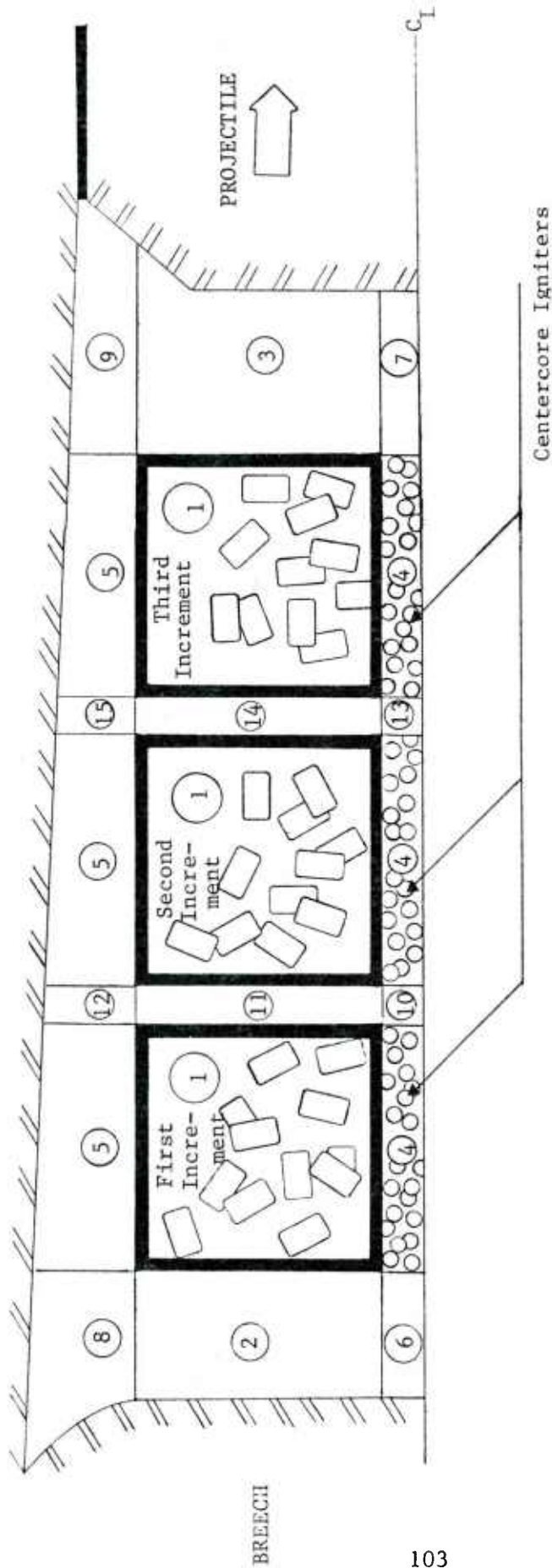
Figure A.2 Nomenclature for Region Labelling in TDNOVA Illustrated for Problem Involving Three Increments

Each region I has attributes NDZ(I), the total number of axial mesh points; NDR(I), the total number of radial mesh points; MODL(I), an indicator of the type of flow equations to be used; and NRBIAS(I), used to construct storage pointers, as described below. The indicator MODL(I) has the following set of values.

MODL(I)	Type of Flow in Region I
1	Lumped Parameter One-Phase (LP1P)
2	Quasi-One-Dimensional One-Phase (1D1P) (Axially directed)
3	Quasi-One-Dimensional One-Phase (1D1P) (Radially directed)
4	Two-Dimensional One-Phase (2D1P)
5	Quasi-One-Dimensional Two-Phase (1D2P)
6	Two-Dimensional Two-Phase (2D2P)

The parenthetical acronyms for each type of region are also present in the names of subroutines dedicated to the integration of each type of region with the further distinguishing characteristic of an initial letter I or B according as the routine pertains to interior or boundary mesh points. The distinction between cases MODL(I) = 2 and 3 is purely formal in the present version of the code.

The state variables are stored in singly indexed arrays. Accordingly, the values pertaining to a given mesh point at a given level of a given time step are located by construction of a suitable pointer.

In order to retain as many of the existing code storage conventions as possible, we have used the previous region labels for those regions which do not lie between successive increments. Thus, as may be seen in Figure A.1, we refer to the propelling charge as region 1 even when several different increments are present. Similarly, regions 4 and 5 extend the length of the entire charge. But these regions--1, 4 and 5 may be interrupted by new regions--10, 11 and 12, for example--when several increments are present.

In our subsequent discussion of the storage pointer construction we will consider first the case when one increment is present. Then we will note the additional considerations which must be taken into account when two or more increments are present and we will note the influence of the presence of stick propellant. Finally, we will comment on the array aliasing which has been incorporated to minimize further increases in storage requirements.

104

As in our previous report[3] we consider, as an example, the gas-phase density, which is stored in the array RHO(J).

When only granular charges are considered, the array RHO contains values of density in the following order. First, the NDZ(1) values pertaining to the line $\eta = 0$ in region 1 (the mixture) are stored. These are followed by successive blocks of NDZ(1) values corresponding to successive increments of the coordinate η. There are, of course, a total of NDR(1) such blocks. Then there are loaded NDZ(2) values corresponding to the line $\eta = 0$ for region 2 and so on through region NRG. It should be noted that NDZ and NDR are each equal to at least one for any type of region. A lumped parameter region has NDZ = NDR = 1.

Following the last value for region NRG, there are loaded NDZ(1) values for the line $\eta = 0$ in region 1 corresponding to the next level of integration. Three such integration level blocks are defined.

The quantity NRBIAS(I) is defined as

$$
\text{NRBIAS(I)} = \begin{cases} \displaystyle\sum_{J=1}^{I-1} \text{NDZ(J)*NDR(J)} & \text{for } I > 1 \\ \\ 0 & \text{for } I = 1 \end{cases}
$$

and the total number of mesh points is given by

$$
\text{NPTOT} = \sum_{J=1}^{NRG} \text{NDZ(J)*NDR(J)}
$$

We also define the quantity

$$
\text{NIBIAS} = (\text{NI} - 1)*\text{NPTOT}
$$

and an analogous definition is given for NPBIAS, NFBIAS which are used to construct pointers to NP- and NF- integration levels, respectively.

Now let $\rho_{IJ,K}^{NI}$ be the value of ρ at the ζ-mesh point I, the η-mesh point J, in region K, at level NI, then

$$
\rho_{IJ,K}^{NI} = \text{RHO(NIBIAS + NRBIAS(K) + (J - 1)*NDZ(K) + I)}
$$

This pattern is followed for all the independent state variables. However for dependent state variables, such as the internal energy, only current storage is maintained. Thus pointers for the array E are constructed similarly to those for RHO, but the quantities NIBIAS, NPBIAS, NFBIAS are not used.

In the preceding discussion it has been assumed that only one increment was present. In fact, when several increments are present only minor revisions to the construction of the storage pointer are required and then only for regions 1, 4 and 5.

Let I_L identify a ζ-mesh point which lies in the L-th increment and let I_L take the value 1 at the left boundary of the increment and the value NSDZ(L) at the right boundary. Define the bias

$$
\text{NSBIAS(L)} = \begin{cases} \sum\limits_{J=1}^{L-1} \text{NSDZ(J)} & \text{for } L > 1 \\\\ 0 & \text{for } L = 1 \end{cases}
$$

Then, with I_L understood to be particularized to the L-th increment, as described above, we have

$$
\rho_{I_L J, K}^{NI} = \text{RHO(NIBIAS} + \text{NRBIAS(K)} + (J - 1)*\text{NDZ(K)} + \text{NSBIAS(L)} + I_L)
$$

It should be emphasized that NDZ(K) is used to construct the pointer and not NSDZ(K).

When stick propellant is present, dual storage is made for all the state variables in region 1. We define the quantity INBIAS as

INBIAS = NDZ(1)*NDR(1)

Then the pointer to exterior properties in region 1 is constructed as before. The pointer to interior properties is defined by adding to the exterior pointer the quantity INBIAS. The region bias NRBIAS is modified to become

$$
\text{NRBIAS(I)} = \sum\limits_{J=1}^{I-1} \text{NDZ(J)*NDR(J)} + \text{INBIAS} \qquad \text{for } I > 1
$$

Storage could be assigned more efficiently if only part of the charge consisted of perforated stick propellant, but only at the expense of further complications in pointer construction.

To minimize storage increases in the present code extension, some aliasing of variables has been done. The following pairs of arrays have been equivalenced:

(HW,H), (TW,D), (QW,TP), (BL,THCK), (SIGW, SIG), (ZMW, EPS),

(UW, UP), (THCKS, UPR)

This equivalencing has been made possible because storage for the first of the quantities is assigned to regions for which the second quantity is undefined. HW, TW, QW and BL are defined only for ullage regions contiguous with the tube wall. SIGW, ZMW and UW are defined only for region 5. THCKS is a special case and the user is referred to function JTHCKS for further information concerning pointer construction for this array.

INPUT AND OUTPUT FILES

TDNOVA is structured to run only one problem. It does not support parametric input, nor does it search for a new data set following problem termination. A given problem, however, may be stored on disc at various points during the solution, as part of the logout procedure. Subsequently, the problem may be restarted from disc at any intermediate point at which logout has been performed. The structure of the input files is described fully in Table A.3 and requires no additional comment here.

We conclude with a description of the output files. Logout may be obtained at multiples of an inputted number of integration steps and at multiples of an inputted increment of time. The logout associated with such intermediate points of the solution consists of printed text, disc storage and plotting, all in accordance with user-selectable options.

When printed logout is requested it is furnished as a table of the current storage of the state variables in the order of storage described in the preceding section. Thus the table proceeds to list the state variables region by region. Within each region, the state variables are tabulated in successive blocks of constant η (which may be thought of as approximately constant radius). For region 1, however, when several increments are present, we print all data for the first increment, followed by all data for the second increment, and so on. The tabulated quantities are, in order: Region number as described in Figure A.2, mesh axial coordinate, mesh radial coordinate, gas-phase pressure, intergranular stress, gas-phase axial velocity, gas-phase radial velocity, solid-phase axial velocity, solid-phase radial velocity, porosity, gas-phase density, gas-phase temperature, solid-phase surface temperature, and, for points on the boundary of the increment, indicators as to whether the increment is permeable and/or ruptured.

Exceptions to the foregoing are as follows. When stick propellant is present, the exterior properties at each location are followed immediately by the interior values at the same location. If a rigidized case is present, the wall velocity and axial stress are tabulated in the columns reserved for solid-phase axial velocity and intergranular stress in the block of data for region 5. Quantities pertaining to the heat

transfer to the wall similarly usurp columns pertaining to the solid-phase but are only defined and printed in blocks of data pertaining to regions of ullage adjacent to the tube wall.

As an option, any of the state variables may be plotted as an isometric view of the surface $\phi(z,r)$ where ϕ is a state variable. Hidden lines are normally deleted, but may be retained as an option. Further information concerning the solution may be had by requesting contour plots of the same surfaces. The isometric and contour plotting options are, however, fully independent of one another. An additional option is the preparation of flow field plots in which the velocity fields of the gas- and solid-phases are represented, separately, as vector fields superimposed on the computational mesh.

If stick propellant is present, the plots are provided for both exterior and interior mixture properties whenever there is a distinction.

A plot of the ignition delay, essentially a contour representation, may also be had. This is prepared just once, at the conclusion of the run. It should be noted that this map is constructed by reference to the initial configuration of the propelling charge.

In addition to the intermediate logout one may request certain summary data. These are accumulated during the run and are printed following the completion of the calculation. A table of summarized interior ballistic data is printed which contains, in order: time, breech pressure, base pressure and space mean pressure, mass fraction of unburnt propellant, mass fraction of unburnt centercore charge, projectile travel, velocity and acceleration. The pressures are all centerline quantities. These tables are always followed by the tabulations of global mass and energy balance. Optionally, these summary data may be followed by pressure histories at user-selectable locations for comparison with experimental pressure gage records. These values of pressure may be obtained at any axial location on either the tube or the centerline. The tabulation of these histories is followed by a tabulation of the histories of pressure difference formed by subtracting the last pressure history from each of the others. Finally, if passive invariant embedding has been used to determine the temperature of the tube wall, the surface temperature histories are tabulated at each of the specified locations.

Table A.1   Summary of TDNOVA Routines and Linkages

TDMAIN

Purpose: Dummy main program. Calls INPUT to read and print data, SETUP to initialize problem and then calls TDXC, which is the principal executive routine, to integrate the solution. The BRL version also executes an optional call to RECAP to plot the summary data.

Calls: INPUT, (RECAP), SETUP, TDXC

Called by: None

AP

Purpose: Function to compute rate of propagation of intergranular disturbances as a function of porosity and direction of loading.

Calls: SIGL

Called by: B1D2P, B2D2P, I1D2P, I2D2P

AREA

Purpose: Function to compute area of quadrilateral defined by four mesh points.

Calls: None

Called by: BCCI, GLOBAL, Q2DBC, SETUP, SUMTAB, TDMESH, XSECT

BAGIBC

Purpose: Subroutine to enforce physical boundary conditions at all mixture boundary mesh points as well as contiguous ullage points.

Calls: BCCI, BCS1, BCS2, B2D1P, B2D2P, CALFLO, CALPRM, CASE, DBUG, DIS, DISBAG, FLUXDR, I1D1P, I1D2P, NAYBOR, TANLOS, TDBCAL

Called by: TDXC

BCCI

Purpose: Subroutine to enforce physical boundary conditions at all mixture corner points as well as contiguous ullage points.

Calls: AREA, BCS1, BCS2, B1D1P, B1D2P, B2D2P, CALFLO, DBUG, DIS, DISBAG, FLUXDR, ILP1P, LOGOUT, NAYBOR, SUMTAB, TDBCAL, XTERB

Called by: BAGIBC

109

BCS1   Purpose: Subroutine to make solid-phase state
                variables compatible with prescribed value of
                normal velocity or of intergranular stress.

                Calls: None

                Called by: BAGIBC, BCCI, BCS2, Q2DBC

BCS2   Purpose: Subroutine to make solid-phase state
                variables on each side of a mixture-to-mixture
                interface compatible with each other.

                Calls: BCS1

                Called by: BAGIBC, BCCI, Q2DBC

BLKDAT   Purpose: Block data initialization

                Calls: None

                Called by: None

B1D1P   Purpose: Subroutine to perform trial update of
                boundary point of a quasi-one-dimensional single-
                phase region.

                Calls: GETFW, GETQW, PSI, YUPD

                Called by: BCCI, Q2DBC, ULLBC, XTERB

B1D2P   Purpose: Subroutine to perform trial update of
                boundary point of a quasi-one-dimensional two-
                phase region.

                Calls: AP, CDB, CDBRG, DELAY, DP, EROSE,
                            GETQW, PROPER, PSI, QP, RDOT, SIGL,
                            YUPD

                Called by: BCCI, Q2DBC, XTERB

B2D1P   Purpose: Subroutine to perform trial update of
                boundary point of a two-dimensional, single-phase
                region.

                Calls: GETQW, LOGOUT, PSI, YUPD

                Called by: BAGIBC, ULLBC, XTERB

110

B2D2P	Purpose: Subroutine to perform trial update of boundary point of a two-dimensional, two-phase region.
	Calls: AP, CDB, CDBRG, DELAY, DP, EROSE, GETQW, LOGOUT, PROPER, PSI, QP, RDOT, YUPD, ZSLOT
	Called by: BAGIBC, BCCI
CALFLO	Purpose: Subroutine to calculate rate of reaction of bag substrate at a given point.
	Calls: IGBAG, JTHCKS, PROPER, RDOT
	Called by: BAGIBC, BCCI, Q2D, Q2DBC, XTERB
CALPRM	Purpose: Subroutine to compute friction factor associated with bag flow resistance at a given mesh point.
	Calls: None
	Called by: BAGIBC, LOGOUT
CASE	Purpose: Subroutine to update state of rigidized case sidewall.
	Calls: DBUG, DIS, DISBAG, JTHCKS
	Called by: BAGIBC
CDB	Purpose: Function to compute friction factor associated with flow resistance through granular bed according to Ergun correlation.
	Calls: None
	Called by: B1D2P, B2D2P, I1D2P, I2D2P, Q2D
CDBRG	Purpose: Function to compute friction factor associated with flow resistance through granular bed according to Robbins-Gough correlation.
	Calls: EPTOR, VIS
	Called by: B1D2P, B2D2P, I1D2P, I2D2P, Q2D

CONTR

Purpose: Subroutine to prepare contour plots of a given state variable.

Calls: None

Called by: PLOTRZ

DBUG

Purpose: Subroutine to determine need for debug print at a given mesh point.

Calls: None

Called by: BAGIBC, BCCI, CASE, I2D2P, Q2D, Q2DBC

DELAY

Purpose: Subroutine to compute delay associated with flamespread over grain surface.

Calls: None

Called by: B1D2P, B2D2P, I1D2P, I2D2P

DIS

Purpose: Function to compute algebraic distance from a given mesh point to a given external boundary element along either a line of constant radius (external boundary given as breech or projectile) or constant axial location (external boundary given as centerline or tube).

Calls: None

Called by: BAGIBC, BCCI, CASE, MSHMOV, PLTLOD, PRMOV, Q2D, Q2DBC, SETUP, TDMESH, TDXC, ULLBC, XSECT, XTERB

DISBAG

Purpose: Function to compute distance from a given mesh point to either front or rear boundary of a given bag. The distance is computed along a line of constant radius.

Calls: None

Called by: BAGIBC, BCCI, CASE, PLTLOD, TDMESH, ULLBC, XSECT, XTERB

DP

Purpose: Function to compute ratio of volume to surface area of a propellant grain as a function of surface regression.

Calls: PERF19

Called by: B1D2P, B2D2P, HEATW, I1D2P, I2D2P, Q2D

EPTOR

Purpose: Function to compute density of gas as a function of internal energy and pressure.

Calls: None

Called by: CDBRG, QP, RFILM, SETUP, TDBCAL, TDXC

EROSE

Purpose: Subroutine to compute erosive contribution to combustion of solid-phase.

Calls: None

Called by: B1D2P, B2D2P, I1D2P, I2D2P

ERTOP

Purpose: Function to compute pressure of gas as a function of internal energy and density.

Calls: None

Called by: ZBRNT

FILLER

Purpose: Subroutine to update motion of compactible case closure elements.

Calls: LOGOUT

Called by: PRMOV, SETUP

FIT

Purpose: Subroutine which replaces NIN equally spaced data by NOUT equally spaced data using a cubic spline interpolation.

Calls: SPLINE

Called by: PLOTRZ

FLUX

Purpose: Subroutine to compute state of gas transported through surface containing multiple reactive substrates.

Calls: None

Called by: FLUXDR, TDBCAL

113

FLUXDR   Purpose: Subroutine to compute partial derivatives of state variables with respect to mass flux added to or subtracted from a given region.

                       Calls: FLUX

                       Called by: BAGIBC, BCCI, Q2D, Q2DBC, ULLBC, XTERB, ZSLOT

GETFW   Purpose: Function to compute flow resistance in a region of quasi-one-dimensional single-phase flow.

                       Calls: None

                       Called by: B1D1P, I1D1P

GETQW   Purpose: Function to compute heat loss per unit volume due to cooling by the wall of the tube.

                       Calls: PRES

                       Called by: B1D1P, B1D2P, B2D1P, B2D2P, ILP1P, I1D1P, I1D2P, I2D1P, I2D2P

GLOBAL   Purpose: Subroutine to compute total mass and energy within computational domain.

                       Calls: AREA

                       Called by: SUMTAB

HEATW   Purpose: Subroutine to compute rate of heat loss to tube wall according to various models.

                       Calls: DP, IMBED, PRES, PROPER, RFILM, RTUBE, VIS, WBC

                       Called by: TDXC

IGBAG   Purpose: Subroutine to compute ignition of reactive substrate due to convective heat flux.

                       Calls: VIS

                       Called by: CALFLO

ILP1P	Purpose:	Subroutine to update state of a lumped parameter, single-phase region.
	Calls:	GETQW, PSI, YUPD
	Called by:	BCCI, Q2DBC
IMBED	Purpose:	Subroutine to update thermal profile in tube wall by method of invariant embedding.
	Calls:	None
	Called by:	HEATW
INPUT	Purpose:	Subroutine to read and print input data used to define problem. See Table A.3 for discussion of input data.
	Calls:	None
	Called by:	TDMAIN
I1D1P	Purpose:	Subroutine to update state of quasi-one-dimensional, single-phase flow at a given interior mesh point.
	Calls:	GETFW, GETQW, PSI, YUPD
	Called by:	BAGIBC, Q2D, ULLBC
I1D2P	Purpose:	Subroutine to update state of a quasi-one-dimensional, two-phase region at a given interior mesh point.
	Calls:	AP, CDB, CDBRG, DELAY, DP, EROSE, GETQW PROPER, PSI, QP, RDOT, SIGL, YUPD
	Called by:	BAGIBC, Q2D
I2D1P	Purpose:	Subroutine to update state of a two-dimensional, single-phase region at all interior mesh points.
	Calls:	GETQW, LOGOUT, PSI, YUPD
	Called by:	ULLBC

115

I2D2P   **Purpose:**   Subroutine to update state of a two-dimensional, two-phase region at all interior mesh points.

                       Calls: AP, CDB, CDBRG, DBUG, DELAY, DP, EROSE, GETQW, LOGOUT, PROPER, PSI, QP, RDOT, YUPD, ZSLOT

                       Called by: TDXC

JTHCKS   **Purpose:**   Function to convert THCK pointer to THCKS pointer.

                       Calls: None

                       Called by: CALFLO, CASE, MAP

LOGOUT   **Purpose:**   Subroutine to print tables of flow-field distributions and execute disc storage, plotting, as required.

                       Calls: CALPRM, PLOTRZ, SUMTAB

                       Called by: BCCI, B2D1P, B2D2P, FILLER, I2D1P, I2D2P, SETUP, TDBCAL, TDMESH, TDXC

MAP   **Purpose:**   Subroutine to establish mesh within a two-dimensional domain to satisfy coupled elliptic equations subject to either Dirichlet or Neumann boundary conditions.

                       Calls: JTHCKS

                       Called by: MSHMOV, SETUP

MSHMOV   **Purpose:**   Subroutine to define boundary distributions of mesh points for all two-dimensional computational regions and, following the definition of the internal distribution by MAP, to set the mesh point velocities.

                       Calls: DIS, MAP, SIDE

                       Called by: TDMESH, TDXC

NAYBOR   **Purpose:**   Subroutine to compute region and mesh pointers as required by BAGIBC.

                       Calls: None

                       Called by: BAGIBC, BCCI, XSECT

PERF19   Purpose: Subroutine to compute surface area and volume of a nineteen-perforation propellant grain following slivering.

          Calls: None

          Called by: DP

PLOTRZ   Purpose: Principal plotting executive for preparation of CALCOMP plots of state variables (isometric, contour, flow field) and ignition delay.

          Calls: CONTR, FIT, PLTFLO, PLTLOD, SEE

          Called by: LOGOUT, TDXC

PLTFLO   Purpose: Subroutine to prepare CALCOMP flow field plots.

          Calls: PLTLOD

          Called by: PLOTRZ

PLTLOD   Purpose: Subroutine to transfer data from computational arrays into plotting arrays.

          Calls: DIS, DISBAG

          Called by: PLOTRZ, PLTFLO

PRES   Purpose: Function to compute gas pressure or inter-granular stress or sum of both at a specified boundary location.

          Calls: SIDE

          Called by: GETQW, HEATW, PRMOV, SUMTAB, TDMESH

PRMOV   Purpose: Subroutine to update motion of projectile.

          Calls: DIS, FILLER, PRES, RESFUN

          Called by: TDXC

PROPER   Purpose: Subroutine to move vector properties of solid-phase into scalar arrays.

          Calls: None

          Called by: B1D2P, B2D2P, CALFLO, HEATW, I1D2P, I2D2P, Q2D, SETUP, TDMESH, TDXC, ZBRNT

117

PRTOE   Purpose: Function to compute internal energy of gas as a function of pressure and density.

Calls: None

Called by: RFILM, TDBCAL, TDXC

PSI   Purpose: Function to compute rate of discharge of externally injected ignition stimulus at a given point and time.

Calls: None

Called by: B1D1P, B1D2P, B2D1P, B2D2P, ILP1P, I1D1P, I1D2P, I2D1P, I2D2P

QP   Purpose: Function to compute interphase heat transfer coefficient and update solid-phase surface temperature according to cubic profile approximation. Also computes flow resistance through stick charges.

Calls: EPTOR, VIS

Called by: · B1D2P, B2D2P, I1D2P, I2D2P

Q2D   Purpose: Subroutine to effect update of solution through one integration step (predictor or corrector) at interior mesh points when a quasi-two-dimensional representation of the propelling charge is in effect.

Calls: CALFLO, CDB, CDBRG, DBUG, DIS, DP, FLUXDR, I1D1P, I1D2P, PROPER, Q2DBC

Called by: TDXC

Q2DBC   Purpose: Subroutine to effect update of solution at boundary mesh points when a quasi-two-dimensional representation of the propelling charge is in effect.

Calls: AREA, BCS1, BCS2, B1D1P, B1D2P, CALFLO, DBUG, DIS, FLUXDR, ILP1P, TDBCAL

Called by: Q2D

RDOT   Purpose: Function to compute rate of surface regression of solid-phase as a function of ambient pressure.

Calls: SPLIND

Called by: B1D2P, B2D2P, CALFLO, I1D2P, I2D2P

RESFUN   **Purpose:**   Function to compute bore resistance exerted on projectile due to interference of rotating band with tube rifling.

         Calls: None

         Called by: PRMOV

RFILM   **Purpose:**   Function to compute density of gas at film temperature in tube wall boundary layer.

         Calls: EPTOR, PRTOE

         Called by: HEATW, WALTEM

RTUBE   **Purpose:**   Function to compute tube radius at a given axial location.

         Calls: None

         Called by: HEATW, WALTEM

SEE   **Purpose:**   Subroutine to assess visibility of given line segment in preparation of isometric views of state variables at a given time.

         Calls: None

         Called by: PLOTRZ

SETUP   **Purpose:**   Subroutine to perform initialization of all state variables and internally set constants.

         Calls: AREA, DIS, EPTOR, FILLER, LOGOUT, MAP, PROPER, SUMTAB, TDMESH, XSECT

         Called by: TDMAIN

SIDE   **Purpose:**   Subroutine to compute pointers to mesh storage along a given side of a given computational region.

         Calls: None

         Called by: MSHMOV, PRES, TDMESH, TDXC, ULLBC

119

SIGL   Purpose: Function to compute intergranular stress as a function of porosity on nominal loading curve.

Calls: None

Called by: AP, B1D2P, I1D2P, TDXC

SPLIND   Purpose: Subroutine to prepare table of values of second derivatives for double precision cubic spline interpolation.

Calls: None

Called by: RDOT

SPLINE   Purpose: Subroutine to prepare table of values of second derivatives for single precision cubic spline interpolation.

Calls: None

Called by: FIT

SUMTAB   Purpose: Subroutine to compile and print tables of summary data.

Calls: AREA, GLOBAL, PRES

Called by: BCCI, LOGOUT, SETUP, TDBCAL, TDXC

TANLOS   Purpose: Subroutine to compute loss of tangential momentum experienced by gas entering mixture from ullage.

Calls: None

Called by: BAGIBC

TDBCAL   Purpose: Subroutine to determine physically compatible boundary values of state variables of gas-phase at a mutually connecting interface or region of lumped properties in the direction of the fluxes.

Calls: EPTOR, FLUX, LOGOUT, PRTOE, SUMTAB

Called by: BAGIBC, BCCI, Q2DBC, ULLBC, XTERB

TDMESH   Purpose: Subroutine to administer region representations and perform mesh point allocations.

                       Calls: AREA, DIS, DISBAG, LOGOUT, MSHMOV, PRES, PROPER, SIDE

                       Called by: SETUP, TDXC

TDXC   Purpose: Subroutine to control overall update and logout procedures. TDXC is the principal executive routine of TDNOVA.

                       Calls: BAGIBC, DIS, EPTOR, HEATW, I2D2P, LOGOUT, MSHMOV, PLOTRZ, PRMOV, PROPER, PRTOE, Q2D, SIDE, SIGL, SUMTAB, TDMESH, ULLBC, WALTEM, XSECT, ZBRNT

                       Called by: TDMAIN

ULLBC   Purpose: Subroutine to control update of all ullage mesh points other than those contiguous with the mixture.

                       Calls: B1D1P, B2D1P, DIS, DISBAG, FLUXDR, I1D1P, I2D1P, SIDE, TDBCAL

                       Called by: TDXC

VIS   Purpose: Function to compute gas viscosity as a function of temperature.

                       Calls: None

                       Called by: CDBRG, HEATW, IGBAG, QP, WALTEM, WBC

WALTEM   Purpose: Subroutine to update tube wall surface temperature by cubic profile approximation and also unsteady boundary layer momentum displacement thickness.

                       Calls: RFILM, RTUBE, VIS

                       Called by: TDXC

WBC   Purpose: Function to compute tube wall heat flux as required by subroutine IMBED.

                       Calls: VIS

                       Called by: HEATW

XSECT
Purpose: Subroutine to compute cross-sectional flow area of quasi-one-dimensional regions and volume of lumped parameter regions.

Calls: AREA, DIS, DISBAG, NAYBOR

Called by: SETUP, TDXC

XTERB
Purpose: Subroutine to update solution at a corner of the bag which is bounded by a fully two-dimensional flow on one or both sides.

Calls: B1D1P, B1D2P, B2D1P, CALFLO, DIS, DISBAG, FLUXDR, TDBCAL

Called by: BCCI

YUPD
Purpose: Subroutine to update fuel mass fraction and gas-phase heating term.

Calls: None

Called by: B1D1P, B1D2P, B2D1P, B2D2P, ILP1P, I1D1P, I1D2P, I2D1P, I2D2P

ZBRNT
Purpose: Subroutine to convert representation of perforated stick propellant to single-voidage mode.

Calls: ERTOP, PROPER

Called by: TDXC

ZSLOT
Purpose: Subroutine to equilibrate interior and exterior pressures for ruptured or slotted stick propellant.

Calls: FLUXDR

Called by: B2D2P, I2D2P

Table A.2 Glossary of Fortran Variables Contained in Common Blocks

Variable	Common Block	Definition
ALFAP	C02	Thermal diffusivity of solid phase, α_p.
ALPHAW	C72	Thermal diffusivity of tube wall.
ANPR	C58	Array of radial components of normal to bag boundary used to define motion of corners by extrapolation.
ANPU	C58	Array of normal velocities of bag boundary used to define motion of corners by extrapolation.
ANPZ	C58	Array of axial components of normal to bag boundary used to define motion of corners by extrapolation.
ANU	C65	Scalar value of XNU.
APL	C65	Scalar value of XAP3.
AP1	C02	Rate of propagation of intergranular disturbances in solid-phase, at settling porosity, under conditions of loading, a_1.
AP2	C02	Rate of propagation of intergranular disturbances in solid phase, under conditions of unloading, a_2.
AP3	C11	$a_1 \varepsilon_o$
ARRC	C70	Scalar value of XARRC.
ARRE	C70	Scalar value of XARRE.
AXC	C34	Array containing cross-sectional areas of quasi-one-dimensional regions and volumes of lumped parameter regions.
BAGMU	C66	Coefficient of friction between rigidized case segment and solid propellant.

Variable	Common Block	Definition
BAGNU	C66	Array of values of Poisson's ratio of bag segment.
BAGSTR	C66	Array of values of tensile strength of bag segment.
BEROS	C70	Scalar value of XBEROS.
BIT	C76	Linear interpolation weight computed by PRES.
BITS	C39	$\zeta_z^2 + \zeta_r^2$ if $\tau - \zeta$ characteristic and $\eta_z^2 + \eta_r^2$ if $\tau - \eta$ characteristic.
BLA	C72	Pre-exponential factor in wall skin friction correlation.
BLB	C72	Exponential factor in wall skin friction correlation.
BLC	C72	Shape factor in integral boundary layer analysis of wall temperature.
BLD	C72	Shape factor in integral boundary layer analysis of wall temperature.
BLX	C76	Value of θ used to interface with invariant embedding analysis of wall temperature.
BV	C02	Covolume of products of combustion of propellant, b.
BX	C76	Value of gas density used to interface with invariant embedding analysis of wall temperature.
CEROS	C70	Scalar value of XCEROS.
CFLON	C39	$\partial \dot{m} / \partial u_n$
CHSO	C14	Charge standoff distance.

Variable	Common Block	Definition
CP	C02	Specific heat at constant pressure of products of combustion of propellant, c_p.
CPBC	C54	Array of specific heats at constant pressure of reactive components of bag.
CPE	C54	Array of internal energies of gas at boundaries of one-dimensional regions terminated by lumped parameter region.
CPF	C11	$0.4\mathrm{Pr}^{-2/3}\gamma R_g/(\gamma - 1)$
CPIG	C51	Specific heat at constant pressure of igniter described by tabular input.
CPSS	C53	Specific heat at constant pressure of surface source term.
CPSSS	C57	Array of specific heats of surface sources used for TDBCAL interface.
CV	C02	Specific heat at constant volume of products of combustion of propellant, c_v.
CVBC	C54	Array of specific heats at constant volume of reactive components of bag.
CVE	C54	Array of internal energies of gas at boundaries of one-dimensional regions terminated by lumped parameter region.
CVIG	C51	Specific heat at constant volume of igniter described by tabular input.
CVSS	C53	Specific heat at constant volume of surface source term.
CVSSS	C57	Array of specific heats of surface sources used for TDBCAL interface.
CPX	C76	Coefficient used to interface with invariant embedding analysis of wall temperature.

Variable	Common Block	Definition
D	C01	Array containing values of d, solid-phase surface regression.
DATFL	SUMCOM	Array inactive.
DATIB	SUMCOM	Array of summarized interior ballistic data as required by BRL routine RECAP.
DATPR	SUMCOM	Array of pressure histories as required by BRL routine RECAP.
DATR	C37	Plot buffer array.
DATV	C37	Plot buffer array.
DATX	C18	Array used to construct plots.
DATY	C18	Array used to construct plots.
DATZ	C37	Plot buffer array.
DB	C34	Computational mesh increment along boundary.
DBAGQI	C84	Characteristic internal length for determination of heat flux to bag wall.
DBAGQO	C84	Characteristic external length for determination of heat flux to bag wall.
DEFF	C11	Effective particle diameter, D_p.
DELIG	C64	Scalar value of XDELIG.
DELX	C72	Invariant embedding mesh spacing.
DENW	C66	Array of values of mass per unit area of a bag sidewall segment.
DGADM	C57	Derivative of ratio of specific heats with respect to mass flux for region with lumped properties in direction of flux.
DGMDM	C57	Derivative of molecular weight with respect to mass flux for region with lumped properties in direction of flux.

Variable	Common Block	Definition
DMDU	C57	Derivative of mass flux with respect to normal velocity at continuum boundary.
DN	C34A	Computational mesh increment normal to boundary.
DPDM	C57	Derivative of pressure with respect to mass flux for region with lumped properties in direction of flux.
DPDU	C57	Derivative of pressure with respect to normal velocity at continuum boundary.
DPERF	C02	Initial diameter of grain perforation, d_o.
DR	C36	$\Delta\eta$
DRDM	C57	Derivative of density with respect to mass flux for region with lumped properties in direction of flux.
DRDP	C57	Derivative of density with respect to pressure at boundary of continuum region.
DRFLO	C46	Estimate of η-variation of gas-phase velocity at corner of two-dimensional region.
DSDEPS	C60	Derivative of intergranular stress with respect to porosity at the boundary of a continuum region.
DSDUS	C60	Derivative of intergranular stress with respect to solid-phase normal velocity at the boundary of a continuum region.
DSDUW	C86	Array of values of $\frac{\partial\sigma}{\partial u_{p_n}}$ used in connection with implicit determination of boundary values for rigidized case analysis.
DT	C09	Time step, $\Delta\tau$.
DTLOG	C05	Time increment for logout.

Variable	Common Block	Definition
DTLOGI	C48	Time increments for logout before and after transition to quasi-two-dimensional flow.
DTLOGM	C48	Array of times at which variably scheduled logout parameters are changed.
DTLOGV	C48	Variable schedule of logout intervals.
DTMAX	C05	Maximum time step consistent with C-F-L condition.
DTSUM	C16	Time increment for storage in summary tables.
DUTDM	C57	Derivative of tangential velocity with respect to normal mass flux for region with lumped properties in direction of flux.
DUTTDM	C57	Derivative of second tangential velocity with respect to normal mass flux for region with lumped properties in direction of flux.
DYDM	C57	Derivative of fuel mass fraction with respect to normal mass flux for region with lumped properties in direction of flux.
DZ	C36	$\Delta\zeta$
DZFLO	C46	Estimate of ζ-variation of gas-phase velocity at corner of two-dimensional region.
E	C01	Array containing current values of e, gas-phase internal energy.
EBAGC	C66	Array of values of compressive modulus of segment of rigidized case.
EBAGT	C66	Array of values of tensile modulus for a segment of rigidized case.

Variable	Common Block	Definition
ECH	C02	Chemical energy released during combustion of solid-phase, e_p.
ECHFRC	C83	Part of chemical energy released in gas-phase as a consequence of finite rate kinetics.
EDDSIG	C44	$\partial\varepsilon/\partial\sigma$ in quasi-one-dimensional two-phase flow.
EFRAC	C70	Scalar value of XEFRAC.
EIG	C02	Chemical energy released by externally injected ignition stimulus, e_{IG}.
EPDSIG	C36	$\partial\varepsilon/\partial\sigma$ in two-dimensional two-phase flow.
EPS	C01	Array containing values of porosity.
EPSØ	C02	Initial porosity of solid-phase.
ER	C30	$(1 - \varepsilon_o)/\varepsilon_o$
ERCT	C25	Array of values of chemical energy released by reactive substrates of bag.
ES	C57	Array of internal energies of surface sources used for TDBCAL interface.
ESS	C27	Local value of ESSIG.
ESSBC	C44	Energy of basepad at boundary of centerline.
ESSIG	C27	Array of values of chemical energy released by bag reactive substrates.
ETAS	C34A	Mesh transformation coefficient, ζ_s, for quasi-one-dimensional regions.
EØ	C02	Settling porosity of solid-phase, ε_o.
EØR	C11	$1/\varepsilon_o$

129

Variable	Common Block	Definition
E1	C30	$1/(1 + 0.02(1 - \varepsilon_o)/\varepsilon_o)$
FAC	C20	Scale factor used in plotting.
FBRES	C26	Array of values of bore resistance.
FEL	FILL	Array of initial resistances to motion of compactible filler elements used in case charges.
FLO	C57	Coefficient to describe pressure loss associated with mass transfer of gas-phase.
FLOIG	C27	Array of values of rate of reactivity of bag substrates.
FLOLOS	C56	Array of pressure loss coefficients.
FLOLP	C41	Array of values of $\dot{m}$ for transfer between quasi-one-dimensional and lumped parameter regions.
FLOLPC	C41	Array of values of $\partial\dot{m}/\partial u$ for transfers between quasi-one-dimensional and lumped parameter regions.
FLON	C34A	Rate of mass flow normal to boundary, positive exiting mixture.
FLORCT	C25	Array of values of rate of bag reactivity.
FLOS	C57	Array of surface source terms used for TDBCAL interface.
FLOSBC	C44	Rate of reactivity of basepad at boundary of centercore.
FLOSS	C27	Local value of FLOIG.
FLXCP1	C81	Interior value of specific heat at constant pressure at mixture boundary.

130

Variable	Common Block	Definition
FLXCP2	C81	Exterior value of specific heat at constant pressure at mixture boundary.
FLXCV1	C81	Interior value of specific heat at constant volume at mixture boundary.
FLXCV2	C81	Exterior value of specific heat at constant volume at mixture boundary.
FLXH1	C81	Interior value of enthalpy at mixture boundary.
FLXH2	C81	Exterior value of enthalpy at mixture boundary.
FLXM1	C81	Interior value of molecular weight at mixture boundary.
FLXM2	C81	Exterior value of molecular weight at mixture boundary.
FLXU1	C81	Interior value of transported velocity component at mixture boundary.
FLXU2	C81	Exterior value of transported velocity component at mixture boundary.
FLXV1	C81	Interior value of transported velocity component at mixture boundary.
FLXV2	C81	Exterior value of transported velocity component at mixture boundary.
FLXY1	C81	Interior value of reactant mass fraction at mixture boundary.
FLXY2	C81	Exterior value of reactant mass fraction at mixture boundary.
FR	C42	Plotting parameter.
FRES	FILL	Inactive.
FS	C20	Length of axis corresponding to state variable being plotted.

Variable	Common Block	Definition
FS1	C69	Component of interphase drag pertinent to stick propellant.
FS2	C69	Component of interphase drag pertinent to stick propellant.
FUEL	C77	Array containing mass fraction of partially reacted gas-phase propellant.
FZ	C42	Plotting parameter.
G	C04	Constant used to reconcile units, g_o.
GAFAC1	C53	Derivative of ratio of specific heats with respect to transverse mass flux entering one-dimensional flow.
GAM	C02	Ratio of specific heats of products of combustion of propellant, γ.
GAMIG	C62	Ratio of specific heats of igniter described in tabular form.
GAMLP	C54	Derivative of ratio of specific heats with respect to mass flux entering lumped parameter region.
GAMM	C01	Array of ratio of specific heats at computational mesh points.
GAMRCT	C51	Array of ratio of specific heats of reactive components of bag.
GAMØ	C02	Initial ratio of specific heats of ambient gas.

Variable	Common Block	Definition
GAM1	C02	$\gamma - 1$
GLEN	C02	Initial length of a grain, L_o.
GMFAC1	C53	Derivative of molecular weight with respect to transverse mass flux entering one-dimensional flow.
GMLSSS	C57	Array of molecular weights of surface source terms used for TDBCAL interface.
GMOL	C02	Molecular weight of products of combustion of propellant, M_w.
GMOLBC	C54	Array of molecular weights of reactive components of bag.
GMOLE	C54	Array of molecular weights of gas at boundaries of one-dimensional regions terminated by lumped parameter region.
GMOLIG	C51	Molecular weight of igniter described by tabular input.
GMOLL	C01	Array of molecular weights at computational mesh points.
GMOLLP	C54	Derivative of molecular weight with respect to mass flux entering lumped parameter region.
GMOLRC	C51	Array of molecular weights of reactive components of bag.
GMOLSS	C53	Array of molecular weights of surface source terms as used for TDBCAL interface.

Variable	Common Block	Definition
GMOLØ	CO2	Initial molecular weight of ambient gas.
H	C01	Array containing values of state variable H used in cubic profile solution of solid-phase surface temperature.
HBAG	C78	Array containing values of state variable H_b used in cubic profile solution of bag surface temperature.
HIDEDR	C42	Plotting parameter.
HIDEDZ	C42	Plotting parameter.
HS	C69	Heat transfer coefficient.
I	C35	Counter used to enumerate side and corners of a two-dimensional region during update of boundary values.
IBRES	FILL	Index to determine functional dependence of bore resistance on projectile velocity.
IBST	SUMCOM	Storage counter for interior ballistic summary data.
IBTABL	SUMCOM	Switch to indicate whether or not summarized interior ballistic data have been prepared.
ICA	C17	Switch used in hidden line algorithm.
ICB	C17	Switch used in hidden line algorithm.
ICL	C17	Switch used in hidden line algorithm.
ICYCL	C80	Switch to indicate to B2D2P whether exterior or interior of perforated stick is under consideration.
IHL	C17	Counter used in hidden line algorithm.
INBIAS	C79	Quantity used to construct pointer to storage internal to perforations of stick propellant.

Variable	Common Block	Definition
INCYCL	C80	Loop counter for dual voidage model.
INDIMR	C07	Number of mesh points allocated to η-coordinate in representation of propelling charge.
INDIMZ	C07	Number of mesh points allocated to ζ-coordinate in representation of propelling charge.
INOUT	C69	Switch to indicate whether flow is external or internal to stick.
INT	C07	Switch used to indicate whether step is predictor or corrector.
INTRL	C29	Array of switches used to indicate whether a given mesh point lies on an internal boundary.
IPLTV	C13	Array of switches used to determine whether or not to create isometric plots of various state variables during logout.
ISWP	C17	Counter used in hidden line algorithm.
ITYP	C31	Pointer to type of solid-phase (propellant or centercore) under consideration.
J	C35	Loop counter enumerating points on a side of a two-dimensional region.
JBAGQ0	C84	Pointer to exterior state variable storage used in modeled bag ignition and combustion.
JDB	C35	Storage increment in direction tangential to boundary.
JDN	C35	Storage increment in direction normal to boundary.

Variable	Common Block	Definition
JF	C35	Pointer to future storage level of a point on the boundary of a two-dimensional region.
JLIS	C74	Array of mesh storage pointers to define diagnostic print requirement.
JP	C35	Pointer to past storage level of a point on the boundary of a two-dimensional region.
JPLTV	C13	Array of switches used to determine whether or not to create contour plots of various state variables during logout.
JPRP	C52	Pointer to propellant property arrays.
JRCT	C25	Number of entries in tables of bag reactivity rates.
JRP	C03	Number of entries in array RPHI.
JTP	C03	Number of entries in array TPHI.
JZP	C03	Number of entries in array ZPHI.
J1	C35	Loop delimiter used in update of side of boundary.
J2	C35	Loop delimiter used in update of side of boundary.
J3	C35	Storage increment along side of two-dimensional region.
J4	C35	Pointer to current storage level of a point on the boundary of a two-dimensional region.
KDIMR	C42	Number of radial points in plot field.
KDIMRM	C42	KDIMR - 1
KDIMZ	C42	Number of axial points in plot field.

136

Variable	Common Block	Definition
KDIMZM	C42	KDIMZ $-$ 1
KDR	C38	Array of values of NDR, a subset.
KDZ	C38	Array of values of NDZ, a subset.
KFL	SUMCOM	Inactive.
KP	C02	Thermal conductivity of solid-phase, k_p.
KPR	SUMCOM	Counter for pressure history tables.
KPT	C55	Array of mesh point storage addresses.
KPTF	C55	Array of mesh point storage addresses biased to NF-level.
KPTHID	C42	Number of points in plot field.
KPTI	C55	Array of mesh point storage addresses biased to NI-level.
KPTP	C55	Array of mesh point storage addresses biased to NP-level.
KREG	C55	Array of pointers to computational regions.
KSDZ	C38	Array of numbers of axial mesh points allocated to successive bag increments and intervening ullage as required for plot interface.
KW	C72	Thermal conductivity of tube wall.
LAGMAP	C73	Switch used to determine whether fully equipotential or solid-phase Lagrangian mesh is to be used in two-dimensional regions occupied by mixture.
LOC	C16	Array for switches indicating whether stations for pressure history summaries are on tube or centerline.

Variable	Common Block	Definition
MAPIT	C15	Maximum allowable number of iterations for convergence of SOR algorithm for equipotential mesh.
MBASIG	C47	Array of pointers to reactivity data bases to describe rear base pads of successive bag increments.
MCCORE	C47	Array of pointers to propellant properties to describe centercore charge for successive bag increments.
MDELX	C72	Parameter used to define invariant embedding mesh.
MEL	FILL	Array of masses of case closure elements.
MFLOWF	C59	Switch used to indicate whether front end of centercore tube is permeable to solid-phase for successive bag increments.
MFLOWR	C59	Switch used to indicate whether rear end of centercore tube is permeable to solid-phase for successive bag increments.
MFORIG	C59	Array of pointers to reactivity data bases to describe forward base pads of successive bag increments.
MODL	C29	Array of values indicating type of flow in each region.
MODWBR	C79	Switch to indicate whether any bag segment has modeled ignition and combustion, as opposed to a purely tabular representation.
MPRP	C47	Array of pointers to propellant properties to describe main charge for successive bag increments.
MSTRNG	C47	Array of switches to indicate whether strong bag option applies to successive bag increments.
NABL	C67	Array of values of switches to indicate whether or not entire heat of combustion is to be released at surface of propellant.

Variable	Common Block	Definition
NABLAL	C79	Switch to indicate whether finite rate chemistry is being modeled for any propellant species.
NABLI	C67	Scalar value of NABL.
NABRB	C35	Pointer to mesh point adjacent to side η = constant at corner of mixture.
NABRBF	C41A	Pointer to future storage level of side η = constant at corner of mixture.
NABRC	C35	Pointer to mesh point adjacent to corner of mixture, in corner region of physical domain.
NABRCF	C41A	Pointer to future storage level of point of physical corner region adjacent to corner of mixture.
NABRN	C35	Pointer to mesh point adjacent to first point on a given side of a two-dimensional region.
NABRND	C35	Storage increment between points adjacent to a given side of a two-dimensional region.
NABRNF	C41A	Pointer to future storage level of mesh point adjacent to boundary of two-dimensional region. Pertains to ζ = constant side of corner of mixture.
NAY	SUMCOM	Inactive.
NBAGS	C47	Number of bags of propellant used to define charge.
NBASIG	C25	Pointer to reactivity data set associated with end of centercore.
NBH1	C17	Counter used in hidden line algorithm.

139

Variable	Common Block	Definition
NBH2	C17	Counter used in hidden line algorithm.
NBH11	C17	Counter used in hidden line algorithm.
NBRES	C26	Number of entries in bore resistance arrays.
NBY	C14	Array containing number of points used to specify bag boundaries initially.
NBYE	C22	Array of number of entries in tables of points used to define external boundaries.
NCASE	C68	Array of switches to indicate whether or not bag sidewall is rigidized.
NCCORE	C25	Switch to determine whether or not a centercore ignition charge is present.
NCHAR	C35	Switch used to indicate whether characteristic is $\tau - \zeta$ or $\tau - \eta$.
NCHOK	C55	Array of switches to indicate whether mass transfer is choked.
NCYCL	C35	Switch used to indicate whether characteristic direction has been altered in call to B2D2P.
NDATA	FILL	Array of counters for files of constitutive data pertaining to case closure elements.
NDBG	C82	Debug print switch.
NDEBUG	C74	Switch used to indicate whether or not diagnostic printing is required.
NDIM	SUMCOM	Inactive.
NDIMR	C35	Number of η-mesh points in a region.
NDIMRM	C35	NDIMR - 1.

Variable	Common Block	Definition
NDIMZ	C35	Number of ζ-mesh points in a region.
NDIMZM	C35	NDIMZ − 1.
NDR	C29	Array of values of η-mesh points allocated to regions.
NDSKR	C06	Switch used to determine whether or not solution is to be initialized by disc read.
NDSKW	C06	Switch used to determine whether or not solutions are to be stored on disc during logout.
NDT	C07	Counter, initialized to zero, bumped by unity on each predictor and each corrector level of each integration step.
NDTOFF	C74	Time step at which diagnostic printing is terminated.
NDTON	C74	Time step at which diagnostic printing begins.
NDTSKP	C32	Switch used to bypass tests of C-F-L criterion four steps out of five.
NDZ	C29	Array of values of number of ζ-mesh points allocated to regions.
NEL	FILL	Number of case closure elements.
NEL1	FILL	NEL + 1.
NEROS	C67	Array of values of switch to indicate whether or not erosive contribution to burning of each propellant is to be considered.
NEROSI	C67	Scalar value of NEROS.
NEW	C17	Counter used in hidden line algorithm.
NF	C07	Pointer to future storage.

Variable	Common Block	Definition
NFBIAS	C12	Quantity used to construct pointer to future storage location in state variable arrays.
NFLAM	SUMCOM	Inactive.
NFORM	C50	Array of switches to indicate whether propellant species consists of cylinders or spheres.
NFORMI	C50	Scalar value of NFORM.
NGRP	C72	Parameter used to define invariant embedding mesh.
NH	C17	Number of points on horizon of visibility in isometric plotting.
NHWLOS	C71	Switch to indicate manner of treatment of heat loss to tube wall.
NI	C07	Pointer to current storage.
NIBIAS	C12	Quantity used to construct pointer to current storage location in state variable arrays.
NINGRP	C72	Parameter used to define invariant embedding mesh.
NJLIS	C74	Number of pairs of mesh storage pointers between which diagnostic printing is to occur.
NJ1	C76	Pointer to storage for interpolation of wall properties.
NJ2	C76	Pointer to storage for interpolation of wall properties.
NLAST	FILL	Pointer to first case closure element currently bounded by a space on the right-hand side.

Variable	Common Block	Definition
NLAST1	FILL	NLAST + 1.
NMPT	C23	Maximum number of mesh points to be used in dynamic allocation mode.
NMSH	C23	Switch used to determine strategy for mesh allocation.
NOC	C17	Switch used in hidden line algorithm.
NOKE	C61	Switch used to indicate form of kinetic energy contributed to heating of gas transferred to region with lumped properties in direction of transfer.
NOLDCD	C85	Switch used to determine whether previous or revised correlations for interphase drag and heat transfer are to be used.
NOMAC	C63	Switch used to reject MacCormack differencing rule for $\partial u / \partial x$ in ullage near point of collapse against external boundary.
NOR	C14	Array of switches indicating whether initial mesh in mixture satisfies Dirichlet or Neumann boundary conditions.
NP	C07	Pointer to past storage.
NPBIAS	C12	Quantity used to construct pointer to past storage location in state variable arrays.
NPERF	C02	Total number of perforations in a grain, N.
NPERM	C24	Array of pointers to bag permeability data sets.
NPLCON	C06	Switch used to determine whether or not contour plots are required on logout.

Variable	Common Block	Definition
NPLFLM	C06	Switch used to determine whether flame-spread map is to be plotted at conclusion of run.
NPLFLO	C06	Switch used to determine whether or not flow field plots are required on logout.
NPLOT	C06	Switch used to determine whether or not isometric plots are required on logout.
NPRINT	C06	Switch used to determine whether or not printed output is required on logout.
NPRM	C25	Number of bag permeability data sets.
NPROP	SUMCOM	Number of propellants to be considered in summary plotting.
NPRPS	C47	Number of propellant species in charge.
NPT	C35	Total number of mesh points in a region.
NPTABL	SUMCOM	Switch used to indicate whether or not pressure histories have been tabulated.
NPTBY	C14	Array indicating numbers of points pre-allocated to various segments of boundaries of bag.
NPTOL	C29	Switch used to indicate whether or not quasi-two-dimensional analysis is in effect.
NPTOT	C07	Total number of mesh points allocated at any time.
NQ2DST	C73	Switch used to determine whether initial part of solution is to be fully two-dimensional or quasi-two-dimensional.
NRBIAS	C29	Array of values used to construct storage pointers.

Variable	Common Block	Definition
NRCT	C25	Number of bag reactivity data sets.
NREACT	C24	Array of pointers to bag reactivity data sets.
NREGB	C35	At a corner of the mixture, NREGB points to the region adjacent to the η = constant side.
NREGC	C35	At a corner of the mixture, NREGC points to a corner region of the physical domain.
NREGN	C35	Pointer to region adjacent to boundary point of two-dimensional region. At a corner, NREGN points to the ζ = constant side.
NRG	C49	Total number of computational regions.
NSBIAS	C49	Array of pointer biases to distinguish mesh storage for successive bag increments.
NSDZ	C49	Number of axial mesh points allocated to successive bag increments.
NSTEP	C06	Number of integration steps for logout.
NSTEPI	C48	Number of integration steps after which logout is to occur.
NSTEPM	C48	Array of integration steps at which variably scheduled logout parameters are changed.
NSTEPV	C48	Variable schedule of logout step cycles.
NSTOP	C06	Number of integration steps for termination of solution.
NSUBSK	C27	Array of pointers to bag permeability data sets.

Variable	Common Block	Definition
NSUBSM	C27	Array of pointers to bag reactivity data sets.
NSUM	C16	Number of stations at which pressure histories are to be summarized.
NSUMRY	C06	Switch used to determine whether or not summary tables are to be prepared for printing at the conclusion of the run.
NTABIG	C25	Switch to determine whether or not an externally injected ignition stimulus is present.
NTB	C21	Array of number of entries in burn rate tables.
NTFL	C79	Array of switches to indicate whether dual-voidage modeling is required in each charge increment.
NTFLAL	C79	Switch to indicate whether any charge increment is subject to dual-voidage modeling.
NTWUPD	C71	Switch to indicate method of analysis of response of wall surface temperature to heat transfer from combustion gas.
NTYPE	FILL	Switch used to indicate constitutive nature of case closure element.
NVHL	C20	Switch used to determine whether or not to delete hidden lines from isometric plots.
NWIB	C71	Number of wall stations at which passive invariant embedding solution is to be obtained of wall temperature profile.
NZPT	SUMCOM	Counter to describe number of stations at which pressure histories are to be plotted.

Variable	Common Block	Definition
OD	C02	Initial diameter of grain D_o.
ORDR	C70	Scalar value of XORDR.
OREL	C15	Overrelaxation factor used to establish equipotential mesh.
P	C01	Array containing values of p, gas-phase pressure.
PBIT	FILL	Force on projectile base, or first case closure element, due to gas pressure and intergranular stress.
PDUN	C36	$\partial p / \partial u_n$
PERIFW	C83	Length of perimeter for calculation of hydraulic diameter in wall friction correlation.
PERM	C27	Array of values of bag friction factor.
PFAC1	C39	$\partial p / \partial \dot{m}$ for quasi-one-dimensional region.
PFAC2	C41	Array of values of $\partial p / \partial u_T$ for boundaries of quasi-one-dimensional regions.
PFACLP	C41	$\partial p / \partial \dot{m}$ for lumped parameter region.
PHI	C03	Array of values used to describe rate of injection of external ignition stimulus, ψ.
PI	C04	π
PR	C04	Prandtl number, Pr.
PR3	C04	$Pr^{1/3}$
PRM	C25	Array of values of initial bag friction factor.
PRMASS	C26	Projectile mass.

Variable	Common Block	Definition
PST	C02	Initial pressure of gas-phase.
PTOL	C23	Fractional pressure difference below which quasi-two-dimensional solution is implemented.
QEDSIG	C56	Array of derivatives of porosity with respect to intergranular stress.
QEDVP	C56	Array of derivatives of porosity with respect to transverse solid-phase velocity of quasi-one-dimensional flow.
QFLON	C45	Array of values of transverse mass fluxes used in quasi-two-dimensional analysis.
QGAFAC	C45	Array of derivatives of ratio of specific heats with respect to mass flux.
QGMFAC	C45	Array of derivatives of molecular weight with respect to mass flux.
QPFAC1	C45	Array of values of $\partial p/\partial \dot{m}$ used in quasi-two-dimensional analysis.
QRFAC1	C45	Array of values of $\partial \rho/\partial \dot{m}$ used in quasi-two-dimensional analysis.
QSDUP	C56	Array of derivatives of intergranular stress with respect to solid-phase velocity.
QSDVP	C56	Array of derivatives of intergranular stress with respect to transverse velocity of solid-phase in quasi-one-dimensional flow.
QUFAC1	C45	Array of values of $\partial u/\partial \dot{m}$ used in quasi-two-dimensional analysis.
R	C04	Universal gas constant, R.
RBY	C14	Array of radial coordinates of points on boundaries of bag.

Variable	Common Block	Definition
RBYE	C22	Array of values of radial coordinate of points on external boundaries.
RESEL	FILL	Array of stresses used to define constitutive properties of case closure elements.
RFAC1	C39	$\partial\rho/\partial\dot{m}$ for quasi-one-dimensional region.
RFAC2	C41	Array of values of $\partial\rho/\partial u_T$ for quasi-one dimensional region.
RFACLP	C41	$\partial\rho/\partial\dot{m}$ for lumped parameter region.
RFRAC	C23	Radial spatial resolution factor.
RG	C04	Gas constant for products of combustion of solid-phase, R_G.
RHO	C01	Array containing values of ρ, gas-phase density.
RHODP	C36	$\partial\rho/\partial p$
RHOIG	C27	Array of densities of solid-phase associated with reactivity of bag material. Index runs over computational mesh.
RHOP	C02	Solid-phase density, ρ_p.
RHORCT	C25	Array of densities of solid-phase associated with reactivity of bag material.
RM	C01	Array containing values of r_m, radial component of mesh point.
RMØ	C43	Array of initial values of r_m.
ROZR	C39	η_r if $\tau - \zeta$ characteristic and ζ_r if $\tau - \eta$ characteristic.
ROZZ	C39	η_z if $\tau - \zeta$ characteristic and ζ_z if $\tau - \eta$ characteristic.

Variable	Common Block	Definition
RPHI	C03	Array of radial positions used to describe externally injected ignition stimulus.
RRA	C39	r_η
RS	C20	Length of r-axis in plots.
RUPINT	C25	Array of values of interval over which bag rupture is completed once rupture strength is exceeded.
RUPSTR	C25	Array of values of bag rupture strength.
RUPT	C27	Array of values of time at which bag rupture is complete locally.
RZA	C39	r_ζ
SAFE	C05	Safety factor used to divide time step allowable by C-F-L criterion.
SDUPN	C36	$\partial\sigma/\partial\hat{u}_{p_n}$
SDVP	C44	$\partial\sigma/\partial V_{p_n}$ where σ is in a quasi-one-dimensional region and V_{p_n} is normal component of velocity of contiguous region.
SGB	C36	Equal to ±1 depending on side of region at which boundary point is located.
SGN	C36	Equal to ±1 depending on side of region at which boundary point is located.
SIG	C01	Array containing values of σ, intergranular stress (N.B. This is a partial stress).
SIGLC	C11	$\rho_p a_1^2 \varepsilon_o^2 / g_o$
SLOT	C65	Scalar value of XSLOT.

Variable	Common Block	Definition
SQUDOT	C11	$[(u - u_p)^2 + (v - v_p)^2]^{1/2}$
SSK	C27	Local value of PERM.
STR	C65	Scalar value of XSTR.
T	C75	Array of thermal profiles as updated by invariant embedding.
TBN	C21	Array of values of burn rate exponents.
TB1	C21	Array of values of burn rate additive constants.
TB2	C21	Array of values of burn rate pre-exponential coefficients.
TDR	C36	$2\Delta\eta$
TDZ	C36	$2\Delta\zeta$
TEMST	C02	Initial temperature of gas phase.
THCK	C01	Thickness of bag material at each computational mesh point.
THK	C24	Array used to input initial thickness of bag material.
THKS	C66	Array of values of thickness of a generic bag segment.
THKV	C66	Total thickness of bag element, including nonstructural components.
TIG	C02	Ignition temperature of solid-phase, T_{ig}.
TIME	C02	Time, τ.
TIMIG	C43	Array of values of time at which ignition occurs.
TITLE	C08	Array containing problem title.

Variable	Common Block	Definition
TKPP	C11	$3k_p^2$
TMAXP	C21	Array of values of maximum pressure for which burn rate coefficients are to be used.
TMAXSM	C33	Pending time for data storage in summary table.
TOL	C15	Maximum allowable fractional displacement of mesh to satisfy equipotential equations.
TP	C01	Array containing current values of T_p, solid-phase surface temperature.
TPHI	C03	Array of times used to describe externally injected ignition stimulus.
TRCT	C25	Array of values of times used to define rate of bag reactivity.
TSBAG	C78	Surface temperature of bag.
TSTOP	C05	Time for termination of solution.
TX	C76	Value of gas temperature used to interface with invariant embedding analysis of wall temperature.
U	C01	Array containing values of u, axial component of gas-phase velocity.
UDOTN	C41	Array of values of $\hat{u}_n$ (not in physical units).
UDOTX1	C69	Inner product of gas velocity relative to solid-phase and longitudinal axis of stick propellant.
UDOTX2	C69	Inner product of gas velocity relative to solid-phase and transverse axis of stick propellant.

Variable	Common Block	Definition
UDUN	C36	$\partial u / \partial \hat{u}_n$
UDUT	C36	$\partial u / \partial \hat{u}_t$
UFAC1	C39	$\partial u_T / \partial \dot{m}$ for quasi-one-dimensional region.
UMR	C01	Radial velocity component of computational mesh.
UMZ	C01	Axial velocity component of computational mesh.
UN	C34A	Gas-phase velocity component normal to boundary (not in physical units).
UOLD	C41	Array of trial boundary values of u_T in quasi-one-dimensional regions.
UP	C01	Array containing values of u_p, axial component of solid-phase velocity.
UPDOTN	C41	Array of values of $\hat{u}_{p_n}$ (not in physical units).
UPN	C36	Component of solid-phase velocity normal to boundary (not in physical units).
UPR	C01	Array containing values of v_p, radial component of solid-phase velocity.
UPT	C36	Component of solid-phase velocity tangential to boundary (not in physical units).
UR	C01	Array containing values of v, radial component of gas-phase velocity.
URDUN	C36	$\partial v / \partial \hat{u}_n$
URDUT	C36	$\partial v / \partial \hat{u}_t$
UT	C34A	Gas-phase velocity component parallel to boundary (not in physical units).

Variable	Common Block	Definition
UTC	C40	Coefficient to convert $\hat{u}_n$ into physical units.
UTI	C84	Internal tangential component of gas-phase velocity.
UTO	C84	External tangential component of gas-phase velocity.
UTSS	C57	Surface source of transverse velocity component at reactive interface.
UTTSS	C57	Surface source of second transverse velocity component at reactive interface.
UX	C76	Value of gas velocity used to interface with invariant embedding analysis of wall temperature.
V	C34A	Array containing current local state variables at boundary point in mixture.
VE	C34A	Current local value of e at boundary point in mixture.
VFRA	C40	$1 + \dfrac{f_s \overline{\Delta\tau}}{\varepsilon\rho\left\|u - u_p\right\|}$ where $\overline{\Delta\tau} = \Delta\tau$ on predictor level and $\overline{\Delta\tau} = \Delta\tau/2$ on corrector level.
VPR	C26	Projectile velocity.
VPRDOT	C26	Projectile acceleration.
VRM	C34A	Current local value of r_m at boundary point in mixture.
VUM	C34A	Mesh velocity in quasi-one-dimensional region.
W	C75	Array containing values of Ricatti variable.

Variable	Common Block	Definition
X	C75	Array containing locations of invariant embedding mesh points.
XA	C17	Coordinate of endpoint of segment to be plotted isometrically.
XALFAP	C28	Array of values of ALFAP.
XAPL	C65	Array of values of longitudinal speed of sound in stick propellant.
XAP1	C28	Array of values of AP1.
XAP2	C28	Array of values of AP2.
XAP3	C28	Array of values of AP3.
XARRC	C70	Array of values of pre-exponents in Arrhenius rate dependence of gas-phase chemical energy release.
XARRE	C70	Array of values of exponents in Arrhenius rate dependence of gas-phase chemical energy release.
XB	C17	Coordinate of endpoint of segment to be plotted isometrically.
XBEROS	C70	Array of values of erosive burning components.
XBOND	C68	Array of values of bonding force between successive charge increments.
XBV	C28	Array of covolumes for propellant species.
XCEROS	C70	Array of values of erosive burning pre-exponential factors.
XCHSO	C64	Array of standoff distances for individual increments of a multi-increment charge.
XCHWT	C28	Array of values of initial mass of solid phase in successive bag increments.

Variable	Common Block	Definition
XCP	C51	Array of specific heats at constant pressure for propellant species.
XCV	C51	Array of specific heats at constant volume for propellant species.
XDELIG	C64	Array of delays associated with flame-spreading over the surface of grains of propellant following ignition by convective flux.
XDPERF	C28	Array of values of DPERF.
XDTA	C34A	Rate of change of cross-sectional area or of volume.
XDTU	C34A	Rate of change of gas-phase velocity at boundary of quasi-one-dimensional region.
XDTUP	C44	$\partial u_p / \partial t$ in quasi-one-dimensional two-phase flow.
XE	C57	Array of internal energies used for TDBCAL interface.
XECH	C28	Array of values of ECH, internal energies of propellant species.
XEFRAC	C70	Array of values of fraction of chemical energy released at surface of propellant.
XEL	FILL	Array of positions of case closure elements.
XEP	C60	Array of porosities used for BCS1, BCS2 interfaces.
XEPSØ	C28	Array of values of EPSØ.
XER	C30	Array of values of ER.
XEØ	C28	Array of values of EØ.

Variable	Common Block	Definition
XEØR	C28	Arrays of values of EØR.
XE1	C30	Array of values of E1.
XGA	C57	Array of ratios of specific heats used for TDBCAL interface.
XGAM	C28	Array of ratios of specific heats of propellant species.
XGLEN	C28	Array of values of GLEN.
XGM	C57	Array of molecular weights used for TDBCAL interface.
XGMOL	C28	Array of molecular weights of propellant species.
XH	C19	Array of abscissae of visibility horizon in hidden line segment.
XI	FILL	Array of positions of case closure elements.
XID	FILL	Array of velocities of case closure elements.
XIDD	FILL	Array of accelerations of case closure elements.
XK	C57	Array of bag pressure loss terms used for TDBCAL interface.
XKP	C28	Array of values of KP.
XM	C57	Array of mass fluxes used for TDBCAL interface.
XNPERF	C28	Array of values of NPERF.
XNU	C65	Array of values of Poisson's ratio for stick propellant.

Variable	Common Block	Definition
XOD	C28	Array of values of OD.
XORDR	C70	Array of values of order of reaction governing gas-phase fuel consumption.
XP	C57	Array of pressures used for TDBCAL interface.
XPR	C26	Projectile displacement.
XR	C57	Array of densities used for TDBCAL interface.
XRHOP	C28	Array of values of RHOP.
XSIG	C60	Array of intergranular stresses used for BCS1, BCS2 interfaces.
XSIGLC	C28	Array of values of SIGLC.
XSLOT	C65	Array of values of initial width of slot in slotted stick propellant.
XSTR	C65	Array of values of pressure differential which can be supported by perforated stick propellant.
XTIG	C28	Array of values of TIG.
XTKPP	C28	Array of values of TKPP.
XU	C57	Array of gas-phase velocities used for TDBCAL interface.
XUP	C57	Array of boundary velocities used for TDBCAL interface.
XUS	C60	Array of solid-phase velocities used BCS1, BCS2 interfaces.
XUT	C57	Array of transverse velocities used for TDBCAL interface.

Variable	Common Block	Definition
XUTT	C57	Second array of transverse velocities used for TDBCAL interface.
XVCP	C53	Specific heat at constant pressure at boundary of two-dimensional region.
XVCV	C53	Specific heat at constant volume at boundary of two-dimensional region.
XVGMOL	C53	Molecular weight at boundary of two-dimensional region.
XWIB	C72	Array of values of axial locations of stations at which passive invariant embedding solution is to be obtained of wall temperature profile.
XXDTA	C45	Array of rates of changes of cross-sectional area at points adjacent to boundaries of successive bag increments.
XXK	C57	Array of bag friction factors used for TDBCAL interface.
XY	C57	Array of values of fuel mass fraction used for TDBCAL interface.
YA	C17	Coordinate of endpoint of segment to be plotted isometrically.
YB	C17	Coordinate of endpoint of segment to be plotted isometrically.
YEL	FILL	Array of compactions used to define constitutive properties of case closure elements.
YH	C19	Array of ordinates of visibility horizon in hidden line algorithm.
YSS	C57	Surface source of fuel mass fraction at reactive interface.

Variable	Common Block	Definition
ZBPR	SUMCOM	Position of projectile as required for summary plots.
ZBRES	C26	Array of projectile displacements used to define bore resistance.
ZBY	C14	Array of axial coordinates of points on boundaries of bag.
ZBYE	C22	Array of axial coordinates of points on external boundaries.
ZFRAC	C23	Axial spatial resolution factor.
ZM	C01	Array containing values of z_m, axial coordinate of mesh point.
ZMØ	C43	Array of initial values of z_m.
ZMQWLP	C83	Axial position for evaluation of wall heat loss in lumped parameter region.
ZORR	C39	ζ_r if $\tau - \zeta$ characteristic and η_r if $\tau - \eta$ characteristic.
ZORZ	C39	ζ_z if $\tau - \zeta$ characteristic and η_z if $\tau - \eta$ characteristic.
ZPHI	C03	Array of axial positions used to describe externally injected ignition stimulus.
ZPT	SUMCOM	Array of positions used to define pressure history summary plots.
ZRA	C39	z_η
ZS	C20	Length of z-axis in plots.
ZSTOP	C05	Projectile displacement for termination of solution.
ZSUM	C16	Array of axial locations of stations at which histories of gas pressure are to be tabulated at conclusion of run.
ZZA	C39	z_ζ

160

Table A.3 Description of TDNOVA Input Files

File 1: One Card (20A4) Problem Title

TITLE   – Problem title, up to 80 alphanumeric characters.

File 2: Two Cards (9I5,4X,11I1/4F10.1)   Logout Options

NPRINT   0 – Tables of the state variables are not printed.
                         1 – Tables of the state variables are printed
                             on a logout schedule determined by NSTEP and
                             DTLOG as described in File 3.

NSUMRY   0 – No summary tables are produced at the conclusion
                             of the run.
                         1 – Summary tables are provided of the histories
                             of the conventional interior ballistic variables
                             and, if NSUM (File 3) is greater than zero,
                             of the histories of pressure at selected
                             positions in the tube.
                         2 – the summary data are not only tabulated at the
                             end of the run but are also plotted by the BRL
                             plot package (RECAP). This option applies only
                             to the code version at BRL.

NPLOT   0 – No isometric plots produced on logout.
                         1 – CALCOMP plots of state variables produced on
                             logout. These plots are isometric views of
                             the state variables as selected in accordance
                             with the values of the array IPLTV defined below.

NVHL   0 – Hidden lines are removed from CALCOMP plots.
                         1 – If not zero, hidden lines are retained and plots
                             are faired with a cubic spline interpolator.

NPLCON   0 – No CALCOMP contour plots produced on logout.
                         1 – Contour plots will be produced in accordance
                             with the values of JPLTV defined below.

NPLFLO   0 – No CALCOMP plots of flow field on logout.
                         1 – Plots are produced of the velocity fields of
                             both the gas and solid phases.

161

NPLFLM   0 - No summary plot of flamespreading.
                       1 - A summary plot is produced at the conclusion
                           of the run to illustrate the path of flame-
                           spreading by reference to contours of the
                           ignition boundary at various times.

NDSKW   0 - No disc storage on logout.
                       1 - Solution saved on disc (Unit 8) on logout.

NDSKR   0 - Initial distributions are constructed from
                           input data.
                      >0 - If not zero, initial distributions are read
                           from Unit 8 and correspond to time step equal
                           to NDSKR.

IPLTV(I),I=1,...,11 - If IPLTV(I) = 1, the quantity tabulated below
                           will be plotted as an isometric view.
                           Otherwise, not.

I	QUANTITY PLOTTED IF IPLTV(I)=1
1	Mesh
2	Porosity
3	Granular Stress
4	Pressure
5	Density
6	Gas Axial Velocity
7	Solid Axial Velocity
8	Gas Radial Velocity
9	Solid Radial Velocity
10	Gas Temperature
11	Particle Surface Temperature

JPLTV(I),I=1,...,11 - As per IPLTV but pertaining to the contour
                           plots. It should be noted that if JPLTV(1)
                           is set equal to one, the result is identical
                           to that produced if IPLTV(1) = 1.

FAC   - Scale factor for CALCOMP plots. (Begin
                           second card).

ZS   - Length of Z-axis in CALCOMP plots (in).

RS   - Length of R-axis in CALCOMP plots (in).

FS   - Length of ordinate axis in isometric plots (in).

File 3: One Card (I5,F10.0,I5,F10.0,I5,F10.0,I5)	Logout Parameters

NSTEPI(1) >0 – Number of integration steps before logout prior to transformation to quasi-two-dimensional analysis.
0 – Logout will occur on every predictor and every corrector step. Disc write is suppressed on the predictor step.
<0 – If |NSTEPI(1)| is not greater than eight, then variably scheduled logout is understood to be required and File 38 is required as defined below.

DTLOGI(1) – Time increment at which logout will occur prior to transformation to quasi-two-dimensional analysis (msec).

NSTEPI(2) >0 – Number of integration steps before logout after transformation to quasi-two-dimensional analysis.
0 – Logout will occur on every predictor and every corrector step. Disc write is suppressed on the predictor step. If NSTEPI(1) is entered as a negative value, both NSTEPI(2) and DTLOGI(2) will be overridden by the variable logout data of File 38.

DTLOGI(2) – Time increment at which logout will occur after transformation to quasi-two-dimensional analysis (msec).

Note: If DTLOGI is less than or equal to zero, logout will occur only in accordance with the value of NSTEPI.

NSUM – Number of stations for storage of pressure summary data, maximum of eight. If NSUM > 0, File 37 is required.

DTSUM – Desired time interval for summary table storage (msec). Automatically increased if table overflow about to occur during execution.

NDEBUG – If not equal to zero, diagnostic printing will be produced. File 39 is then required to specify the range of integration steps and mesh points at which the printing is to occur.

163

File 4:	One Card	(I5,2F10.0)	Termination Parameters

NSTOP
- Number of integration steps before termination. If problem involves a disc start, NSTOP is taken to include all steps up to the point of restart.

TSTOP
- Time for termination of solution (msec).

ZSTOP
- Projectile displacement for termination of solution (cm).

File 5:	Two Cards	(10I5/7F10.0)	Charge Representation Parameters

NPRPS
- Number of types of propellant in charge. Maximum of 10.

NBAGS
- Number of bags of propellant. Maximum of 10.

NMSH

0 - The propelling charge is initially represented by means of INDIMZ axial mesh points and INDIMR radial mesh points, unless NQ2DST (see below - this file) is set equal to one in which case the entire problem is analyzed in the quasi-two-dimensional mode. The propelling charge will continue to be given a fully two-dimensional representation until the PTOL criterion is satisfied as defined below. Moreover, in this case the ullage contiguous with each side of the charge will be represented as quasi-one-dimensional for that period in which the charge is treated as two-dimensional. It should be noted that the quasi-two-dimensional analysis applies only in the case NMSH = 0 in the present version of the code.

1 - The treatment of the propelling charge will be the same as in the case when NMSH = 0. However, the mesh will be allocated to the ullage regions dynamically in such a fashion as to constrain the total number of storage points to a value less than or equal to NMPT defined below, and so that no region has an axial mesh spacing less than ZFRAC times the distance between the breech face and the base of the projectile or a radial mesh spacing less than RFRAC times the radius of the bore, where ZFRAC and RFRAC are input quantities as defined below. Thus, in this case, the ullage may be treated as either quasi-one-dimensional or as fully two-dimensional according as its geometry dictates.

NMPT — Maximum number of storage points to be used in dynamic allocation of mesh as occurs when NMSH is equal to one. It should be noted that NMPT is a grand total and includes the points allocated to the propelling charge as well as those to be allocated dynamically to the ullage.

INDIMZ — Number of axial mesh points used to represent the propelling charge in both the fully two-dimensional and quasi-one-dimensional modes. When more than one bag is present, the axial mesh is allocated to the bags on the basis of their initial lengths, the total number being equal to INDIMZ.

INDIMR — Number of radial mesh points used to represent the propelling charge in the fully two-dimensional mode.

MAPIT — Maximum number of iterations to be used in determining mesh distributions by successive overrelaxation of elliptic system. Applies to initial mesh of propelling charge and to all two-dimensional regions subsequently, unless LAGMAP = 1.

LAGMAP 0 — An equipotential mesh is used for all fully-two-dimensional mixture regions.
1 — A solid-phase Lagrangian mesh is used. Two-dimensional regions of ullage are nevertheless represented by equipotential meshes.

NQ2DST 0 — The initial analysis will be fully two-dimensional.
1 — A quasi-two-dimensional representation is used from the initial instant and throughout the entire calculation.

NOLDCD 0 — The revised constitutive laws are used for interphase drag and heat transfer in granular propellant beds.
1 — The correlations as encoded in the previous version are used.

SAFE — Safety factor to be applied to CFL stability criterion. Must be greater than or equal to 1.

TOL   - Maximum fractional displacement of mesh coordinates for equipotential mesh to be accepted as converged.

OREL   - Overrelaxation factor. Must be between 1 and 2.

PTOL   - Quantity used to determine point in solution at which a quasi-two-dimensional representation of the flow is adequate to complete the solution. The value of PTOL is inspected only after the completion of flamespreading and when bag rupture is complete on the sidewalls. It should be noted that the transition to a quasi-two-dimensional treatment may occur prior to the rupture of the outer sidewall of a given bag if the relevant value of MSTRNG (File 11) has been set equal to one.
If the maximum value of pressure difference in each cross section of the tube does not exceed PTOL times the pressure at the centerline, the solution is continued according to a quasi-two-dimensional representation until all radial ullage has disappeared or until burnout occurs and according to a quasi-one-dimensional representation thereafter.

ZFRAC   - Dimensionless quantity used to allocate axial distribution of mesh to individual regions when NMSH is equal to one.

RFRAC   - Dimensionless quantity used to allocate radial distribution of mesh to individual regions when NMSH is equal to one.

CRIT   - Source stability factor. If entered as zero, it is ignored.

File 6: One Card   (4F10.0)   Ambient Conditions

TEMST   - Initial temperature of both phases (°K).

PST   - Initial pressure of gas phase (MPa).

GAMØ   - Ratio of specific heats of ambient gas (-).

GMOLØ   - Molecular weight of ambient gas (gm/gm-mol).

Note: Files 7, 8, 9, 10 are repeated, as a group, NPRPS times, once for each of the NPRPS types of propellant present in the charge. The centercore igniter is considered to be a distinct propellant for this purpose, but a basepad, treated as a reactive bag component, may or may not be. Reactive components of the bag may require that Files 7-10 be partially defined to support modeled ignition and combustion. In such cases, the discussion of File 36 should be consulted to determine the required data. It should be noted that the subscript used to distinguish the various types of propellant is suppressed in the subsequent discussion.

File 7:   One Card   (8F10.0)   Solid Phase Constitutive Data

XE$\emptyset$ – Settling porosity of bed (-).

XAP1   – Rate of propagation of compressive wave in settled bed (m/sec).

XAP2   – Rate of propagation of unloading wave (m/sec).

XRHOP   – Density of solid phase (gm/cc).

XKP   – Thermal conductivity of solid phase (J/cm-sec-°K).

XALFAP   – Thermal diffusivity of solid phase (cm^2/sec).

XAPL   – Rate of propagation of axial stresses in unconfined stick propellant (m/sec).

XNU   – Poisson ratio of stick propellant (-).
 Note: XAPL and XNU are only required for stick charges. If the propellant consists of sticks, XAP1 and XAP2 describe the load/unload characteristics of the bundle when subjected to transverse loads. Moreover, XNU refers to the longitudinal strain induced by the transverse loads.

File 8:	One Card	(3F10.0)	Gas Phase Constitutive Data

XGAM   - Ratio of specific heats (-).

XGMOL   - Molecular weight (gm/gm-mol).

XBV   - Covolume (cc/gm).

File 9:	Four or more Cards	(3I5/(8F10.0))	Solid Phase Combustion Characteristics

NTB   - Number of tabular data to define burn rate. Maximum of 10.

NEROS   0 - Erosive burning of the propellant is not considered.
                         1 - Erosive burning is considered and values of CEROS and BEROS must be supplied on the next card.

NABL   0 - The entire heat of combustion is assumed to be released at the surface of the propellant.
                         1 - A fraction XEFRAC of the energy is released at the surface and the balance is released in the gas-phase according to an Arrhenius kinetic law with pre-exponent XARRC and exponent XARRE as defined on the next card. In the present version of the code, at most one propellant type may have NABL = 1.

XTIG   Ignition temperature of solid-phase (°K). This quantity starts a new card.

XECH   - Chemical energy released in combustion (J/gm).

XDELIG   - Delay for flamespread over surface of grain following ignition (msec). If XDELIG is not equal to zero, the burn rate will rise linearly in time to the steady state value over the interval XDELIG following the instant at which the temperature first exceeds XTIG.

168

XCEROS   - Erosive burning pre-exponential factor (cm^2-°K/N) as required by Lenoir-Robillard model.

XBEROS   - Erosive burning exponential factor (-).

XEFRAC   - Fraction of chemical energy released at the surface of the propellant (-).

XARRC   - Pre-exponent of Arrhenius law governing rate of release of energy in the gas-phase $((gm/cc)**(1 - XORDR)/sec)$.

XARRE   - Exponent of Arrhenius law governing rate of release of energy in the gas-phase (J/gm).

XORDR   - Order of reaction governing gas-phase reactant consumption (-). This quantity starts a new card.

TMAXP(1)   - Maximum pressure for which corresponding coefficients are applicable in the law RDOT = TB1(1) + TB2(1)*P**TBN(1) where P is pressure and RDOT is regression rate. This quantity starts a new card.

TB1(1)   - Burn rate additive constant (cm/sec).

TB2(1)   - Burn rate pre-exponential factor (cm/sec-MPa^{BN}).

TBN(1)   - Burn rate exponent (-).

.
.
.

TMAXP(NTB)   - Maximum pressure for which corresponding coefficients are applicable in the law RDOT = TB1(NTB) + TB2(NTB)*P**TBN(NTB) where P is pressure and RDOT is regression rate.

TB1(NTB)   - Burn rate additive constant (cm/sec).

TB2(NTB)   - Burn rate pre-exponential factor (cm/sec-MPa^{BN}).

TBN(NTB)   - Burn rate exponent (-).
 Notes: (1) A new card is started for TMAXP(1), TMAXP(3) etc., but
              not for TMAXP(2), TMAXP(4) etc.
         (2) If the pressure exceeds TMAXP(NTB), the corresponding
              data are used as default values.

File 10: One Card (I5,6F10.0) Grain Geometry

NFORM   0 - Grain is a cylinder.
                         1 - Grain is a sphere.
                         2 - Grain is an unperforated stick.
                         3 - Grain is a perforated stick. In this case,
                             separate analyses are made of the gas flow
                             and combustion history in the interstices
                             and the perforations.
                             In the present version of the code, this
                             option pertains only to the main charge
                             increments.

XOD   - External diameter (cm).

XGLEN   - Length (cm)
                           Note: This datum is not required for sticks.

XDPERF   - Diameter of perforation (cm).

XNPERF   - Number of perforations (-).

XSLOT   - Width of slot (cm).
                           Note: This datum is only required for perforated
                                  sticks and may be entered as zero, if the
                                  sticks are not slotted.
                                  The initial value of XSLOT must not be less
                                  than 10^{-10} if the propellant is slotted.
                                  Current coding assumes that a slotted
                                  stick has just one perforation.

XSTR   - Maximum pressure differential which may be
                           supported by unslotted perforated stick pro-
                           pellant (MPa).
                           Note: This datum is required only for perforated
                                  sticks.
 Note: Files 11, 12, 13, 14, 15 are repeated as a group, NBAGS times,
        once for each of the NBAGS bags of propellant. It should be
        noted that the subscript used to distinguish the various bags
        of propellant is suppressed in the subsequent discussion.

File 11:	Two Cards	(12I5/6F10.0)	Description of Bag

NBY(1) — Number of entries in file for tabular description of rear of bag. Maximum of ten.

NBY(2) — Number of entries in file for tabular description of front of bag. Maximum of ten.

NBY(3) — Number of entries in file for tabular description of properties of internal circumferential boundary of bag. Maximum of ten.

NBY(4) — Number of entries in file for tabular description of properties of external circumferential boundary of bag. Maximum of ten.

MPRP — Pointer to file of propellant properties which characterize the main charge contained in the bag. MPRP must be greater than zero and less than or equal to NPRPS (File 5).

MCCORE 0 — A centercore igniter is not considered for the bag in question.
>0 — A centercore igniter is assumed to occupy the region interior to the bag, namely that defined by Files 14 and 19, over the axial extent of the charge. In this case MCCORE is a pointer to a file of propellant properties and is subject to the same restrictions as MPRP.

MBASIG — When MCCORE is not equal to one, MBASIG points to a reactivity data set in the same sense as NREACT (File 12) and defines the discharge characteristics of that part of a basepad which overlaps the rear section of the centercore igniter tube.

MFORIG — MFORIG is analogous to MBASIG but refers to the front of the centercore ignition tube.

MFLOWR 0 — The rear boundary of the centercore tube will not admit efflux of the solid-phase.
1 — The solid-phase is permitted to exit the centercore tube.

MFLOWF — MFLOWF is analogous to MFLOWR but refers to the front of the centercore tube.

171

Note: At a bag-to-bag interface in which MFLOWF and MFLOWR are both set equal to one on their respective sides of the interface, the solid-phase fluxes through the centercore are made mechanically compatible. Accordingly, mass transfer may occur from one tube to its neighbor not only for the gas-phase but also for the solid-phase. However, influx of the solid-phase to the extreme ends of the charge never occurs. Moreover, no account is taken of the influence of solid effluents from the extreme ends of the centercore subsequent to their discharge.

MSTRNG 1 - The conversion to a quasi-two-dimensional representation will occur independently of the rupture of the bag outer sidewall. In Q2D no radial sidewall motion will be allowed.

NCASE 0 - The increment is assumed to be contained in a flexible bag.
1 - The increment is assumed to be contained in a rigidized case and the pertinent data of File 35 must be defined for all segments of the outer circumferential boundary.

XCHWT(1) - Initial mass of main charge in bag (kg).

XEPS∅(1) - Initial porosity of main charge in bag (-).

XCHWT(2) - Initial mass of centercore igniter in bag (kg).

XEPS∅(2) - Initial porosity of centercore igniter in bag (-).

XCHSO - Increment standoff (cm). This datum is added to the axial coordinates of all points used to define the increment in question and also all increments in front of it. Values of XCHSO are therefore cumulative as one moves forward through the increments. Care must be taken not to define the initial charge distribution so that it penetrates the external boundaries.

XBOND - Strength of bond to next increment (N). This datum is applicable to all bags except the last. If the bag is initially separated from the next increment XBOND is defaulted internally to zero. The value of XBOND is only used, however, if both the increment in question and the next one are contained in rigid cases.

172

Note: The following conventions apply to each pair of values XCHWT and XEPSØ for each charge component of each bag.

If XCHWT is entered as zero, a value is computed from XEPSØ and is printed following the tabulation of all the input data.

If a nonzero value of XCHWT is entered, the value of XEPSØ will be replaced by a value which is consistent with the entered value of XCHWT.

The following default procedure applies to the datum XEØ (see File 7) for each type of propellant present in the charge as a whole.

If XEØ is entered as zero, it will automatically be replaced by the minimum value of XEPSØ which occurs among all bags in which the given type of propellant is present, following the preceding tests of consistency of XEPSØ with XCHWT. Internally revised values of XEPSØ and XEØ are printed following the tabulation of all input data.

File 12: NBY(1) Cards (3F10.0,4I5) Properties of Rear of Bag

ZBY(1,1)   – Axial location of first point on rear (cm).

RBY(1,1)   – Corresponding radial location (cm).

THK(1,1)   – Thickness of rear of bag at first point (cm).

NPERM(1,1)   – Pointer to data set (File 35) to describe the flow resistance of a section of the bag wall defined by (ZBY(1,1), RBY(1,1)) and (ZBY(2,1), RBY(2,1)). May take any integer value from zero to ten.

NREACT(1,1)   – Pointer to data set (File 36) to describe the reactivity of the same segment. May take any integer value from 0000 to 9999.

N.B.   See Note (15) following discussion of File 15.

NPTBY(1,1)   – Number of points pre-allocated to interior of line segment defined by (ZBY(1,1),RBY(1,1)) and (ZBY(2,1),RBY(2,1)).

NOR(1,1)   0 – Dirichlet data will be assumed for the initial distribution of mesh points on the line segment defined by (ZBY(1,1),RBY(1,1)) and (ZBY(2,1), RBY(2,1)).

            1 – Neumann data will be assumed for the initial distribution of mesh points on the line segment defined by (ZBY(1,1),RBY(1,1)) and (ZBY(2,1), RBY(2,1)). The mesh will be made orthogonal on the boundary segment.

.
.

ZBY(NBY(1),1)	- Axial location of last point on rear (cm).
RBY(NBY(1),1)	- Corresponding radial location (cm).
THK(NBY(1),1)	- Corresponding thickness (cm).

File 13: NBY(2) Cards   (3F10.0,4I5)   Properties of Front of Bag

ZBY(1,2)   - Axial location of first point on front (cm).

RBY(1,2)   - Corresponding radial location (cm).

THK(1,2)   - Thickness of front of bag at first point (cm).

NPERM(1,2)   - Pointer to data set (File 35) to describe the
                          flow resistance of a section of the bag wall
                          defined by (ZBY(1,2),RBY(1,2)) and (ZBY(2,2),
                          RBY(2,2)). May take any integer value from
                          zero to ten.

NREACT(1,2)   - Pointer to data set (File 36) to describe the
                          reactivity of the same segment. May take any
                          integer value from 0000 to 9999.
 N.B.   See Note (15) following discussion of File 15.

NPTBY(1,2)   - Number of points pre-allocated to interior
                          of line segment defined by (ZBY(1,2),RBY(1,2))
                          and (ZBY(2,2),RBY(2,2)).

NOR(1,2)   0 - Dirichlet data will be assumed for the initial
                          distribution of mesh points on the line segment
                          defined by (ZBY(1,2),RBY(1,2)) and (ZBY(2,2),
                          RBY(2,2)).
                       1 - Neumann data will be assumed for the initial
                          distribution of mesh points on the line segment
                          defined by (ZBY(1,2),RBY(1,2)) and (ZBY(2,2),
                          RBY(2,2)). The mesh will be made orthogonal
                          on the boundary segment.

.
.

ZBY(NBY(2),2)   - Axial location of last point on front (cm).

RBY(NBY(2),2)   - Corresponding radial location (cm).

THK(NBY(2),2)   - Corresponding thickness (cm).

File 14: NBY(3) Cards (3F10.0,4I5)	Properties of Internal Circumferential Boundary of Bag

ZBY(1,3)   - Axial location of first point on internal
                                   boundary of bag (cm).

RBY(1,3)   - Corresponding radial location (cm).

THK(1,3)   - Thickness of inside of bag at first point (cm).

NPERM(1,3)   - Pointer to data set (File 35) to describe
                                   the flow resistance of a section of the bag wall
                                   defined by (ZBY(1,3),RBY(1,3)) and (ZBY(2,3),
                                   RBY(2,3)). May take any integer value from
                                   zero to ten.

NREACT(1,3)   - Pointer to data set (File 36) to describe the
                                   reactivity of the same segment. May take any
                                   integer value from 0000 to 9999.
  N.B.   See Note (15) following discussion of File 15.

NPTBY(1,3)   - Number of points pre-allocated to interior of
                                   line segment defined by (ZBY(1,3),RBY(1,3))
                                   and (ZBY(2,3),RBY(2,3)).

NOR(1,3)   0 - Dirichlet data will be assumed for the initial
                                   distribution of mesh points on the line segment
                                   defined by (ZBY(1,3),RBY(1,3)) and (ZBY(2,3),
                                   RBY(2,3)).
                            1 - Neumann data will be assumed for the initial
                                   distribution of mesh points on the line segment
                                   defined by (ZBY(1,3),RBY(1,3)) and (ZBY(2,3),
                                   RBY(2,3)). The mesh will be made orthogonal
                                   on the boundary segment.

         .
         .
ZBY(NBY(3),3)   - Axial location of last point (cm).

RBY(NBY(3),3)   - Corresponding radial location (cm).

THK(NBY(3),3)   - Corresponding thickness (cm).

File 15: NBY(4) Cards   (3F10.0,4I5)   Properties of External
                                             Circumferential Boundary of Bag

ZBY(1,4)   - Axial location of first point on external
                             boundary of bag (cm).

RBY(1,4)   - Corresponding radial location (cm).

THK(1,4)   - Thickness of outside of bag at first point (cm).

NPERM(1,4)   - Pointer to data set (File 35) to describe the
                             flow resistance of a section of the bag wall
                             defined by (ZBY(1,4),RBY(1,4)) and (ZBY(2,4),
                             RBY(2,4)). May take any integer value from
                             zero to ten.

NREACT(1,4)   - Pointer to data set (File 36) to describe the
                             reactivity of the same segment. May take any
                             integer value from 0000 to 9999.
  N.B. See Note (15) following discussion of File 15.

NPTBY(1,4)   - Number of points pre-allocated to interior of
                             line segment defined by (ZBY(1,4),RBY(1,4))
                             and (ZBY(2,4),RBY(2,4)).

NOR(1,4)   0 - Dirichlet data will be assumed for the initial
                             distribution of mesh points on the line segment
                             defined by (ZBY(1,4),RBY(1,4)) and (ZBY(2,4),
                             RBY(2,4)).
                       1 - Neumann data will be assumed for the initial
                             distribution of mesh points on the line segment
                             defined by (ZBY(1,4),RBY(1,4)) and (ZBY(2,4),
                             RBY(2,4)). The mesh will be made orthogonal
                             on the boundary segment.

   .
   .
ZBY(NBY(4),4)   - Axial location of last point (cm).

RBY(NBY(4),4)   - Corresponding radial location (cm).

THK(NBY(4),4)   - Corresponding thickness (cm).

Notes on Files 12 through 15:

   (1)   Note that a new card is started for each value of ZBY(I,K), all I and K.

   (2)   Values of NPTBY and NOR are only required for the first NBY-1 cards of each boundary set, at most.

   (3)   Files 12 through 15 must be consistent with each other in the sense that the end points must match to define a continuous closed boundary for the computational domain.

   (4)   In Files 12 and 13, the first point must correspond to the internal boundary of the domain and the last point must correspond to the external boundary.

   (5)   In Files 14 and 15, the first point must correspond to the rear and the last must correspond to the front of the bag.

   (6)   Only endpoints of Files 12 through 15 are treated as explicit corners of the computational domain. All other corners, defined implicitly by the tabular data within a given file are treated as though they lay on a continuously differentiable curve.

   (7)   A mesh point is always located at the initial location defined by ZBY(I,K),RBY(I,K), all I and K.

   (8)   If NPERM is set equal to zero for any line segment, the segment in question is assumed to be fully permeable to the gas-phase. A similar convention applies to NREACT for which a zero value implies that the segment in question is nonreactive.

   (9)   With regard to the initial description of the properties of the bag, it should be noted that a fully independent analysis is not made of the permeability and reactivity of the corners. Instead, values of flow resistance and surface mass generation are established by extrapolation of either the source terms or of the state variables themselves along each side of the bag boundary.

  (10)   For a given segment of the bag, the designated resistance and reactivity models are applied to all mesh points in the interior of the segment and to the mesh point at the end of the segment, but not to the mesh point at the start of the segment.

177

(11)　It is assumed that if flow resistance and reactivity models are specified, then the initial distribution of boundary points is to be determined by Dirichlet data.

(12)　In contrast to the resistance and reactivity pointers, the values of THK are understood to apply only at the given points on each side.　Initial distributions along each segment are defined by linear interpolation of the entered values.
However, if nonzero thickness data are supplied to characterize the segment in the mechanical data File 35, the values in File 35 supersede those of Files 12 through 15 and, moreover, the value in File 35 is taken to apply uniformly over the segment in question.

(13)　When nonzero values of THK are specified, it is understood that the values of ZBY and RBY define the outside of the bag.　The values of THK therefore define the extent to which the bag material--cloth, wear-reducing additive, basepad, centercore tube,and flash suppressant--intrude on the volume available to the propellant within the bag.
Accordingly, the initial distribution of mesh points on the boundary of each bag will be displaced inwardly from the exterior surface defined by ZBY and RBY.

(14)　In the present version of the code it is assumed that when more than one bag is present, the mesh distributions coincide on the bag-to-bag interfaces.　This represents a constraint on the specification of ZBY and RBY on the bag-to-bag interfaces which may be relaxed when future need so warrants.

(15)　In contrast to versions of the code preceding version 5.0, the reactivity pointer is required to be a four digit number.　Each of the four digits is an individual pointer to a reactivity data set in accordance with the following convention.

DIGIT	SOURCE OF REACTIVITY
1	Internal Attached Component
2	Interior of Bag Segment
3	Exterior of Bag Segment
4	External Attached Component

File 16: One Card (4I5) External (Breech, Tube and Projectile) Boundary File Counters

NBYE(1)
- Number of entries in file for tabular description of breech geometry. Maximum of fifty.

NBYE(2)
- Number of entries in file for tabular description of geometry of projectile base. Maximum of fifty.

NBYE(3)
- Number of entries in file for tabular description of geometry of internal circumferential boundary of tube (normally centerline). Maximum of fifty.

NBYE(4)
- Number of entries in file for tabular description of geometry of external circumferential boundary of tube. Maximum of fifty.

File 17: NBYE(1) Cards (2F10.0) Geometry of Breech

ZBYE(1,1)
- Axial location of first point on breech (cm).

RBYE(1,1)
- Corresponding radial location (cm).

ZBYE(2,1)
- Axial location of second point. Starts a new card.

.
.
.

ZBYE(NBYE(1),1)
- Axial location of last point on breech (cm).

RBYE(NBYE(1),1)
- Corresponding radial location (cm).

File 18: NBYE(2) Cards (2F10.0) Geometry of Projectile Base

ZBYE(1,2)
- Axial location of first point on projectile base (cm).

RBYE(1,2)
- Corresponding radial location (cm).

.
.
.

ZBYE(NBYE(2),2)
- Axial location of last point on projectile base (cm).

RBYE(NBYE(2),2)
- Corresponding radial location (cm).

File 19:	NBYE(3) Cards	(2F10.0)	Geometry of Internal Circumferential Boundary

ZBYE(1,3)   – Axial location of first point on internal boundary (cm).

RBYE(1,3)   – Corresponding radial location (cm).

.
.

ZBYE(NBYE(3),3)   – Axial location of last point (cm).

RBYE(NBYE(3),3)   – Corresponding radial location (cm).

File 20:	NBYE(4) Cards	(2F10.0)	Geometry of External Circumferential Boundary

ZBYE(1,4)   – Axial location of first point on external boundary (cm).

RBYE(1,4)   – Corresponding radial location (cm).

.
.

ZBYE(NBYE(4),4)   – Axial location of last point (cm).

RBYE(NBYE(4),4)   – Corresponding radial location (cm).

File 21:	One Card	(4I5)	Igniter Discharge Table Counters and Options

NTABIG

     0 – A tabular representation of an ignition stimulus viewed as an externally injected source is not considered.

     1 – An externally injected ignition source is considered. Values of JZP, JRP and JTP must be specified and Files 22, 23, 24, 25 and 26 must be included.

JZP

     – Number of axial stations in discharge table for case when NTABIG equals one. JZP must not exceed twenty.

JRP	– Number of radial stations in discharge table when NTABIG equals one. JRP must not exceed eight.
JTP	– Number of time levels in discharge table for case when NTABIG equals one. JTP must not exceed twenty.

File 22:   One Card   (3F10.0)   Properties of External Ignition Source

---

Note: This file is required if and only if NTABIG is equal to one.

EIG   – Energy of igniter gas (J/gm).

GAMIG   – Ratio of specific heats of igniter gas (-).

GMOLIG   – Molecular weight of igniter gas (gm/gmol).

File 23:   One to Three Cards   (8F10.0)   Axial Positions for
                                                    Discharge Table

---

Note: This file is required if and only if NTABIG is equal to one.

ZPHI(I),I=1,JZP   – Axial positions (cm).

File 24:   One Card   (8F10.0)   Radial Positions for Discharge Table

---

Note: This file is required if and only if NTABIG is equal to one.

RPHI(I),I=1,JRP   – Radial positions (cm).

File 25:   One to Three Cards   (8F10.0)   Time Levels for
                                                    Discharge Table

---

Note: This file is required if and only if NTABIG is equal to one.

TPHI(I),I=1,JTP   – Time levels (msec).

File 26:   JRP*JTP to 3*JRP*JTP Cards   (8F10.0)   Discharge Table

Note: This file is required if and only if NTABIG is equal to one.

PHI(1,1,1)   - First value of rate of discharge per unit
                              volume (gm/cc-sec).

PHI(2,1,1)   - Second value.

.
.

PHI(JZP,1,1)   - Value at last axial position, first radial
                              position and first time.

PHI(1,2,1)   - Value at first axial, second radial position.
                              This entry starts a new card.

.
.

PHI(JZP,JRP,JTP)   - Last value.

File 27:   One Card   (F10.0, 5I5)   Projectile Mass, Bore Resistance
                                         and Heat Loss Data

PRMASS   - Projectile mass (kg).

NBRES   - Number of entries in tabular description of
                              bore resistance. Must not exceed 10.

IBRES   - Type of law for bore resistance.
                          1 - Resistance given directly by interpolation
                              of tabular data of File 28.
                          2 - Interpolated value multiplied by $7.2/V^{0.6}$
                              where V is projectile velocity in ft/sec.
                          3 - Interpolated value multiplied by
                              $(1 + .0004414V)/(1 + .005046V)$
                              where V is projectile velocity in in/sec.
                      N.B. If IBRES <1 or >3, the value is internally
                              defaulted to 2.

NEL   - Number of filler elements to be interposed
                              between the propellant and the projectile
                              base. $0 \leq NEL \leq 10$. If NEL > 0, then
                              Files 33 and 34 are required.

182

```
NHWLOS                  0 - Heat loss to tube is neglected.
                        1 - Heat loss is calculated by empirical
                            correlation for turbulent flow past a
                            flat plate.
                        2 - Heat loss is calculated by empirical
                            correlation for fully developed pipe flow.
                        3 - Heat loss is calculated by unsteady
                            boundary layer model.
                            File 30 is required for this case.

NTWUPD                  0 - Wall temperature is not updated.
                        1 - Wall temperature is updated by cubic
                            profile approximation.
                            File 29 is required in this case.
                        2 - Passive invariant embedding analysis is
                            performed in addition to the cubic profile
                            analysis.
                            Files 29, 31 and 32 are required in this case.
               N.B.     It is presently assumed that NHWLOS = 3 if
                        this level of wall temperature response is
                        of interest.
```

File 28:   One to Three Cards   (8F10.0)   Bore Resistance Table

ZBRES(1)   - First value of projectile displacement at
                             which bore resistance is specified (cm).

FBRES(1)   - Corresponding value of bore resistance (MPa).

  .
  .

ZBRES(NBRES)   - Last value of displacement.

FBRES(NBRES)   - Corresponding value of bore resistance.

File 29:   One Card   (2F10.0)   Tube Thermal Properties

Note: This file is required if and only if NTWUPD is not equal to zero.
       (See File 27.)

KW   - Thermal conductivity of wall (J/cm-sec-°K).

ALPHAW   - Thermal diffusivity of wall (cm^2/sec).

File 30:   One Card   (4F10.0)   Parameters for Boundary Layer Analysis

   Note: This file is required if and only if NHWLOS is equal to three.
           (See File 27.)

BLA   - Pre-exponential factor in skin friction
                             correlation.   Suggested value is BLA = 0.016527.

BLB   - Exponential factor in skin friction correlation.
                             Suggested value is BLB = 0.268.

BLC   - Shape factor.   Suggested value is BLC = 8.

BLH   - Shape factor.   Suggested value is BLH = 9/7.

File 31:   Two Cards   (I5/8F10.0)   Wall Stations for Invariant
                                            Embedding Analysis

   Note: This file is required if and only if NTWUPD is equal to two.
           (See File 27.)

NWIB   - Number of stations.   Maximum of two.

XWIB(1)   - Axial location of first station (cm).
                             Starts second card.

   .
   .

XWIB(NWIB)

File 32:   One Card   (F10.0,3I5)   Parameters to Define Mesh in
                                           Invariant Embedding Analysis

   Note: This file is required if and only if NTWUPD is equal to two.
           (See File 27.)

DELX   - Mesh spacing in group closest to heated surface
                             $(sec^{\frac{1}{2}})$.   Value refers to computational
                             coordinate x/DSQRT(ALPHAW) where x is distance
                             from surface and ALPHAW is thermal diffusivity.

NINGRP   - Number of intervals per group (-).   NINGRP*NGRP
                             must not exceed 100.

184

MDELX   – Integer multiple by which mesh spacing
                               increases from group to group as one moves
                               away from the heated surface (–).

NGRP   – Number of groups (–).
                               May take any integer value between one and ten.

File 33: NEL Cards   (3F10.0,2I5)   Filler Element Data

Note: This file is required if and only if NEL is not zero.
       One card is used to describe each element.

XEL   – Position of left hand boundary of element (cm).
                               It is assumed that successive values of XEL
                               increase monotonically.

MEL   – Mass of element (kg). If $<10^{-10}$, element
                               is interpreted as a space. MEL must not be $<10^{-10}$
                               for the first element.

FEL   – Initial resistance to motion of element (N).

NTYPE   – Indicator of constitutive behavior of element.

NTYPE	CONSTITUTIVE RESPONSE
0	Plastic––no deformation when unloading.
1	Elastic.
2	Rigid.
3	Incompressible.

NDATA   – Number of pairs of entries in stress–strain
                               table for given element, $0 \leq NDATA \leq 10$. If
                               NDATA > 0, then File 34 is required for the
                               given element.
                               Note that all files of the type 33 are entered
                               first and that the files of the type 34 follow
                               as a group.

**File 34: Zero to 3*NEL Cards   (8F10.0)   Filler Element
                                                 Constitutive Data**

Note: This file is required only if NEL is greater than zero.
       The element in question has nonzero mass, and is of either
       type 0 (plastic) or type 1 (elastic).

YEL(1)   - First value of engineering strain (-).

RESEL(1)   - Corresponding stress (MPa). Taken positive
                            in compression.

.
.

RESEL(NDATA)   - Last value of stress. Should exceed maximum
                            pressure in gun.

Notes: (1) The array YEL must be well-ordered for each element.
             The values must lie in the interval (0,1).
        (2) The array RESEL must have nonzero entries (except
             possibly for the first) and must be nondecreasing
             for each element.

File 35: 1 + NPRM Cards   (I5/(8F10.0))   Bag Mechanical Properties

NPRM   - Total number of bag resistance data sets.
                            May take any integer value from zero to ten.
                            The subsequent data of this file are required
                            if and only if NPRM is greater than zero.

PRM(1)   - Initial friction factor for normal flux
                            through bag element (-).

RUPSTR(1)   - Pressure difference supportable by bag
                            element before rupture commences (MPa).
                            This datum applies to flexible outer
                            sidewalls, to all endwalls and to all inner
                            sidewalls. Rupture of a rigidized outer
                            sidewall is determined by reference to the
                            datum BAGSTR, defined below.

RUPINT(1)   - Time interval over which bag flow resistance
                            decreases to zero in a linear fashion (msec).
                            May have any nonnegative value, including
                            zero.

THKV(1)   - Thickness of segment (cm). If a non-zero
                            value is entered for this datum, it supersedes
                            the data supplied in Files 12 through 15
                            wherever referenced. See note (12) following
                            the description of Files 12 through 15.
                            THKV is understood to define the volumetric
                            presence of the case and may therefore be
                            larger than the structural or load-carrying
                            thickness THKS.

Note: The following seven data are required only if at least one charge increment is loaded in a rigidized container.

THKS(1)   – Structural thickness of segment (cm).

DENW(1)   – Density of structural part of segment (gm/cc).

Note: The following five data pertain only to the external sidewall of the bag.

EBAGT(1)   – Young's modulus for tension of segment (MPa).

EBAGC(1)   – Young's modulus for compression of segment (MPa).

BAGNU(1)   – Poisson's ratio (–). (New card).

BAGSTR(1)   – Tensile strength (MPa).

BAGMU(1)   – Coefficient of friction between container wall and solid propellant (–).

PRM(2)   – (New card).

.
.

BAGSTR(NPRM).

Note: The impediment to gas flow is controlled by the friction factor. However, the motion of the solid phase at the external circumferential boundary is also influenced by the state of integrity of the bag. Dilation of the bag beyond its initial radius will not occur until it is completely ruptured locally. Thus by setting PRM = 0 and RUPSTR equal some large number (or RUPINT equal to some period which exceeds the firing interval) one may characterize a bag segment as impeding the motion of the solid-phase alone.

File 36:　1 + NRCT*(2 or 3) Cards　(I5/(I5,4F10.0/(8F10.0)))
Bag Reactivity Data

NRCT
- Total number of reactivity data sets. May take any integer value from zero to nine.
The subsequent data of this file are required if and only if NRCT is greater than zero.

JRCT(1)
- Number of pairs of data in tabular description of mass generation rate for element type 1. (New card). Maximum of eight.
If JRCT is entered as a negative quantity, it is understood that the ignition and combustion of the given segment is to be modeled using data for propellant of type |JRCT| for those quantities not provided in the subsequent field of this card.
Required data are as follows:
File 7 - XKP,XALFAP
File 8 - None
File 9 - XTIG, NTB, TMAXP, TB1, TB2, TBN
File 10 - None
Blanks may be entered for those data which are not noted above, unless of course, the file refers also to a main charge increment or a centercore igniter increment.
At present, this option is only linked to the static mesh representation due to constitutive uncertainties associated with the heat transfer to the bag.
If this latter option is exercised, then the dimensions of the arrays in common block /C78/ must be enlarged to the following:
/C78/ HBAG(999,4), TSBAG(333,4)

ERCT(1)
- Chemical energy released by reaction of bag material (J/gm). Positive if reaction is exothermic.

RHORCT(1)
- Density of solid-phase consumed by reaction of bag (gm/cc).

GAMRCT(1)
- Ratio of specific heats of gas created by reaction of bag (-).

GMOLRC(1)
- Molecular weight of gas created by reaction of bag (gm/gmol).

TRCT(1,1)   - Value of time (msec). (New card--only required
                               if JRCT is positive).

FLORCT(1,1)   - Corresponding rate of reaction of bag element
                               (gm/cm^2-sec).

   .
   .
FLORCT(JRCT(1),1).

JRCT(2)   - (New Card).

   .
   .
FLORCT(JRCT(NRCT),NRCT).

File 37: Two Cards   (8F10.0/8I5)   Pressure Summary Table Locations

---

  Note: This file is required if and only if NSUM is not zero. (See
         File 3.)

ZSUM(1)   - Axial location of first station (cm).

   .
   .
ZSUM(NSUM)   - Axial location of last station (cm).

LOC(1)   0 - First station is assumed to be on the tube wall.
                          1 - First station is assumed to be on the centerline
                              of the tube.

   .
   .
LOC(NSUM)   - Location of the last station.

**File 38: Two or Three Cards   (16I5/(8F10.0))   Variably Scheduled
                                                        Logout Data**

  Note: This file is required if and only if NSTEPI(1) is less than
         zero. (See File 3.)

NSTEPM(1)   - Last integration step at which MSTEPV(1) is
                               used to define logout schedule based on the
                               number of steps.

NSTEPV(1)   - Number of integration steps before logout.

    .
    .

NSTEPM($|$NSTEPI(1)$|$) - Last value of NSTEPM.

NSTEPV($|$NSTEPI(1)$|$) - Last value of NSTEPV.

DTLOGM(1)   - Last value of integration time at which
                                     DTLOGV(1) is used to define logout schedule
                                     based on integration time (msec).
                                     Starts a new card.

DTLOGV(1)   - Time increment before logout (msec).

    .·
    .

DTLOGM($|$NSTEPI(1)$|$) - Last value of DTLOGM.

DTLOGV($|$NSTEPI(1)$|$) - Last value of DTLOGV.
 Note: For values of integration step or integration time outside
        the table range defined by File 38, the final entries are
        used.

File 39: Two to Eleven Cards (3I5/(2I5))	Diagnostic Print Parameters

 Note: This file is required if and only if NDEBUG is equal to one.
        (See File 3.)

NDTON   - Integration step at which diagnostic print begins.

NDTOFF   - Integration step after which diagnostic print stops.

NJLIS   - Number of pairs of data to define mesh pointers
                                     for diagnostic printing. Maximum of 10.

JLIS(1,1)   - Diagnostic printing occurs for all mesh points
                                     lying between JLIS(1,1) and JLIS(1,2) inclusive.
                                     Starts a new card.

JLIS(1,2)
JLIS(2,1)   - Starts a new card.

    .
    .

JLIS(NJLIS,2)

Nomenclature

A	Cross-sectional area of tube
a	Rate of propagation of intergranular stresses
a_L	Longitudinal rate of propagation of stresses in stick charge
a_T	Transverse rate of propagation of stresses in stick charge
a_w	Rate of propagation of stresses in rigidized case sidewall
B_1, B_2	Burn rate coefficients
D_p	Effective diameter of a grain
$\dot{d}$	Burn rate
e	Internal energy
$\vec{f}$	Interphase drag
g_o	Constant used to reconcile units of measurement
h	Heat transfer coefficient
$\overleftrightarrow{I}$	Unit tensor of order two
K	Dimensionless friction factor used to characterize bag flow resistance
k	Thermal conductivity
M_{end}	Mass of rigidized container endwall
M_w	Molecular weight
$\dot{m}$	Mass rate of propellant combustion per unit volume
$\dot{m}_i$	Rate of mass transfer into a region
$\dot{m}_o$	Rate of mass transfer out of a region
Nu	Nusselt number

n	Burn rate exponent
$\vec{n}$	Normal vector
n_{end}	Normal to endwall of rigidized container
Pr	Prandtl number
p	Pressure
q	Rate of interphase heat transfer per unit surface area of solid-phase
q_w	Rate of heat loss to tube wall per unit volume
R	Intrinsic average intergranular pressure
Re	Reynolds number
R_i	Radius of surface at which mass enters a region
R_o	Radius of surface at which mass exits a region
R_{tube}	Radius of tube
r	Radial coordinate
S_n	Center-to-center spacing of sticks
S_p	Surface area of a grain
s_p	Total solid-phase surface area per unit volume
T	Temperature
t	Time
$\vec{u}$	Gas-phase velocity, components (u,v)
$\vec{u}_p$	Solid-phase velocity, components (u_p,v_p)
u_w	Velocity of rigidized case sidewall
V_p	Volume of a grain

w	Gas-phase velocity ζ-component in computational coordinates
w_p	Solid-phase velocity ζ-component in computational coordinates
x	Gas-phase velocity η-component in computational coordinates
x_p	Solid-phase velocity η-component in computational coordinates
Y	Reactant mass fraction
y	Characteristic root
z	Axial coordinate

Greek Symbols

γ	Ratio of specific heats
Δp_{res}	Pressure drop due to normal flux through bag
$\overline{\Delta t}$	$\overline{\Delta t} = \Delta t$ on predictor step and $\Delta t/2$ on corrector step where Δt is time increment used to integrate equations
δ_w	Displacement of sidewall of rigidized case
ε	Porosity or void fraction. Fraction of a unit volume occupied by gas-phase
ζ	Computational coordinate, generally aligned with z
η	Computational coordinate, generally aligned with r
Θ	Quantity related to momentum displacement thickness in unsteady boundary layer theory
θ	Thickness of container wall
θ_s	Structural thickness of container wall
μ	Viscosity

ν Coefficient of friction

ξ Inhomogeneous term in characteristic analysis

ρ Density

$\overset{\leftrightarrow}{\sigma}$ Solid-phase intrinsic average stress tensor

τ Time in computational coordinate frame

ϕ Angle of rotation of sticks

ψ Rate of injection of external ignition stimulus

Subscripts and Special Symbols

In the dual-voidage analysis we use subscripts e and i to distinguish exterior and interior gas-phase properties.

Subscripts p, sℓ, w, f and IG respectively identify solid-phase properties, attributes of the slot in slotted stick charges, attributes of the sidewall of a rigidized case, properties at the film temperature, and attributes of the external ignition stimulus.

D/Dt and D/Dt_p respectively denote total derivatives with respect to time along the gas-phase and solid-phase streamlines.

A dot placed over a quantity indicates a derivative with respect to time.

DISTRIBUTION LIST

No. Of Copies	Organization	No. Of Copies	Organization
12	Administrator Defense Technical Info Center ATTN: DTIC-DDA Cameron Station Alexandria, VA 22314	3	Commander US Army Materiel Development and Readiness Command ATTN: DRCDMD-ST DCRSF-E, Safety Office DRCDE-DW 5001 Eisenhower Avenue Alexandria, VA 22333
1	Office of the Under Secretary of Defense Research & Engineering ATTN: R. Thorkildsen Washington, DC 20301	13	Commander ARDC, USAAMCCOM ATTN: DRSMC-TD, A. Moss DRSMC-TSS DRSMC-TDC D. Gyorog DRSMC-LCA
1	HQDA/SAUS-OR, D. Hardison Washington, DC 20301		J. Lannon A. Beardell D. Downs S. Einstein
1	HQDA/DAMA-ZA Washington, DC 20310		L. Schlosberg S. Westley S. Bernstein P. Kemmey
1	HQDA, DAMA-CSM, E. Lippi Washington, DC 20310		C. Heyman Dover, NJ 07801
1	HQDA/SARDA Washington, DC 20310	9	Commander ARDC, USAAMCCOM ATTN: DRSMC-SCA, L. Stiefel B. Brodman
1	Commander US Army War College ATTN: Library-FF229 Carlisle Barracks, PA 17013		DRSMC-LCB-I, D. Spring DRSMC-LCE, R. Walker DRSMC-LCU-CT E. Barrieres
1	Director Ballistic Missile Defense Advanced Technology Center P. O. Box 1500 Huntsville, AL 35804		R. Davitt DRSMC-LCU-CV C.Mandala E. Moore
1	Chairman DOD Explosives Safety Board Room 856-C Hoffman Bldg. I 2461 Eisenhower Avenue Alexandria, VA 22331		DRSMC-LCM-E S. Kaplowitz Dover, NJ 07801

DISTRIBUTION LIST

No. Of Copies	Organization
1	Commander ARDC, USAAMCCOM ATTN: DRSMC-QAR, J. Rutkowski Dover, NJ 07801

5	Project Manager
	Cannon Artillery Weapons
	  System
	ATTN: DRCPM-CW,
	    F. Menke
	  DRCPM-CWW
	    H. Noble
	  DRCPM-CWS
	    M. Fisette
	  DRCPM-CWA,
	    R. DeKleine
	    H. Hassmann
	Dover, NJ 07801

2	Project Manager Munitions Production Base Modernization and Expansion ATTN: DRCPM-PMB, A. Siklosi SARPM-PBM-E, L. Laibson Dover, NJ 07801

3	Project Manager
	Tank Main Armament System
	ATTN: DRCPM-TMA, K. Russell
	    DRCPM-TMA-105
	    DRCPM-TMA-120
	Dover, NJ 07801

3	Commander
	ARDC, USAAMCCOM
	ATTN: DRSMC-LCW-A
	    M.Salsbury
	  DRSMC-LCS
	  DRSMC-LC, J. Frasier
	Dover, NJ 07801

No. Of Copies	Organization

5	Commander
	ARDC, USAAMCCOM
	ATTN: DRSMC-LEP-L
	    DRSMC-LC, L. Ambrosini
	    DRSMC-IRC, G. Cowan
	    DRSMC-LEM, W. Fortune
	        R. Zastrow
	Rock Island, IL 61299

1	Commander US Army Watervliet Arsenal ATTN: SARWV-RD, R. Thierry Watervliet, NY 12189
1	Director US Army AMCCOM Benet Weapons Laboratory ATTN: DRSMC-LCB-TL Watervliet, NY 12189
1	Commander US Army Aviation Research and Development Command ATTN: DRDAV-E 4300 Goodfellow Blvd. St. Louis, MO 63120
1	Commander US Army TSARCOM 4300 Goodfellow Blvd St. Louis, MO 63120
1	Director US Army Air Mobility Research and Development Laboratory Ames Research Center Moffett Field, CA 94035

1	Commander
	US Army Communications
	  Research and Development
	  Command
	ATTN: DRSEL-ATDD
	Fort Monmouth, NJ 07703

DISTRIBUTION LIST

No. Of Copies	Organization	No. Of Copies	Organization
1	Commander US Army Electronics Research and Development Command Technical Support Activity ATTN: DELSD-L Fort Monmouth, NJ 07703	1	Project Manager Fighting Vehicle Systems ATTN: DRCPM-FVS Warren, MI 48090
1	Commander US Army Harry Diamond Lab. ATTN: DELHD-TA-L 2800 Powder Mill Road Adelphi, MD 20783	1	Director US Army TRADOC Systems Analysis Activity ATTN: ATAA-SL White Sands Missile Range NM 88002
2	Commander US Army Missile Command ATTN: DRSMI-R DRSMI-YDL Redstone Arsenal, AL 35898	1	Project Manager M-60 Tank Development ATTN: DRCPM-M60TD Warren, MI 48090
1	Commander US Army Natick Research and Development Command ATTN: DRDNA-DT Natick, MA 01762	1	Commander US Army Training & Doctrine Command ATTN: ATCD-A Fort Monroe, VA 23651
1	Commander US Army Tank Automotive Command ATTN: DRSTA-TSL Warren, MI 48090	2	Commander US Army Materials and Mechanics Research Center ATTN: DRXMR-ATL Tech Library Watertown, MA 02172
1	US Army Tank Automotive Command ATTN: DRSTA-CG Warren, MI 48090	1	Commander US Army Research Office ATTN: Tech Library P. O. Box 12211 Research Triangle Park, NC 27709
1	Project Manager Improved TOW Vehicle ATTN: DRCPM-ITV US Army Tank Automotive Command Warren, MI 48090	1	Commander US Army Mobility Equipment Research & Development Command ATTN: DRDME-WC Fort Belvoir, VA 22060
2	Program Manager M1 Abrams Tank System ATTN: DRCPM-GMC-SA Warren, MI 48090	1	Commander US Army Logistics Center Defense Logistics Studies Fort Lee, VA 23801

DISTRIBUTION LIST

No. Of Copies	Organization
2	Commandant US Army Infantry School ATTN: ATSH-CD-CSO-OR Fort Benning, GA 31905
1	US Army Armor & Engineer Board ATTN: STEBB-AD-S Fort Knox, KY 40121
1	Commandant US Army Aviation School ATTN: Aviation Agency Fort Rucker, AL 36360
1	Commandant Command and General Staff College Fort Leavenworth, KS 66027
1	Commandant US Army Special Warfare School ATTN: Rev & Tng Lit Div Fort Bragg, NC 28307
1	Commandant US Army Engineer School ATTN: ATSE-CD Ft. Belvoir, VA 22060
1	Commander US Army Foreign Science & Technology Center ATTN: DRXST-MC-3 220 Seventh Street, NE Charlottesville, VA 22901
1	President US Army Artillery Board Ft. Sill, OK 73504
2	Commandant US Army Field Artillery School ATTN: ATSF-CO-MW, B. Willis Ft. Sill, OK 73503

No. Of Copies	Organization
3	Commandant US Army Armor School ATTN: ATZK-CD-MS/ M. Falkovitch Armor Agency Fort Knox, KY 40121
1	Chief of Naval Materiel Department of the Navy ATTN: J. Amlie Washington, DC 20360
1	Office of Naval Research ATTN: Code 473, R. S. Miller 800 N. Quincy Street Arlington, VA 22217
2	Commander Naval Sea Systems Command ATTN: SEA-62R2, J. W. Murrin R. Beauregard National Center, Bldg. 2 Room 6E08 Washington, DC 20360
1	Commander Naval Air Systems Command ATTN: NAIR-954-Tech Lib Washington, DC 20360
1	Strategic Systems Project Office Dept. of the Navy Room 901 ATTN: J. F. Kincaid Washington, DC 20376
1	Assistant Secretary of the Navy (R, E, and S) ATTN: R. Reichenbach Room 5E787 Pentagon Bldg. Washington, DC 20350
1	Naval Research Lab Tech Library Washington, DC 20375

DISTRIBUTION LIST

No. Of Copies	Organization
5	Commander Naval Surface Weapons Center ATTN: Code G33, J. L. East W. Burrell J. Johndrow Code G23, D. McClure Code DX-21, Library Br. Dahlgren, VA 22448
2	Commander US Naval Surface Weapons Center ATTN: J. P. Consaga C. Gotzmer Indian Head, MD 20640
4	Commander Naval Surface Weapons Center ATTN: S. Jacobs/Code 240 Code 730 K. Kim/Code R-13 R. Bernecker Silver Spring, MD 20910
2	Commanding Officer Naval Underwater Systems Center Energy Conversion Dept. ATTN: CODE 5B331, R. S. Lazar Tech Lib Newport, RI 02840
4	Commander Naval Weapons Center ATTN: Code 388, R. L. Derr C. F. Price T. Boggs Info. Sci. Div. China Lake, CA 93555
2	Superintendent Naval Postgraduate School Dept. of Mechanical Engineering ATTN: A. E. Fuhs Code 1424 Library Monterey, CA 93940

No. Of Copies	Organization
6	Commander Naval Ordnance Station ATTN: P. L. Stang J. Birkett S. Mitchell C. Christensen D. Brooks Tech Library Indian Head, MD 20640
1	AFSC/SDOA Andrews AFB Andrews AFB, MD 20334
1	Program Manager AFOSR Directorate of Aerospace Sciences ATTN: L. H. Caveny Bolling AFB, DC 20332
6	AFRPL (DYSC) ATTN: D. George J. N. Levine B. Goshgarian D. Thrasher N. Vander Hyde Tech Library Edwards AFB, CA 93523
1	AFFTC ATTN: SSD-Tech Lib Edwards AFB, CA 93523
1	AFATL/DLYV Eglin AFB, FL 32542
1	AFATL/DLJM ATTN: W. Dittrich Eglin AFB, FL 32542
1	AFATA/DLD ATTN: D. Davis Eglin AFB, FL 32542
1	AFATL/DLDL ATTN: O. K. Heiney Eglin AFB, FL 32542

DISTRIBUTION LIST

No. Of Copies	Organization	No. Of Copies	Organization
1	AFATL/DLODL ATTN: Tech Lib Eglin AFB, FL 32542		
1	AFFDL ATTN: TST-Lib Wright-Patterson AFB, OH 45433	1	General Applied Sciences Lab ATTN: J. Erdos Merrick & Stewart Avenues Westbury Long Island, NY 11590
1	NASA HQ 600 Independence Avenue, SW ATTN: Code JM6, Tech Lib. Washington, DC 20546	1	General Electric Company Armament Systems Dept. ATTN: M. J. Bulman, Room 1311 Lakeside Avenue Burlington, VT 05412
1	NASA/Lyndon B. Johnson Space Center ATTN: NHS-22, Library Section Houston, TX 77058	1	Hercules, Inc. Allegany Ballistics Laboratory ATTN: R. B. Miller P. O. Box 210 Cumberland, MD 21501
1	Aerodyne Research, Inc. Bedford Research Park ATTN: V. Yousefian Bedford, MA 01730	1	Hercules, Inc Bacchus Works ATTN: K. P. McCarty P. O. Box 98 Magna, UT 84044
1	Aerojet Solid Propulsion Co. ATTN: P. Micheli Sacramento, CA 95813		
1	Atlantic Research Corporation ATTN: M. K. King 5390 Cherokee Avenue Alexandria, VA 22314	1	Hercules, Inc. Eglin Operations AFATL DLDL ATTN: R. L. Simmons Eglin AFB, FL 32542
1	AVCO Everett Rsch Lab ATTN: D. Stickler 2385 Revere Beach Parkway Everett, MA 02149	1	IITRI ATTN: M. J. Klein 10 W. 35th Street Chicago, IL 60616
2	Calspan Corporation ATTN: Tech Library P. O. Box 400 Buffalo, NY 14225	2	Lawrence Livermore Laboratory ATTN: M. S. L-355, A. Buckingham M. Finger P. O. Box 808 Livermore, CA 94550
1	Foster Miller Associates ATTN: A. Erickson 135 Second Avenue Waltham, MD 02154		

DISTRIBUTION LIST

No. Of Copies	Organization	No. Of Copies	Organization
1	Olin Corporation Badger Army Ammunition Plant ATTN: R. J. Thiede Baraboo, WI 53913		
1	Olin Corporation Smokeless Powder Operations ATTN: R. L. Cook P. O. Box 222 St. Marks, FL 32355	3	Thiokol Corporation Huntsville Division ATTN: D. Flanigan R. Glick Tech Library Huntsville, AL 35807
1	Paul Gough Associates, Inc. ATTN: P. S. Gough 1048 South Street Portsmouth, NH 03801	2	Thiokol Corporation Wasatch Division ATTN: J. Peterson Tech Library P. O. Box 524 Brigham City, UT 84302
1	Physics International Company 2700 Merced Street San Leandro, CA 94577		
1	Princeton Combustion Research Lab., Inc. ATTN: M. Summerfield 475 U.S. Highway One Monmouth Junction, NJ 08852	2	Thiokol Corporation Elkton Division ATTN: R. Biddle Tech Lib. P. O. Box 241 Elkton, MD 21921
1	Pulsepower Systems, Inc. ATTN: L. C. Elmore 815 American Street San Carlos, CA 94070	2	United Technologies Chemical Systems Division ATTN: R. Brown Tech Library P. O. Box 358 Sunnyvale, CA 94086
2	Rockwell International Rocketdyne Division ATTN: BA08 J. E. Flanagan J. Grey 6633 Canoga Avenue Canoga Park, CA 91304	1	Universal Propulsion Company ATTN: H. J. McSpadden Black Canyon Stage 1 Box 1140 Phoenix, AZ 85029
1	Science Applications, Inc. ATTN: R. B. Edelman 23146 Cumorah Crest Woodland Hills, CA 91364	1	Veritay Technology, Inc. ATTN: E. B. Fisher P. O. Box 22 Bowmansville, NY 14026
1	Scientific Research Assoc., Inc. ATTN: H. McDonald P. O. Box 498 Glastonbury, CT 06033	1	Southwest Research Institute Institute Scientists ATTN: W. H. McLain 8500 Culebra Road San Antonio, TX 78228

No. Of Copies	Organization	No. Of Copies	Organization
1	Battelle Memorial Institute 505 King Avenue Columbus, OH 43201	3	Georgia Institute of Tech School of Aerospace Eng. ATTN: B. T. Zinn E. Price W. C. Strahle Atlanta, GA 30332
1	Brigham Young University Dept. of Chemical Engineering ATTN: M. Beckstead Provo, UT 84601	1	Institute of Gas Technology ATTN: D. Gidaspow 3424 S. State Street Chicago, IL 60616
1	California Institute of Tech 204 Karman Lab Main Stop 301-46 ATTN: F. E. C. Culick 1201 E. California Street Pasadena, CA 91125	1	Johns Hopkins University Applied Physics Laboratory Chemical Proplsion Information Agency ATTN: T. Christian Johns Hopkins Road Laurel, MD 20707
1	California Institute of Tech Jet Propulsion Laboratory 4800 Oak Grove Drive Pasadena, CA 91103	1	Massachusetts Institute of Technology Dept of Mechanical Engineering ATTN: T. Toong Cambridge, MA 02139
1	University of Illinois Department of Mech Engr ATTN: H. Krier 144 MEB, 1206 W. Green Street Urbana, IL 61801	1	Pennsylvania State University Applied Research Lab ATTN: G. M. Faeth P. O. Box 30 State College, PA 16801
1	University of Massachusetts Dept. of Mechanical Engineering ATTN: K. Jakus Amherst, MA 01002	1	Pennsylvania State University Dept. Of Mechanical Engineering ATTN: K. Kuo University Park, PA 16802
1	University of Minnesota Dept. of Mechanical Engineering ATTN: E. Fletcher Minneapolis, MN 55455	1	Purdue University School of Mechanical Engineering ATTN: J. R. Osborn TSPC Chaffee Hall West Lafayette, IN 47906
1	Case Western Reserve University Division of Aerospace Sciences ATTN: J. Tien Cleveland, OH 44135	1	Rensselaer Polytechnic Inst. Department of Mathematics Troy, NY 12181

DISTRIBUTION LIST

No. Of Copies	Organization
1	Rutgers University Dept. of Mechanical and Aerospace Engineering ATTN: S. Temkin University Heights Campus New Brunswick, NJ 08903
1	SRI International Propulsion Sciences Division ATTN: Tech Library 333 Ravenswood Avenue Menlo Park, CA 94025
1	Stevens Institute of Technology Davidson Laboratory ATTN: R. McAlevy, III Hoboken, NJ 07030
2	Los Alamos Scientific Lab ATTN: T.D. Butler, MS B216 M. Division, B. Craig P. O. Box 1663 Los Alamos, NM 87545
1	University of Southern California Mechanical Engineering Dept. ATTN: OHE200, M. Gerstein Los Angeles, CA 90007
2	University of Utah Dept. of Chemical Engineering ATTN: A. Baer G. Flandro Salt Lake City, UT 84112
1	Washington State University Dept. of Mechanical Engineering ATTN: C. T. Crowe Pullman, WA 99163

No. Of Copies	Organization
1	AFWL/SUL Kirtland AFB, NM 87117

Aberdeen Proving Ground

Dir, USAMSAA
ATTN: DRXSY-D
DRXSY-MP, H. Cohen
Cdr, USATECOM
ATTN: DRSTE-TO-F

Cdr, USAAPG
ATTN: STEAP-MT, S. Walton
G. Rice
D. Lacey
C. Herud
Director, HEL
ATTN: J. Weisz

Director, USACSL
ATTN: DRSMC-CLB-PA
DRSMC-CLJ-L
DRSMC-CLN

USER EVALUATION OF REPORT

Please take a few minutes to answer the questions below; tear out this sheet, fold as indicated, staple or tape closed, and place in the mail. Your comments will provide us with information for improving future reports.

1. BRL Report Number _____

2. Does this report satisfy a need? (Comment on purpose, related project, or other area of interest for which report will be used.)

_____

_____

_____

3. How, specifically, is the report being used? (Information source, design data or procedure, management procedure, source of ideas, etc.) _____

_____

_____

4. Has the information in this report led to any quantitative savings as far as man-hours/contract dollars saved, operating costs avoided, efficiencies achieved, etc.? If so, please elaborate.

_____

_____

5. General Comments (Indicate what you think should be changed to make this report and future reports of this type more responsive to your needs, more usable, improve readability, etc.) _____

_____

_____

_____

6. If you would like to be contacted by the personnel who prepared this report to raise specific questions or discuss the topic, please fill in the following information.

              Name: _____

    Telephone Number: _____

Organization Address: _____

_____

_____